TA-16

Los Alamos National Laboratory/University of California
Risk Reduction & Environmental Stewardship (RRES)
Remediation Services (RS), MS M992
Los Alamos, New Mexico 87545
(505) 667-0808/FAX (505) 665-4747

National Nuclear Security Administration.
Los Alamos Site Operations, MS A316
Environmental Restoration Program
Los Alamos, New Mexico 87544
(505) 667-7203/FAX (505) 665-4504

Date: July 25, 2003
Refer to: ER2003-0484

JUL 2003

Mr. John Young, Corrective Action Project Leader
Permits Management Program
NMED – Hazardous Waste Bureau
2905 Rodeo Park Drive East
Building 1
Santa Fe, NM 87505-6303

Mr. Carl Will, LANL Permits Project Leader
Permits Management Program
NMED – Hazardous Waste Bureau
2905 Rodeo Park Drive East
Building 1
Santa Fe, NM 87505-6303

SUBJECT: SUBMITTAL OF BEDROCK FRACTURE CHARACTERIZATION AT MATERIAL DISPOSAL AREA (MDA) P SITE: PHASE II CLOSURE INVESTIGATION REPORT

Dear Mr. Young and Mr. Will:

Enclosed are two copies of the Los Alamos National Laboratory (LANL) Risk Reduction Environmental Stewardship-Environmental Characterization and Remediation (RRES-ECR) Bedrock Fracture Characterization at MDA P Site: Phase II Closure Investigation Report. This report was originally submitted to your office on January 31, 2003 (ER2003-0095) as Annex III in the MDA P Area Closure Certification Report (ER2002-0773). Per your letter dated April 30, 2003, the aforementioned annex has been augmented to address your concerns and is now being resubmitted.

If you have any questions, please contact William Criswell at (505) 665-5886 or Lance Woodworth at (505) 665-5820.

Sincerely,

David McInroy, Acting Deputy Project Director
Remediation Services
Los Alamos National Laboratory

Sincerely,

for Thomas F. Wheeler

David Gregory, Project Manager
Department of Energy
Los Alamos Site Operations

6425

DM/DG/NR/vn

Enclosure: Bedrock Fracture Characterization at MDA P Site: Phase II Closure Investigation Report (ER2003-0467)

Cy:(w/enc)
W. Criswell, RRES-RS, MS M992
D. Hickmott, RRES-RS, MS M992
R. Mirenda, RRES-RS, MS M992
N. Quintana, RRES-RS, MS M992
N. Riebe, RRES-RS, MS M992
K. VanDerpoel, RRES-RS, MS M992
D. Gregory, LASO, MS A316
S. Yanicak, NMED-OB
V. Maranville, NMED-HWB
K. Olsen, NMED-HWB
J. Davis, NMED-SWB
L. King, EPA Region 6
RRES-RS File, MS M992
IM-5, MS A150
RPF MS M707

Cy:(w/o enclosure)
S. Den Baars, Shaw, MS M892
D. McInroy, RRES-RS, MS M992
B. Newman, EES-2, MS J495
B. Ramsey, RRES-DO, MS J591
R. Romero, RRES-SWRC, MS M992
J. Salazar, EES –2, MS J495
A. Sherrard, ESA-OPS, MS C924, FMU-ESH
M. Tardiff, Neptune, MS M969
M. Wade, Weston, MS M992
S. Wirth, Shaw, MS M992
B. Tongate, NMED-HWB
N. Dhawan, NMED-HWB
D. Goering, NMED-HWB
J. Kieling, NMED-HWB
C. Voorhees, NMED-OB

Remediation Program

RRES

LA-UR-02-7200
July 2003
ER2003-0467

Bedrock Fracture Characterization at Material Disposal Area P Site: Phase II Closure Investigation Report

1943 - 2003
Los Alamos
NATIONAL LABORATORY
Ideas That Change the World

Disclaimer

This document contains data regarding radioactive wastes, the management of which is regulated under the Atomic Energy Act and specifically excluded from regulation under the Resource Conservation and Recovery Act and the New Mexico Hazardous Waste Act. These data are provided to the New Mexico Environment Department for information purposes only.

Produced by
Risk Reduction and Environmental Stewardship Division–Remediation Services

Los Alamos National Laboratory, an affirmative action/equal opportunity employer, is operated by the University of California for the United States Department of Energy under contract W-7405-ENG-36.

This report was prepared as an account of work sponsored by an agency of the United States Government. Neither the Regents of the University of California, the United States Government nor any agency thereof, nor any of their employees make any warranty, express or implied, or assume any legal liability or responsibility for the accuracy, completeness, or usefulness of any information, apparatus, product, or process disclosed, or represent that its use would not infringe privately owned rights. Reference herein to any specific commercial product, process, or service by trade name, trademark, manufacturer, or otherwise does not necessarily constitute or imply its endorsement, recommendation, or favoring by the Regents of the University of California, the United States Government, or any agency thereof.

Los Alamos National Laboratory strongly supports academic freedom and a researcher's right to publish; as an institution, however, the Laboratory does not endorse the viewpoint of a publication or guarantee its technical correctness. By acceptance of this article, the publisher recognizes that the U.S. Government retains a nonexclusive, royalty-free license to publish or reproduce the published form of this contribution, or to allow others to do so, for U.S. Government purposes. Los Alamos National Laboratory requests that the publisher identify this article as work performed under the auspices of the U.S. Department of Energy.

EXECUTIVE SUMMARY

This report correlates and augments the fracture characterization measurements of Material Disposal Area (MDA P) with (1) geophysical measurements taken in six boreholes, (2) observations of fractures, and (3) geochemical data from cores to create an initial conceptual model of fracture transport of shallow groundwater in the bedrock beneath the MDA P Site. The Phase II activities conducted at the MDA P Site had three major components: exploratory drilling to investigate the subsurface geophysical and geochemical regime of the bedrock; fracture survey and mapping to define the characteristics of the bedrock fractures at the site; and the final confirmation sampling and analysis.

MDA P, Flash Pad 387, and Solid Waste Management Unit (SWMU) 16-016(c)-99 (referred to collectively as the MDA P Site) are located within a small open watershed with no springs or internal sources of water. Excavation and removal of the MDA P waste pile, as part of the Phase I closure activities, resulted in removal of most of the unconsolidated, surficial materials and exposure of the bedrock surfaces at the MDA P Site. The resulting bedrock exposures provide excellent exposures for surface mapping of stratigraphy and fractures. The geologic mapping delineates the stratigraphy of the Tshirege Member of the Bandelier Tuff at MDA P, including Units 3, 3T, and 4l, from bottom to top, respectively. Within the regional structure, MDA P is within the deformation zone of the Pajarito Fault Zone. Personnel from Risk Reduction and Environmental Stewardship–Remediation Services collaborated with personnel from the Seismic Hazards Program to perform the mapping and surface fracture investigations. Lewis et al. (2002, 73785) provides complete descriptions and discussions of the stratigraphic assignments.

MDA P lies on the southern rim of Cañon de Valle at the transition from a graben structure to the west and a bedrock promontory to the east. A fracture zone on the west side of the MDA P footprint exhibits distributed deformation consisting of a series of small faults, a small graben, elevated fracture density, and larger apertures in Bandelier Tuff Units 3 and 3T and is attributed to deeper seated normal faulting. The east side of the MDA P footprint exhibits fewer fractures, with generally smaller apertures. The apparent occurrences of larger, more frequent clay accumulations on the west side are interpreted to indicate a greater capacity for transmitting suspended solids. Measurements of induced water flow made with the heat pulse flowmeter in selected boreholes indicate that the larger, more frequent fractures in the western area are capable of transmitting larger volumes of water to greater depths under saturated conditions. Under unsaturated conditions that prevail naturally, the fractures with larger apertures or more densely fractured areas have higher air permeability, which will enhance air movement and evaporation.

The borehole geophysical measurements that were performed included natural gamma, caliper, electromagnetic (EM) conductivity, neutron, heat pulse flowmeter, and optical televiewer. Results of the EM conductivity measurements indicate that anomalies of increased conductivity are present in all boreholes at depths that range from 35 to 90 ft. The EM conductivity highs at the MDA P footprint range from 35- to 55-ft depths and are consistent from east to west. These anomalies strongly correlate with caliper logs and fractures observed in cores.

After inspection of the borehole geophysical logs, samples were collected from the core for anion and cation analyses. Forty-seven samples were leached and analyzed for anions and selected cations. The results indicate that nitrate, chloride, sodium, calcium, and potassium exhibit concentration increases at 35 to 90 ft below ground surface after sharp decreases from the surface. The concentrations of the anions, nitrate, and chloride are generally mirrored with the cations, sodium, and potassium. Results are reported in mg/kg because moisture data from the cores are not available. The EM conductivity highs are thus interpreted to result from the high ionic strength solutions in the rock matrices. Barium is found to be approximately 1 mg/kg throughout the cores measured, with the exception of 116 mg/kg at the surface of core 526 on the east side of the MDA P footprint.

From the empirical data, a conceptual model was developed that states that the fracture flow system is unsaturated, with local infiltration of precipitation and downward percolation, but dominated by matrix absorption and evaporation. The latter processes have resulted in an accumulation zone of nitrate, chloride, and sulfate salts at 30- to 90-ft depths below the current land surface in the partially welded Unit 3. The salts are interpreted to be the result of dissolution of surface salts and redistribution in the subsurface through percolation and evaporation. The zone is apparent in all boreholes and is located entirely above the stream level of Cañon de Valle. It is interpreted that evaporation is promoted by connection of the fracture system with the atmosphere near the canyon walls. Pressure changes are propagated through the fracture system in response to barometric pressure changes, a process recognized at many other arid and semi-arid sites across the western United States and the Pajarito Plateau. Hence, the larger fractures promote exchange of atmospheric gases; the smaller fractures promote retention of moisture and provide the initial paths of rewetting.The data in this report support the suggestion by Neeper and Gilkeson (1996, 56025) and Newman (1996, 59372) that the process of moisture removal from within the mesa by evaporation forms a hydraulic barrier. Thus, vapor phase transport is the dominant subsurface mechanism for moisture transport. The zone of salt accumulation is interpreted to represent the response of the fracture system to the semi-arid climate and probably required thousands of years to develop.

The removal of all unconsolidated deposits across the MDA P footprint has resulted in the elimination of all potentially near-saturated and ponded water sources at the surface, so that current conditions promote runoff and inhibit infiltration. The hydrology of the fracture flow system has been permanently altered from that which existed historically. The lack of water observed in any boreholes during or after drilling indicates that the saturated conditions along the Cañon de Valle alluvial aquifer do not extend laterally to produce a perched water table beneath the MDA P footprint.

CONTENTS

1.0 INTRODUCTION **1**
1.1 General Site Description 1
1.2 Previous and Concurrent Work 6

2.0 GEOLOGIC SETTING **6**
2.1 Topographic Mapping 8
2.2 Geologic Mapping 8
2.3 Unconsolidated Deposits 9
2.4 Bedrock Stratigraphy 9

3.0 BOREHOLES **11**
3.1 Drilling Methods and Collection of Core 12
3.2 Field Screening and Sampling and Sampling of Core 12
3.3 Lithologic Descriptions of Cores 13

4.0 FRACTURE CHARACTERIZATION **13**
4.1 Methods of Surface Measurements 13
4.2 Results of Surface Measurements 14
4.3 Methods of Observations of Fractures in Core 17
4.3.1 Results of Observations of Fractures in Core 18
4.4 Methods of Measurement of Fractures in Boreholes 20
4.4.1 Results of Measurement of Fractures in Boreholes 21

5.0 BOREHOLE GEOPHYSICS **23**
5.1 Natural Gamma 24
5.1.1 Results and Discussion of Natural Gamma Logs 24
5.2 Caliper 24
5.2.1 Results of Caliper Logs 25
5.3 Electromagnetic Conductivity 25
5.3.1 Results of Electromagnetic Conductivity Logs 26
5.4 Neutron Logs 26
5.4.1 Results of Neutron Logs 26
5.5 HPF Measurements 27
5.5.1 Results of HPF Measurements 28

6.0 GEOCHEMICAL PROFILES **28**
6.1 Results of Geochemical Profiles 29

7.0 DISCUSSION **30**
7.1 Characteristics of the Eastern Part of the MDA P Footprint 30
7.2 Characteristics of the Western Part of the MDA P Footprint 32
7.3 Characteristics of Flash Pad 387 at the Watershed Divide 34

8.0 CONCEPTUAL MODEL OF THE FRACTURE FLOW SYSTEM AT MDA P WATERSHED 36

9.0 REGIONAL SETTING OF MDA P 40

10.0 DISCUSSION OF MDA P AND THE CAÑON DE VALLE STREAM 41

11.0 IMPLICATIONS FOR THE TA-16 CONCEPTUAL MODEL 43

12.0 CONCLUSIONS 43

13.0 REFERENCES 44

Appendix A. Field Boring Logs, Lithologic Field Logs

Appendix B. Surface Fracture Data Tables and Subsurface Fracture Data Tables Generated from Borehole Optical Televiewer

Appendix C. Descriptions of Selected Fractures in Cores

Appendix D. Summary Plots of Borehole Geophysics

Appendix E. Heat Pulse Flowmeter Data Tables

Appendix F. Summary Tables of Geochemical Anion/Cation Analyses

Plate 1. Geologic Map of MDA P: Completion of Phase I Closure Implementation

List of Figures

Figure 1.0-1. Location of the MDA P Site within TA-16, Los Alamos National Laboratory 2
Figure 1.1-1. Map of the MDA P Site showing boundaries of MDA P, Flash Pad 387, and the TA-16 Burning Ground 4
Figure 2.0-1. Generalized stratigraphic column of Bandelier Tuff 7
Figure 2.4-1. Stratigraphic and lithologic correlations of boreholes at MDA P, Flash Pad 387, and measured section north of Cañon de Valle 10
Figure 4.2-1. Orientations of surface and subsurface fractures 15
Figure 4.2-2. Map view of fracture apertures measured along traverses at MDA P 16
Figure 4.4-1. Plot of anion concentrations in core samples from Borehole 554 22
Figure 7.1-1. Empirical correlation diagram for Borehole 526, west side of the MDA P footprint 31
Figure 7.2-1. Empirical correlation diagram for Borehole 554, east side of the MDA P footprint 33
Figure 7.3-1. Empirical correlation diagram for Borehole 273 and Flash Pad 387 at the watershed divide 35
Figure 8.0-1. Conceptual model of fracture flow in bedrock at MDA P 38
Figure 9.0-1. Generalized regional structure map of the MDA P Site 42

List of Photographs

Photograph 1.1-1. The MDA P Site viewed from the north, after completion of Phase I excavation activities (October 2002) 5
Photograph 4.3-1. Natural fracture in core from Borehole 526 at 36.5-ft depth (center row of core) 19
Photograph 4.3-2. Natural fracture in core from Borehole 554 at 77.3-ft depth (top row of core) 20

List of Tables

Table 3.1-1. Summary of Boreholes at the MDA P Site 12
Table 4.2-1. Summary of Surface Fracture Density Measured at MDA P 17
Table 5.0-1. Summary of Borehole Geophysical Logging Suite 23

List of Acronyms and Abbreviations

bgs	below ground surface
BH	borehole
CFR	Code of Federal Regulations
EES	Earth and Environmental Sciences (a Laboratory division)
EM	eletromagnetic
EPA	US Environmental Protection Agency
ER	environmental restoration
FWS	full-waveform sonic (log)
GIS	geographic information system
HE	high explosives
HPF	heat pulse flowmeter
HRMB	Hazardous and Radioactive Materials Bureau
HWB	Hazardous Waste Bureau
MDA	material disposal area
msl	mean sea level
NMAC	New Mexico Administrative Code
NMED	New Mexico Environment Department
OBI	optical borehole imaging
RPF	Records Processing Facility
RRES-RS	Risk Reduction and Environmental Stewardship–Remediation Services (a Laboratory project)
SAL	screening action level
SWMU	solid waste management unit
TA	technical area
USGS	US Geological Survey
VCA	voluntary corrective action
XRF	x-ray fluorescence

Glossary

abandonment — The plugging of a well or borehole in such a manner as to preclude migration of surface runoff or ground water along the length of the well.

alluvial — Relating to geologic deposits or features formed by running water.

aquifer — Body of permeable geologic material whose saturated portion is capable of readily yielding groundwater to wells.

area of contamination (AOC) — Discrete areas of generally dispersed contamination.

ash-flow tuff — A tuff deposited by a hot, dense volcanic current. Ash-flow tuff can be either welded or nonwelded.

background level — Naturally occurring concentrations (levels) of an inorganic chemical and naturally occurring radionuclides in soil, sediment, and tuff.

breccia — Coarse-grained rock that consists of angular fragments cemented together or embedded in a fine-grained matrix.

caldera — An approximately circular volcanic depression, generally on the order of tens of kilometers in diameter, formed during the eruption of large volumes (tens to hundreds of cubic kilometers) of dense rock equivalent, ash-flow tuff, and ash-fall tuff deposits.

chemical — Any naturally occurring or man-made substance characterized by a definite molecular composition, including molecules that contain radionuclides.

Code of Federal Regulation (CFR) — A codification of all regulations developed by federal government agencies and finalized by publication in the Federal Register.

colluvium — Loose rock debris that accumulates at the base of a cliff or on a slope principally by the action of gravity.

decontamination — Removal of unwanted material from the surface of or from within another material.

evapotranspiration — The combined discharge of water from the earth's surface to the atmosphere by evaporation from lakes, streams, and soil surfaces, and by transpiration from plants.

fault — A fracture, or zone of fractures, in rock along which there has been vertical or horizontal movement; adjacent rock layers or bodies are displaced.

Federal Register — The official daily publication for Rules, Proposed Rules, and Notices of federal agencies and organizations, as well as Executive Orders and other Presidential Documents.

geohydrology — The science that applies hydrologic methods to the understanding of geologic phenomena.

groundwater — Water in a subsurface saturated zone; water beneath the regional water table.

hazardous waste — Any solid waste is generally a hazardous waste if it

- is not excluded from regulation as a hazardous waste,
- is listed in the regulations as a hazardous waste,
- exhibits any of the defined characteristics of hazardous waste (ignitability, corrosivity, reactivity, or toxicity), or
- is a mixture of solid waste and hazardous waste.

See 40 CFR 261.3 for a complete definition of hazardous waste.

Hazardous and Solid Waste Amendments (HSWA) — The Hazardous and Solid Waste Amendments of 1984 (Public Law No. 98-616, 98 Stat. 3221), which amended the Resource Conservation and Recovery Act of 1976, 42 U.S.C. § 6901 et seq.

hydraulic conductivity — The rate at which water moves through a medium in a unit of time under a unit hydraulic gradient through a unit area measured perpendicular to the direction of flow.

hydraulic gradient — The rate of change of hydraulic head per unit of distance in the direction of groundwater flow.

hydraulic head — Elevation of the water table or potentiometric surface as measured in a well.

interflow — A runoff process that involves lateral subsurface flow in the soil zone.

intermittent stream — A stream that flows only in certain reaches due to losing and gaining characteristics of the channel bed.

matrix — Relatively fine material in which coarser fragments or crystals are embedded; also called "ground mass" in the case of igneous rocks.

nonwelded

percolation — Gravity flow of soil water through the pore spaces in soil or rock below the ground surface.

piezometric surface — The surface that represents the static head in an aquifer: applies to both confined and unconfined aquifers (also called potentiometric surface).

porosity — The ratio of the volume of interstices in a soil or rock sample to its total volume expressed as a percentage or as a fraction.

porphyritic — Said of the texture of an igneous rock in which larger crystals (phenocrysts) are set in a finer ground mass.

Quaternary — The second period of the Cenozoic Era, following the Tertiary, and including the last 2–3 million years.

radionuclide — A nuclide (species of atom) that exhibits radioactivity.

recharge — The process by which water is added to the zone of saturation, either directly from the overlying unsaturated zone or indirectly by way of another material in the saturated zone.

regional aquifer — Geologic material(s) or unit(s) of regional extent whose saturated portion yields significant quantities of water to wells, contains the regional zone of saturation, and is characterized by the regional water table or potentiometric surface.

Resource Conservation and Recovery Act (RCRA) — The Solid Waste Disposal Act as amended by the Resource Conservation and Recovery Act of 1976. (40 CFR 270.2)

sample — A portion of a material (e.g., rock, soil, water, air), which, alone or in combination with other samples, is expected to be representative of the material or area from which it is taken. Samples are typically sent to a laboratory for analysis or inspection or are analyzed in the field. When referring to samples of environmental media, the term field sample may be used.

screening action level (SAL) — Medium-specific concentration level for a chemical derived using conservative criteria below for which it is generally assumed that there is no potential for unacceptable risk to human health. The derivation of a SAL is based on conservative exposure and land-use assumptions. However, if an applicable regulatory standard exists that is less than the value derived by risk-based computations, it will be used for the SAL.

sediment — (1) A mass of fragmented inorganic solid that comes from the weathering of rock and is carried or dropped by air, water, gravity, or ice; or a mass that is accumulated by any other natural agent and that forms in layers on the earth's surface such as sand, gravel, silt, mud, fill, or loess. (2) A solid material that is not in solution and either is distributed through the liquid or has settled out of the liquid.

site conceptual model — A qualitative or quantitative description of sources of contamination, environmental transport pathways for contamination, and biota that may be impacted by contamination (called receptors) and whose relationships describe qualitatively or quantitatively the release of contamination from the sources, the movement of contamination along the pathways to the exposure points, and the uptake of contaminant by the receptors.

soil gas — Those gaseous elements and compounds that occur in the void spaces in unsaturated rock or soil. Such gases can move through or leave the rock or soil, depending on changes in pressure.

soil water — Water in the unsaturated zone, regardless of whether it occurs in soil or rock.

solid waste management unit (SWMU) — Any discernible unit at which solid wastes have been placed at any time, irrespective of whether the unit was intended for the management of solid or hazardous waste. Such units include any area at a facility at which solid wastes have been routinely and systematically released. This definition includes regulated units (i.e., landfills, surface impoundments, waste piles, and land treatment units) but does not include passive leakage or one-time spills from production areas and units in which wastes have not been managed (e.g., product-storage areas).

stratigraphy — The science dealing with the succession, age, composition, and history of strata.

technical area (TA) — The Laboratory established technical areas as administrative units for all its operations. There are currently 49 active TAs spread over 43 square miles.

transmissivity — A measure of the rate at which water is transmitted through a cross-section of aquifer having the dimensions unit width and total saturated thickness as height, under a unit hydraulic gradient; also hydraulic conductivity times aquifer thickness.

tuff — A compacted deposit of volcanic ash and dust that contains rock and mineral fragments accumulated during an eruption.

vadose zone — The unsaturated zone. Portion of the subsurface above the regional water table in which pores are not fully saturated.

unconfined — Said of water in a saturated zone that is open to the atmosphere (that is, not beneath a confining bed or under artesian pressure).

unsaturated zone — The zone between the land surface and the regional water table and between perched zones of saturation. Generally, fluid pressure in this zone is less than atmospheric pressure, and some of the voids may contain air or other gases at atmospheric pressure.

water balance — The relationship between water input (precipitation) and output (runoff, evapotranspiration, and recharge) in a hydrological system; the partitioning of precipitation among these components of the hydrological cycle.

watershed — The region drained by, or contributing waters to, a stream, lake or other body of water and separated from adjacent drainage areas by a divides such as a ridge or summit of high ground.

water table — The top of the regional saturated zone; the piezometric surface associated with an unconfined aquifer.

welded tuff — A volcanic deposit hardened by the action of heat, pressures from overlying material, and hot gases.

Metric Units to US Customary Conversions

Multiply SI (Metric) Unit	by	To Obtain US Customary Unit
kilometers (km)	0.622	miles (mi)
kilometers (km)	3281	feet (ft)
meters (m)	3.281	feet (ft)
meters (m)	39.37	inches (in.)
centimeters (cm)	0.03281	feet (ft)
centimeters (cm)	0.394	inches (in.)
millimeters (mm)	0.0394	inches (in.)
micrometers or microns (µm)	0.0000394	inches (in.)
square kilometers (km^2)	0.3861	square miles (mi^2)
hectares (ha)	2.5	acres
square meters (m^2)	10.764	square feet (ft^2)
cubic meters (m^3)	35.31	cubic feet (ft^3)
kilograms (kg)	2.2046	pounds (lb)
grams (g)	0.0353	ounces (oz)
grams per cubic centimeter (g/cm^3)	62.422	pounds per cubic foot (lb/ft^3)
milligrams per kilogram (mg/kg)	1	parts per million (ppm)
micrograms per gram (µg/g)	1	parts per million (ppm)
liters (l)	0.26	gallons (gal.)
milligrams per liter (mg/l)	1	parts per million (ppm)
degrees Celsius (°C)	9/5 + 32	degrees Fahrenheit (°F)

1.0 INTRODUCTION

This report documents the results of field investigation activities conducted to support the closure of Material Disposal Area (MDA) P (also known as Solid Waste Management Unit [SWMU] 16-018) (Figure 1.0-1), the closure of Flash Pad 387 [SWMU 16-010(b)], and a voluntary corrective action (VCA) at adjacent sites known as consolidated SWMU 16-016(c)-99. MDA P, Flash Pad 387, and SWMU 16-016(c)-99 are referred to collectively in this report as the MDA P Site. All these sites are located within a small watershed that is referred to in this report as the MDA P watershed. The MDA P watershed is located within Los Alamos National Laboratory (the Laboratory), at the Technical Area 16 (TA-16) Burning Ground, within the high explosives (HE) exclusion area.

The sites that make up the MDA P Site are a contiguous group with overlapping boundaries and similar characteristics. Therefore, the VCA and closures were integrated to promote efficient and effective field operations while achieving a common cleanup goal and satisfying the following requirements:

- Demonstrating that the appropriate closure performance standards have been met for MDA P and Flash Pad 387, pursuant to 20.4.1.500 and 600 of the New Mexico Administrative Code, which incorporates 40 CFR 264 and 265; and
- Demonstrating that the appropriate no further action criterion has been met for SWMU 16-016(c)-99, pursuant to Module VIII of the Laboratory's Hazardous Waste Facility permit.

The decision to consolidate the fieldwork at these sites was agreed upon during discussions between personnel from the Laboratory's Risk Reduction and Environmental Stewardship–Remediation Services (RRES-RS) (formerly the Environmental Restoration [ER] Project) and personnel from the New Mexico Environment Department (NMED) Hazardous Waste Bureau (HWB) (formerly the Hazardous and Radioactive Materials Bureau [HRMB]). The field investigations were conducted as part of Phase II closure activities after the Phase I excavation and waste removal activities were largely complete (LANL 2003, 76054). The area that was occupied by the waste pile is referred to in this report as the MDA P footprint.

The field investigation focused on the bedrock fracture regime beneath the MDA P Site. The objectives of this investigation were to (1) define the vertical and lateral variations in the frequency and distribution of fractures as they affect the potential to transmit groundwater in the bedrock; (2) define the relationship between the shallow bedrock fracture regime and the stream in Cañon de Valle; and (3) define the regional setting of MDA P. The characterization program consisted of compiling a surface bedrock map, taking field measurements of surface fractures within the footprint of MDA P, drilling boreholes in and adjacent to the footprint of MDA P, and taking limited geophysical measurements in the open boreholes. Upon inspection of the borehole geophysical data, samples were collected from the cores for geochemical analysis of soluble anions and cations. This report describes the methods used and the results of these field investigations and interprets the lithology, fracture, geophysical, and geochemical characteristics in a conceptual model of fracture flow at MDA P.

1.1 General Site Description

The TA-16 Burning Ground is located within a topographic saddle on an east-trending mesa of the Pajarito Plateau. The MDA P Site is located on the north side of the TA-16 Burning Ground (Figure 1.1-1 and Photograph 1.1-1) within a small open watershed that drains into Cañon de Valle, a small tributary of Water Canyon. The watershed is defined by the topographic hills to the east and west sides, with elevations of 7466 and 7515 ft above mean sea level (msl), respectively. A broad saddle runs between these hills that has a low elevation of 7454 ft above msl. The access road to the area and to Flash Pad 387 trends along this topographic saddle. The saddle creates a divide between the area of MDA P to the north and a larger watershed to the south that eventually drains to Cañon de Valle.

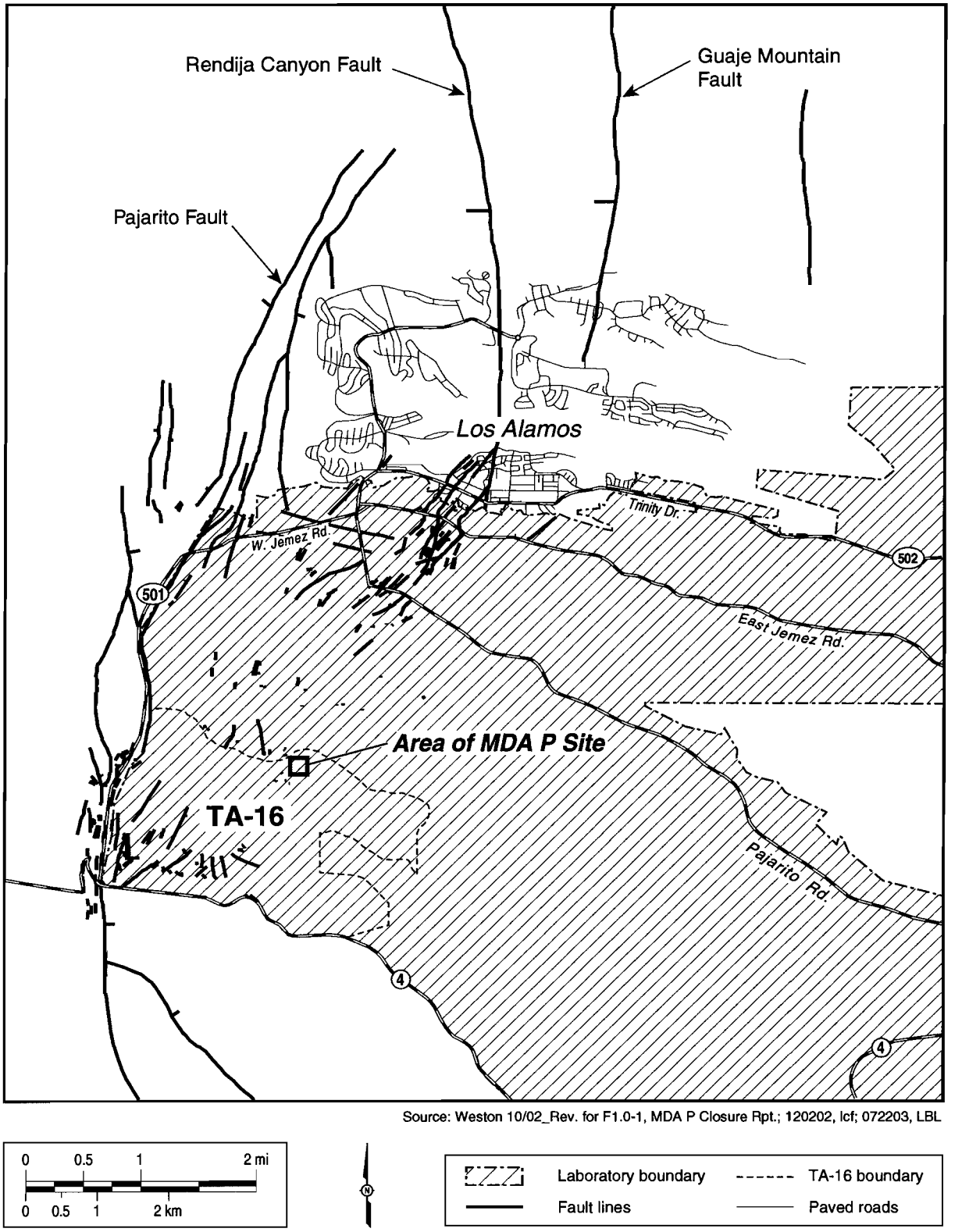

Source: Weston 10/02_Rev. for F1.0-1, MDA P Closure Rpt.; 120202, lcf; 072203, LBL

Figure 1.0-1. Location of the MDA P Site within TA-16, Los Alamos National Laboratory

The climate is semi-arid with approximately 18.7 in. of average annual precipitation which occurs as a combination of winter snowfall and warm-season thunderstorms in approximately equal proportions. Vegetation on the slopes and hills surrounding MDA P is characterized by the Rocky Mountain Montane Conifer Forest, whereas Cañon de Valle is characterized by the Rocky Mountain Riparian Deciduous Forest (Cross 1997, 59096). The vegetation in the area was affected, but not totally destroyed, by the Cerro Grande Fire in May 2000.

There are no ponds, springs, seeps, or other natural perennial water sources within the MDA P watershed (Nyhan 1989, 06890). The bar ditch along the north side of the access road leading from the west into the TA-16 Burning Ground is diverted through a culvert to the drainage south of the saddle. The active facilities at the burning ground are now located either on the saddle of the divide or in the watershed on the south side of the saddle. Ephemeral drainages within the watershed from the adjacent hills trend northward across the margins of the MDA P waste pile footprint to Cañon de Valle. Overland flow from Flash Pad 387 is currently diverted through a remnant of the MDA P run-on trench to the drainage on the east side of the waste pile footprint. Overland flow from SWMU 16-016(c)-99 currently trends north across a riprap-lined swale to the drainage on the west side of the waste pile footprint. Cañon de Valle possesses perennial flow through the reach north of the toe of the waste pile footprint. The stream is fed from upstream springs west of the MDA P watershed.

The burning ground was built at its present location on the southern margin of Cañon de Valle circa 1950. The area was originally remote and heavily forested. To construct the flash pad, the trees were cut and the slash and timber were burned in a central location. The soils and colluvium in the footprint of MDA P and Flash Pad 387 were regraded and several thousand cubic yards of backfill were brought in to provide a barren roughly flat surface on which to construct the flash pad. The backfill consisted of crushed Bandelier Tuff matrix with angular boulders up to 2 m across. The placement of the backfill resulted in a lobate mesa of dirt that extended northward from Flash Pad 387 to a large talus slope on the south side of Cañon de Valle. The waste pile resulted from burned debris from the flash pad which was disposed of at the leading edge of the lobate fill.

The MDA P waste pile, Flash Pad 387, and the contaminated soil at SWMU 16-016(c)-99 were removed completely by excavation in 1999–2002 (Figure 1.1-1). Most of the waste pile was found to be underlain by a dry soil, with bedrock only locally exposed directly under the waste pile materials. The footprint is represented by the boundary of the SWMU in Figure 1.1-1. The excavated area is larger than the waste pile footprint because contaminated soils extended beyond the footprint. The northern part of the footprint is composed of the steep slopes and cliffs adjacent to Cañon de Valle. The southern part is composed of the gentle slopes that grade southward to the topographic saddle. Flash Pad 387 was located south of MDA P near the saddle of the watershed divide. Contaminated soil at the flash pad was removed to bedrock, the excavation extending eastward of the pad fence line. The slope that is north of the flash pad yet south of the MDA P waste pile was found to be locally underlain by a moist, thick clay horizon that may have represented the original soil in the area. No other exposures of this clay were found during the excavations. The soil and fill materials underlying the waste pile were found to be entirely dry (LANL 2003, 76054). Phase I excavation, waste removal, and site-stabilization activities at the MDA P Site were completed in April 2002. Area restoration is currently pending the design and implementation of a reclamation plan.

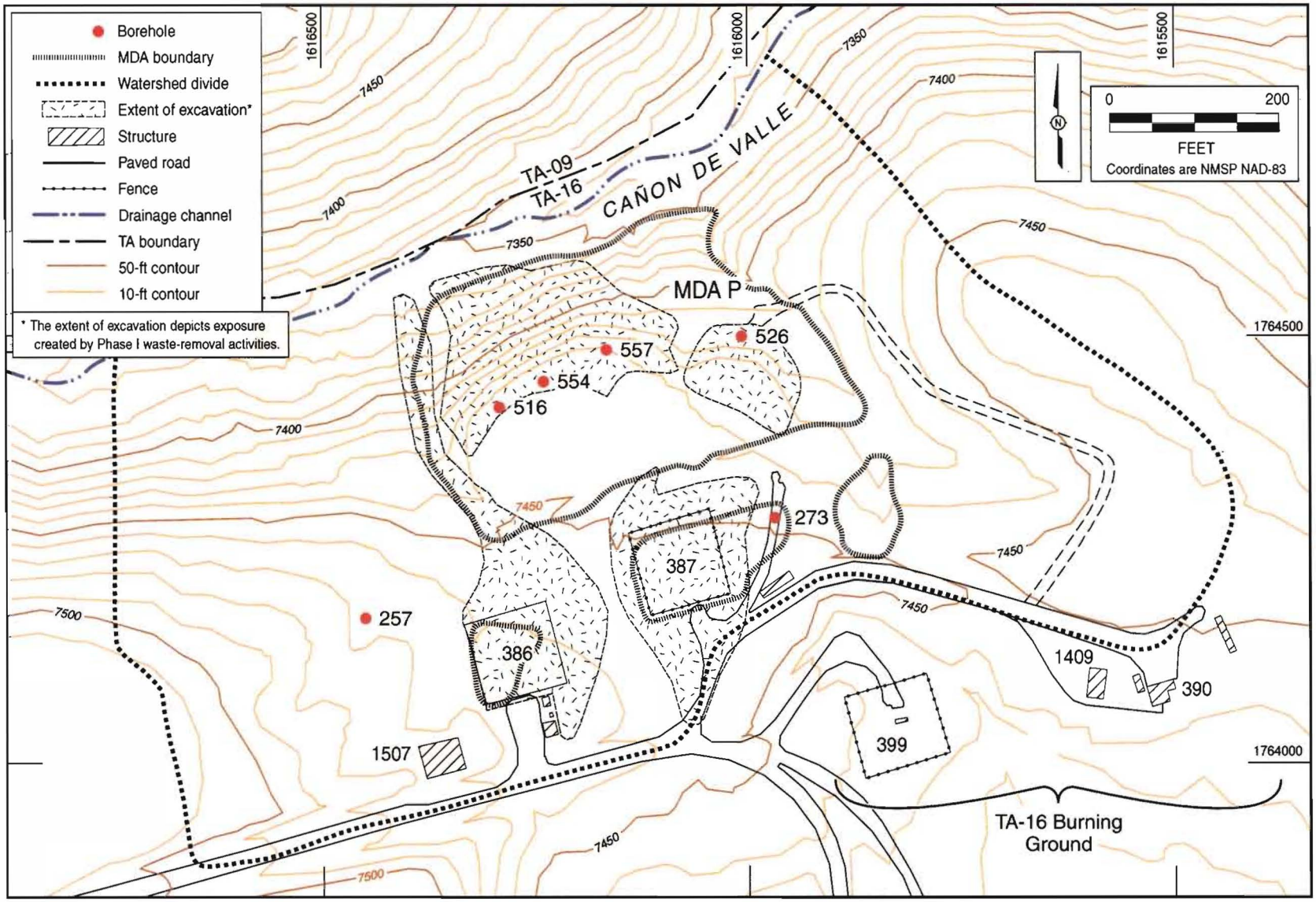

Source: FIMAD G109756 and G109758, 053101_Rev. as F1.1-1 in MDA P Closure Certification Rpt., Annex III Phase II, 121202, lcf

Figure 1.1-1. Map of the MDA P Site showing boundaries of MDA P, Flash Pad 387, and the TA-16 Burning Ground

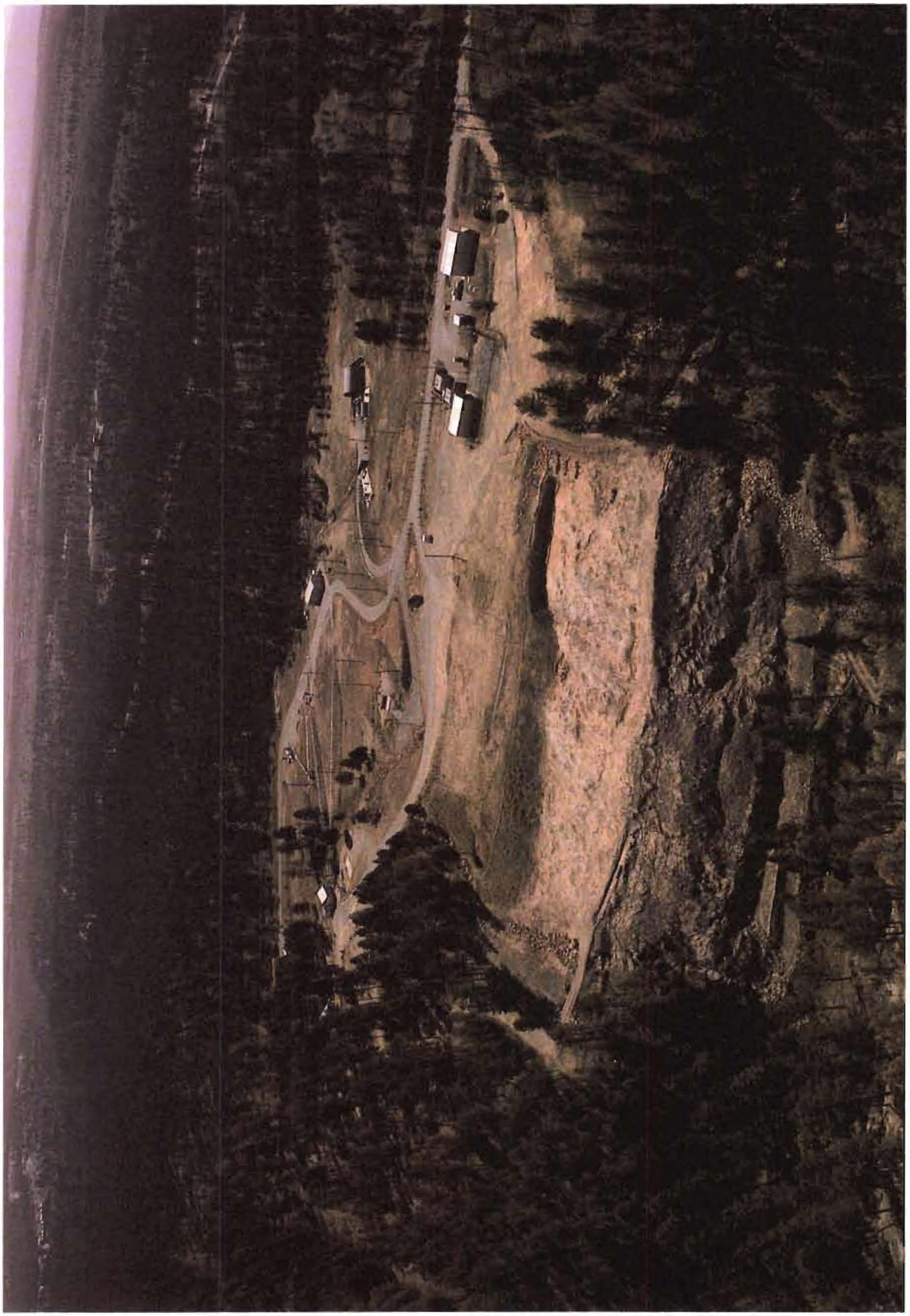

Photograph 1.1-1. The MDA P Site viewed from the north, after completion of Phase I excavation activities (October 2002)

1.2 Previous and Concurrent Work

No groundwater has been recognized below the MDA P footprint. McLin (1989, 11718) installed a vadose zone monitoring system adjacent to or into the waste pile materials and collected soil and tuff core samples. Moisture determinations and measurements for hydraulic properties were performed on cuttings or core (Brown et al. 1988, 06871). Moisture inventories were consistently higher in the waste pile wells than adjacent undisturbed areas, indicating that waste pile infiltration rates were higher than in surrounding undisturbed areas. Lysimeters in the underlying tuff did not yield any water, leading McLin (1989, 11718) to conclude that the tuff underlying the waste pile restricted all deep infiltration below the waste pile. Subsequent water balance studies focused on the upper flat portion of the waste pile that existed prior to excavation and waste removal (Nyhan 1989, 06890). Brown et al. (1988, 06871) used the drilling data to establish the geology and hydrology at MDA P and the regional setting within the Pajarito Plateau. They attributed hydrologic characteristics of the tuff to the degree of welding, with porosity and hydraulic conductivity decreasing with the increasing degree of welding.

As part of this study, personnel from the Laboratory's Seismic Hazards Program collaborated to collect fracture and stratigraphic data at MDA P. The Laboratory Seismic Hazard Program was then focused on evaluating a portion of TA-16 for seismic surface rupture potential. Initial inspection indicated that a zone of open and filled fractures is present on the west side of MDA P but is not apparent on the east side. The exceptional exposure of the bedrock units as a result of the excavations at MDA P provided the opportunity to measure a large number of surface fractures in three dimensions. The results of that study are reported by Lewis et al. (2002, 73785) and indicate that no large fault transects MDA P. The spatial association of a small fault, a graben, elevated fracture density, and fractures of large aperture appear to indicate that a zone of diffuse deformation is present in the western part of MDA P. Specific methods and results of Lewis et al. (2002, 73785) are discussed in the relevant sections of this report.

2.0 GEOLOGIC SETTING

The MDA P Site is known to be underlain by the Tshirege Member of the Bandelier Tuff, a series of volcanic deposits erupted from the Valles Caldera. The Tshirege Member forms much of the upland areas of the Pajarito Plateau. Broxton and Reneau (1995, 49726) examined nomenclature systems used by previous workers at the Laboratory, and other Environmental Restoration (ER) Program studies to evaluate the criteria for identifying and naming the subunits of the Bandelier Tuff. They used cooling units as the fundamental mapping units of the tuffs (Figure 2.0-1). A cooling unit consists of a sequence of pyroclastic flow deposits, here referred to as ashflow deposits, that were emplaced as a mixture of ash, stones, and gases that cooled, and perhaps welded, as a single entity. The lithologic characteristics of the units of the Bandelier Tuff were determined to be sufficiently distinct to be recognized in both outcrop and boreholes. Mapping efforts by Broxton et al. (1996, 54948) as part of the preparatory activities for the MDA P closure established that Tshirege Member Units 3 and 4 are exposed in Cañon de Valle and underlie MDA P. These units compose the cliffs and slopes, respectively. The hill to the west of MDA P is additionally underlain by a welded tuff that forms a caprock that terminates west of MDA P. The slopes of this hill are composed of weathered bedrock, colluvium, and isolated outcrops of the El Cajete pumice layer. The welded tuff caprock and the outcrops of the El Cajete pumice are largely absent at MDA P and on the hill to the east (Lewis et al. 2002, 73785).

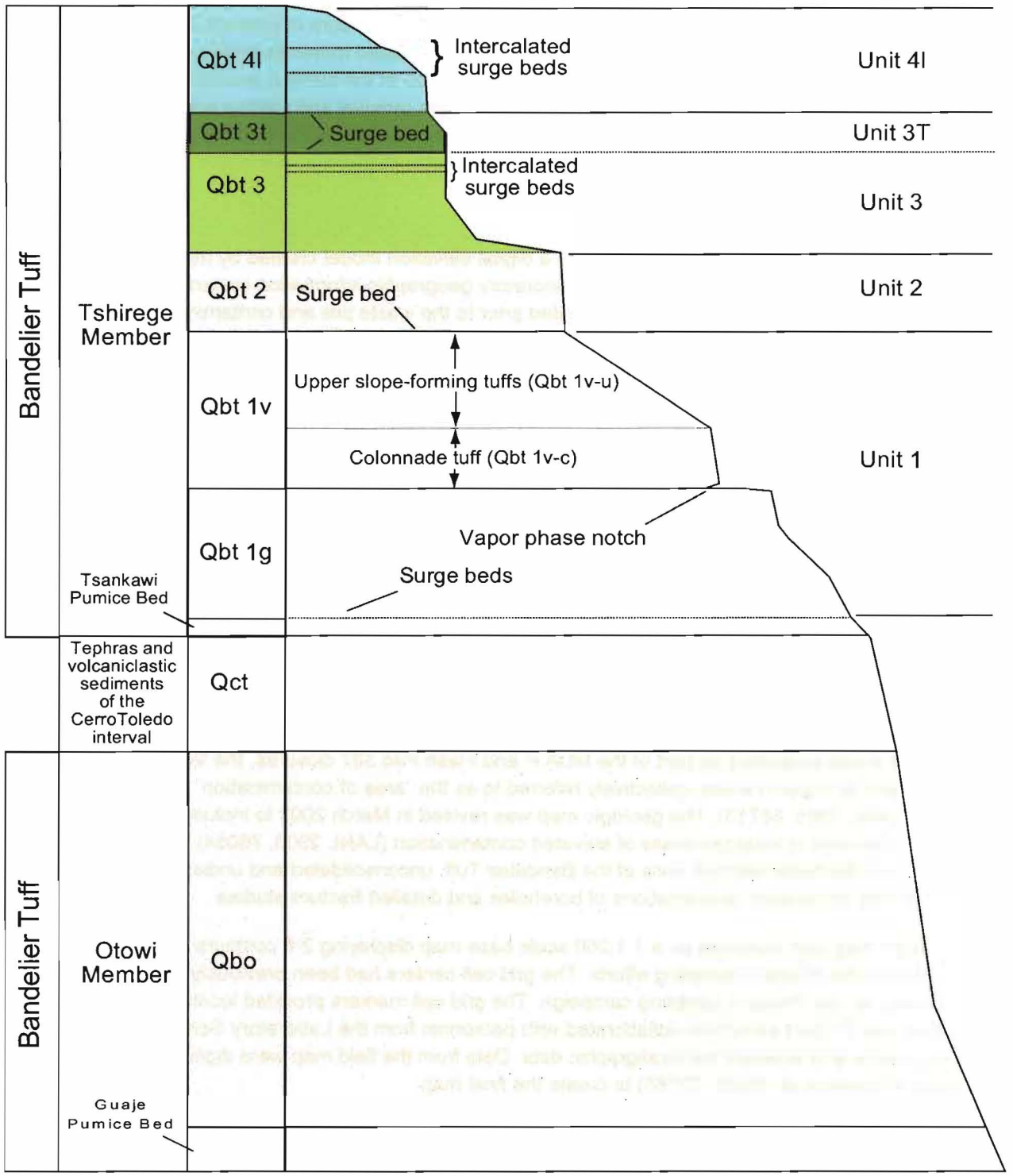

(modified from Broxton and Reneau 1995, 49726)

Figure 2.0-1. Generalized stratigraphic column of Bandelier Tuff

Preparation of staging areas and roads, and excavation of wastes and contaminated materials from MDA P, Flash Pad 387, and SWMU 16-016(c)-99 resulted in the exposure of bedrock in the waste pile footprint and isolated locations within the MDA P Site. Unconsolidated materials locally cover or veneer the bedrock. These materials consist of fill imported for construction of the burning ground, and fills and gravels imported for the construction of support areas for the waste removal and staging activities. Soil and colluvial materials adjacent to the project area remain largely undisturbed by the burning ground activities or the remediation activities.

2.1 Topographic Mapping

The topographic base map was generated from a digital elevation model created by modifying the 1991 topographic map of TA-16 maintained by the Laboratory geographic information system (GIS) lab group. This map consisted of terrain contours that existed prior to the waste pile and contaminated soil removal. Topographic data collected during and after the excavations were electronically inserted into the affected area to produce the final map. The high-resolution, topographic data set of Carey and Cole (2002, 73784) were utilized to refine the digital elevation model for the final map production.

The elevation and location information associated with field data at MDA P were determined by several geodetic surveys conducted between March 3, 2000, and July 31, 2002, using a Wild/Leica TC 1000 total station with electronic data memory. Control for the survey was Stations 1420, 1421, and the Pajarito Tower identified in the 1992 Laboratory-wide control network. Field measurements were reduced using LisCad Plus 5.0 surveying software. Horizontal coordinates are New Mexico State Plane Grid Coordinates, Central Zone, North American Datum, 1983, and are expressed in US Survey ft. Elevation is expressed in ft above msl relative to the National Geodetic Vertical Datum of 1929.

2.2 Geologic Mapping

The field studies for the geologic map of the excavated areas associated with the closures and VCA was conducted in July 2001 after the majority of contamination excavation was complete. The map area includes the areas excavated as part of the MDA P and Flash Pad 387 closures, the VCA for SWMU 16-016(c)-99, and all support areas, collectively referred to as the "area of contamination" in the MDA P closure plan (LANL 1995, 58713). The geologic map was revised in March 2002 to include excavations required for removal of localized areas of elevated contamination (LANL 2003, 76054). The objectives of the map are to delineate bedrock units of the Bandelier Tuff, unconsolidated and undisturbed units exposed during excavation, and locations of boreholes and detailed fracture studies.

The geologic map was compiled on a 1:1,200 scale base map displaying 2-ft contours and the grid cells established for the Phase II sampling efforts. The grid cell centers had been previously surveyed to establish the basis for the Phase II sampling campaign. The grid cell markers provided location control across the project site. Project personnel collaborated with personnel from the Laboratory Seismic Hazards Program to compile and evaluate the stratigraphic data. Data from the field map were digitized using methods described in Lewis et al. (2002, 73785) to create the final map.

For the MDA P Site, five general mapping units have been established, including bedrock, unconsolidated deposits, undisturbed deposits, alluvial deposits, and post-excavation units emplaced for erosion control. The excavations of the waste materials, as well as areas locally used for decontamination and materials staging, resulted in exposure of bedrock Units 3 and 4 across the project site. Some bedrock outcrops were locally exposed prior to the excavations along the ephemeral drainages on the eastern and western margins of MDA P, and locally at the toe of the east lobe of MDA P. Unconsolidated units consist of soil, alluvial and colluvial sediments, and gravels or fill materials used during the remediation or placed afterward for erosion stabilization. The inefficiency of removal of all of the unconsolidated materials on the

steeper, bedrock slopes resulted in residual, thin veneers of mixed soil, sediment and older fill. The geologic map is provided as Plate 1.

2.3 Unconsolidated Deposits

Unconsolidated deposits are mapped where the thickness obscures the ability to identify the immediately underlying bedrock unit. These deposits generally include gravels and fill materials placed to support the remediation, fill materials existing in the area prior to remediation, and residual materials on the steeper, south slopes of Cañon de Valle on the footprint of the former waste pile. The latter could not be removed by conventional excavation equipment due to access limitations. Thicknesses range from a few inches (5 to 20 cm) on the steep, north slope of the MDA P footprint to approximately 6 ft (2 m) on the slopes south of the MDA P footprint leading to Flash Pad 387. Thicknesses of the residual and placed soil at the flash pad are approximately 1 ft (30 cm). Similar thicknesses remain at SWMU 16-016(c)-99. A layer of crushed gravel covers the area used for the support facilities, parking and haul roads.

Undisturbed deposits consist of soils and colluvium on the slopes adjacent to the remediation project. Colluvium is defined as coarse- to fine-grained materials that have been weathered from the bedrock, but have not been transported far by natural hillslope processes. They typically consist of angular rocks that rest near the angle of repose on the bedrock slopes. These areas are generally vegetated with Ponderosa pine and white fir and may have a heavy mantle of needle litter. Portions of these areas were affected by the Cerro Grande Fire in May 2000.

The alluvium along the Cañon de Valle stream is divided only where the surface height indicates that an older terrace exists above the active streambed. No effort is made to differentiate geomorphic deposits in this area. The alluvial materials at the immediate toe of the waste pile footprint were partially excavated to remove materials where the waste pile talus lapped onto the terrace. The area was generally re-graded and stabilized after excavation to facilitate runoff and prevent ponding of water on the terrace surface.

The post-excavation deposits depicted on the map (Plate 1) include riprap and reclaimed soils. The riprap consists of coarse rock and boulders placed along active stream courses to slow water velocities and create an environment for deposition of sediments. The reclaimed areas include areas reseeded to control surface erosion. Some soil was placed and reseeded to prevent ponding of water at the flash pad, as the area was excavated below the adjacent grade and would not have had an outlet for overland flow.

2.4 Bedrock Stratigraphy

Field and laboratory methods were used to delineate the stratigraphy of the Tshirege Member of the Bandelier Tuff at MDA P. The outcrop at MDA P exposed by the excavations provides excellent exposures in terrain that is normally covered by soils and colluvium that would make mapping and identification of individual units impractical. Lewis et al. (2002, 73785) employed physical and textural characteristics of measured sections at outcrops and cores at MDA P and other TA-16 localities, petrographic variations of MDA P and other TA-16 samples, as well as major and trace element geochemistry by whole-rock x-ray fluorescence (XRF) analysis for unit identification and correlation. Stratigraphic thicknesses were determined from the MDA P cores, a measured section north of MDA P in Cañon de Valle, and map patterns of outcrop in adjacent areas of TA-16 (Figure 2.4-1). The stratigraphy of the Tshirege Member of the Bandelier Tuff at MDA P reported by Lewis et al. (2002, 73785) differs in detail from that reported by Broxton et al. (1996, 54948) in that both Units 3 and 4 are now subdivided. The reader is referred to Lewis et al. (2002, 73785) for complete descriptions and discussions. Tshirege Member stratigraphic units exposed at MDA P include Units 3, 3T, and 4l, from bottom to top, respectively.

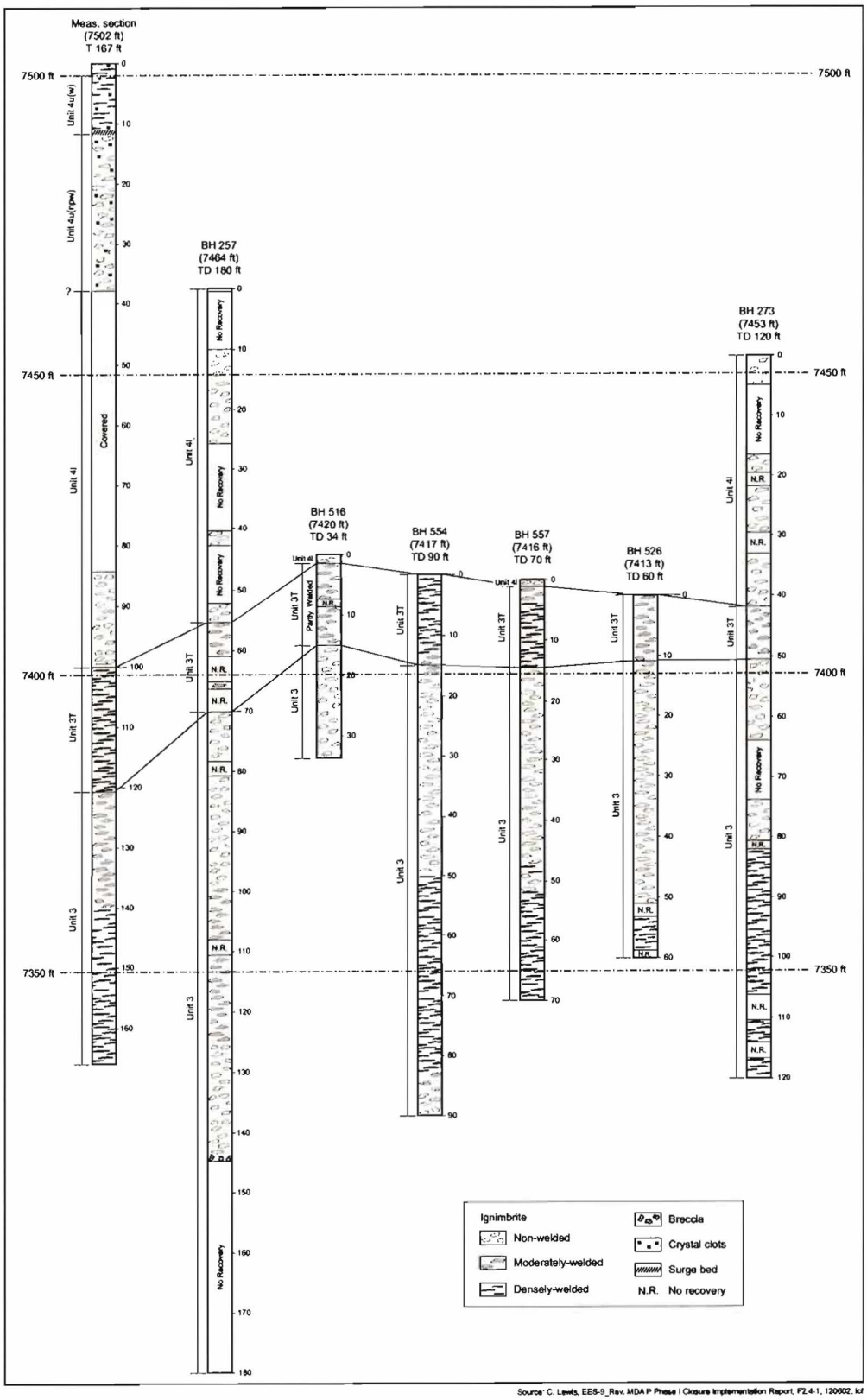

Source: C. Lewis, EES-9_Rev. MDA P Phase I Closure Implementation Report, F2.4-1, 120602. icf

Figure 2.4-1. Stratigraphic and lithologic correlations of boreholes at MDA P, Flash Pad 387, and measured section north of Cañon de Valle (modified from Lewis et al. 2002, 73785)

Unit 3 is the lowest member of the Bandelier Tuff exposed in outcrop at MDA P. It consists of welded to partially welded tuffs that form the steep cliffs and benches of the lower MDA P footprint on the north-facing slopes of Cañon de Valle. At MDA P, Unit 3 is welded at the upper contact with Unit 3T. The degree of welding decreases downward, a partially welded zone that varies from 29 to 39 ft thick forms many of the outcrops in Cañon de Valle. This grades downward to a welded zone, over 30 ft thick in Borehole 554 that forms the lower few feet of cliff-forming outcrop at stream level. In cores 257 and 273, Unit 3 is at least 110 ft (34 m) thick, and the base is not exposed. Recovery of core below this depth was not possible, probably due to a change to partial or non-welding through this zone. Unit 3 is relatively porhyritic (30 percent crystals) and pumice-rich. It contains abundant lithic fragments, and compared to other units, contains relatively coarse crystals.

Unit 3T overlies Unit 3 at MDA P with a contact that is difficult to identify without careful examination of the textural and geochemical characteristics. The unit is typically welded from its base to its top. At MDA P, Unit 3T is the cliff-forming unit that creates the abrupt east-west break in slope across the central footprint of the waste pile. The unit is densely welded in the central portion of the waste pile footprint across Boreholes 554 and 557. Unit 3T ranges from 9 to 15 ft (5 m) thick at MDA P, and generally thins from west to east. The unit is moderately porphyritic (20 to 25 percent crystals) with bimodal crystal sizes.

Unit 4l is the highest member of the Tshirege Member exposed at MDA P. The contact with the underlying Unit 3T is sharp and is observable along the east-west break in slope across the central footprint of the waste pile. In Borehole 516 the basal portion of Unit 4l is welded. Unit 4l is generally poorly welded to non-welded, and it forms the gentle slopes that underlie the footprint of Flash Pad 387, SWMU 16-016(c)-99, and the southern slopes of the MDA P footprint. The exposed surface of Unit 4l displays local irregular topography including shallow drainages, depressions, and arroyos. Unit 4l is 42 ft (13 m) thick in core 273 and 55 ft (17 m) thick in core 257. It is pumice- and crystal-poor with rare accidental lithic fragments. A zone of coarse, subangular lithic fragments (10 to 30 cm across) is exposed near the base of the unit in the eastern part of the waste pile footprint near Borehole 526.

3.0 BOREHOLES

A total of six boreholes were drilled within the MDA P watershed in August 2001. The objectives of the boreholes were to (1) provide continuous core for sample material to investigate the potential for residual contamination in the bedrock; (2) provide continuous core for lithologic and fracture descriptions of the bedrock beneath MDA P; (3) provide open boreholes for geophysical measurements; and (4) provide open boreholes to measure water levels. All boreholes were dry with no water observed during or after drilling. All boreholes were filled with grout and abandoned in October 2001.

Four of the boreholes were located within the MDA P footprint. These four boreholes were originally planned to be located in grid cells within the MDA P footprint that were determined to have the greatest potential for residual contamination. They were to be drilled to approximately 30-ft depth. After discussions between Laboratory and NMED personnel, two boreholes with target depths of approximately 10 ft below the level of the Cañon de Valle stream elevation, or 60 ft total depth, were drilled where local drainage may have concentrated contaminants. These two boreholes were located in grid cells 526 and 557 in the central and eastern part of the MDA P footprint, respectively. An elevational survey error resulted in the target depth for Boreholes 526 and 557 not achieving the objective of 10 ft below the level of the Cañon de Valle stream.

Two additional boreholes, 516 and 554, were drilled once the increased fracture density on the western side of the waste pile footprint was recognized. The objective of Borehole 516 was to examine the potential for coring within the fracture zone. Borehole 554 was located adjacent to a potential bounding fault, and

cored to a total depth of 100 ft. Although Boreholes 526 and 557 did not reach the depth target, together the group of four boreholes in this region accomplished the overall objectives. The results of the contaminant sampling are beyond the scope of this report.

Two boreholes were located outside the MDA P footprint. These two boreholes were located in grid cells that were determined to have the least potential for residual contamination from MDA P operations, to provide further evidence of whether or not there was contamination at depth below the MDA P Site. Borehole 273 was located in a grid cell adjacent to Flash Pad 387, and Borehole 257 was located on the far southwestern, upgradient corner of the project site. These boreholes had original target depths of 170 ft to try to exploit geophysical tools to investigate the fracture regime within the bedrock.

3.1 Drilling Methods and Collection of Core

All boreholes were drilled with a small trailer-mounted diamond-coring rig, fitted with compressed air for cuttings removal, using an NQ-sized coring bit and rods to drill 4-in. boreholes and recover 2.5-in. core. An alcohol-based drilling foam was used in the deeper parts of some boreholes to facilitate core recovery. A small pump was plumbed into the air line and intermittent water bursts were introduced into the airstream for dust suppression. The core barrel was decontaminated with an Alconox solution and rinsed with dionized water between core runs. The cores were rinsed with dionized water to remove cuttings and other drilling debris before placed in core boxes. The core retrieved was boxed and labeled with borehole number and depths at the time of recovery.

For each borehole, a borehole summary log was compiled (Appendix A). Table 3.1-1 provides a summary of the boreholes, dates, locations and depths of each. Continuous core was not extracted from all boreholes to the total depths drilled. The initial depth represents the depths drilled and the final depths represent the depths of the open boreholes (Table 3.1-1). No recovery was possible from Boreholes 257 and 273 below approximately 144- and 120-ft depths, respectively. Drilling continued in both of these holes to a target depth of approximately 170 ft. The boreholes remained open, but no core was recovered at these lower depths. It is believed that the non-welded and unconsolidated nature of the rocks in this zone contributed to no recovery, as the compressed air simply blew the drill cuttings and unconsolidated core out the stack.

Table 3.1-1
Summary of Boreholes at the MDA P Site

Borehole Number	Surface Elevation[a]	Initial Depth[b]	Final Depth[c]	Drilling Method	Completion Date
257	7467.8	180.0	158.7	Air/water-foam	8/23/2001
273	7452.8	170.0	145.8	Air/water-foam	8/15/2001
516	7423.5	33.7	32.0	Air/water-foam	8/27/2001
526	7420.6	59.4	59.4	Air/water-foam	8/1/2001
554	7422.2	100.0	96.5	Air/water-foam	8/29/2001
557	7419.4	69.5	69.5	Air/water	8/2/2001

[a] elevation mean sea level (msl).

[b] Depth below ground surface (bgs).

[c] Depth bgs.

3.2 Field Screening and Sampling and Sampling of Core

Once the cores were boxed, they were moved to an on-site storage facility. Each core was visually examined for occurrences of fractures and obvious staining that might indicate residual contamination. Each

core was then field-screened for metals contamination with a field XRF instrument, and for radiological contamination with a beta-gamma counter. Elevated concentrations of barium identified in shallow fractures were recorded in a logbook and marked for laboratory analyses. No radiological readings above background were observed, and the cores were freely released for unrestricted use. The logbooks and radiological release forms are archived in the RRES-RS Records Processing Facility.

3.3 Lithologic Descriptions of Cores

For this study, a summary log form was created to document the lithologic and structural characteristics of each core. The log form includes depth, lithologic characteristics, and natural and induced fracture characteristics. The lithologic characteristics included the estimates of pumice, lithic and crystal contents, crystal size, and degree of welding. These estimates were made according to standard practices. The lithologic characteristics, when combined with geochemical data, are indicative of individual members and units of the Bandelier Tuff, as described in section 5.0. The fracture characteristics of the cores were also recorded on the summary log form. The methods and results are described in section 6.0. The completed summary log forms for each core are included in Appendix A.

4.0 FRACTURE CHARACTERIZATION

As part of site characterization after completion of waste pile removal activities, an investigation of the fracture regime was conducted. The fractures were investigated by surface mapping, investigation of borehole cores, and in-situ observations of fractures within boreholes.

Initial inspection indicated that a zone of open and filled fractures is present on the west side of MDA P that is not apparent on the east side. This observation prompted personnel from the Laboratory's Seismic Hazards Program to collaborate with the investigation of the fracture regime at the MDA P Site. The objectives of the investigation from the perspective of seismic hazards was to identify patterns in orientation, density and aperture that may indicate their mode of formation, either as the results of cooling and contraction of the tuff, or as the result of tectonic influences, such as faulting or folding. These objectives overlap with the objective of this study to define the vertical and lateral variations in the frequency and distribution of fractures as they affect the potential to transmit groundwater in the bedrock.

In this report, fracture refers to any break or physical discontinuity in the rock caused by stresses that exceed the rock's physical strength. This definition includes the terms fault and joint. A joint is a fracture whose opposing faces have demonstrable opening without shear. The Bandelier Tuff was formed from a series of hot, ashflow tuff deposits that exhibit various degrees of compaction and welding after emplacement. Contraction of the welded deposits upon cooling produced tension fractures, called cooling joints. The non-welded to partially welded units typically do not exhibit cooling joints, because they did not experience the thermal stresses upon cooling. Lewis et al. (2002, 73785) discuss the methods used to distinguish joints with random and preferred orientations, as they relate to the abilities to distinguish cooling joints from those that may have tectonic origins. At least part of the fractures observed at the MDA P Site are interpreted to have likely resulted from tectonic reactivation of cooling joints (Lewis et al. 2002, 73785).

4.1 Methods of Surface Measurements

The surface fracture mapping was conducted in August 2001. Personnel from the Laboratory's Seismic Hazards Program conducted much of the fieldwork, and led the analysis and reporting efforts. The exceptional exposure of the bedrock units as a result of the excavations at the MDA P Site provided the opportunity to measure a large number of fractures in three-dimensions. Eight traverse lines were established within the footprint of MDA P. Two long east-west traverse lines were established on the gently sloping surface of non-welded Unit 4I, and three shorter lines on Unit 3T and Unit 3. This surface has been scraped

clean during the excavations. Compressed air was used to clean surface debris so that each fracture could be examined for orientation and trace length. Three orthogonal north-south traverse lines were established that extended across the east-west lines. In all cases, location control was established by the utilization of a set of 30-ft grid center markers that had been surveyed according to the methods described in section 2.1. Compressed air was used locally to clean the fracture exposures, but the veneer deposits on the steeper, north slope of the waste pile footprint were too thick for this method.

The study located and measured 454 fractures and small faults along the 8 traverses that covered 1891 ft (576 m) of exposure. Data collected for each fracture included distance along traverse, strike, dip, trace length, aperture, and characteristics of the fracture terminations and the materials filling the fracture aperture. Strike and dip were measured to an accuracy of ±2° with a Brunton compass. Fracture apertures were measured perpendicular to the fracture faces. The surface fracture data are included in Appendix B. Rose diagrams were plotted to determine preferred orientations. Classes of 10° intervals were established, and mean strikes with 95% confidence intervals were calculated (Lewis et al. 2002, 73785).

4.2 Results of Surface Measurements

A structural analysis of the surface fractures measured at MDA P was performed by Lewis et al. (2002, 73785). They performed a statistical analysis of preferred directions, apertures, and fracture density. The reader is referred to Lewis et al. (2002, 73785) for analysis methods and discussions. In summary, these analyses indicate that the fracture set, as a whole, has a statistically significant north-northwest preferred orientation of N15W±26° (Figure 4.2-1). Fracture dip angles vary from sub-horizontal to steep. The data set as a whole was interpreted to have been derived from a population of fractures with preferred orientations. A schematic representation of the measured fractures is shown on the geologic map (Plate 1).

Fracture trace lengths were measured where the exposures allowed. The trace lengths were best exposed on the Unit 4l outcrops. Most fractures were observed to terminate at other fractures, indicating that a polygonal pattern is present, suggesting that the nonwelded Unit 4l was influenced by thermal fracturing during cooling and contraction of the welded units.

The fracture density and apertures measured at MDA P were observed to vary across the footprint. Table 4.2-1 summarizes fracture density measured at MDA P. Fracture density within units 3 and 3T is higher than in Unit 4l. From east to west fracture densities in Units 3 and 3T vary from 20 fractures per 100 ft (approximately 30 m) to 40 fractures per 100 ft (Table 4.2-1). There are also larger apertures in Units 3 and 3T than in Unit 4l. Apertures exceeding 20 mm in Units 3 and 3T are dispersed throughout the east and west side of the footprint whereas apertures in Unit 4l that exceed 20 mm are located on the west side of the footprint only (Figure 4.2-2). Apertures in Unit 4l are generally 1 to 2 mm, with only seven fractures reaching values between 20 mm and 50 mm. The largest recorded aperture in Unit 4l is 50 mm. Apertures recorded along traverse lines in Units 3 and 3T reach values of 10 cm in the western part but larger apertures are observed. No consistent spatial variation was apparent in the statistical analyses of aperture, but as noted by Lewis et al. (2002, 73785) examination of the outcrop indicates that higher fracture apertures are present in the western parts of the MDA P footprint compared to the eastern parts. The higher aperture values in the western part of MDA P suggest post-cooling extension in this area. A small graben on the north side of Cañon de Valle appears to line up with the zone of high apertures and high fracture density, but no major faults were identified to be associated with the fracture zone in the western part of MDA P. Small faults with minor displacements were observed and are shown on the map (see Plate 1). The spatial association of a series of small faults and a small amount of horizontal extension appear to indicate that a zone of diffuse structural deformation is present in the western part of MDA P, possibly related to deep-seated normal faulting that is not expressed as any significant stratigraphic offset at the surface (Lewis et al. 2002, 73785).

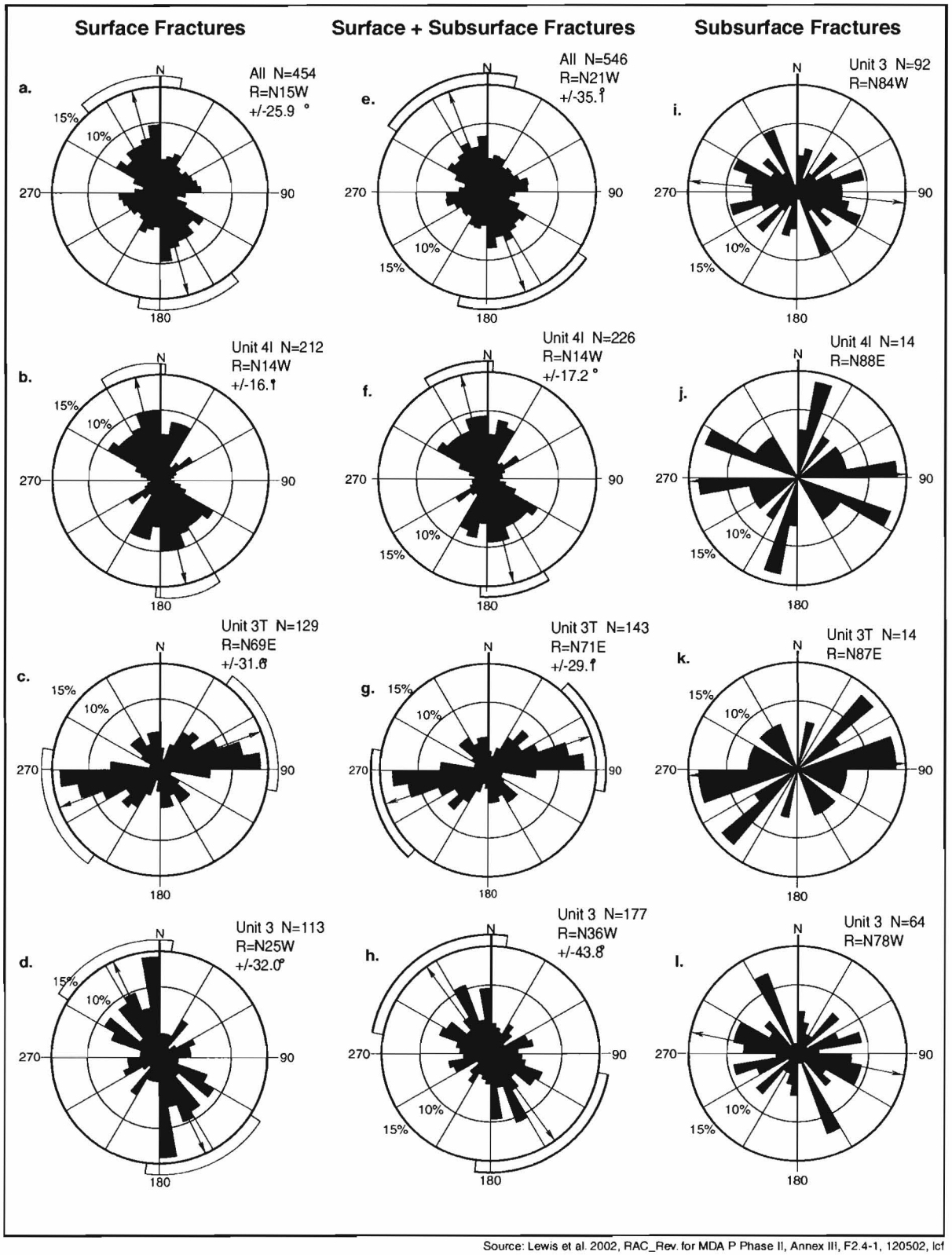

Source: Lewis et al. 2002, RAC_Rev. for MDA P Phase II, Annex III, F2.4-1, 120502, lcf

Note: Surface fracture data from Lewis et al. (2002, 73785); orientations of subsurface fractures interpreted from borehole optical televiewer log

Figure 4.2-1. Orientations of surface and subsurface fractures

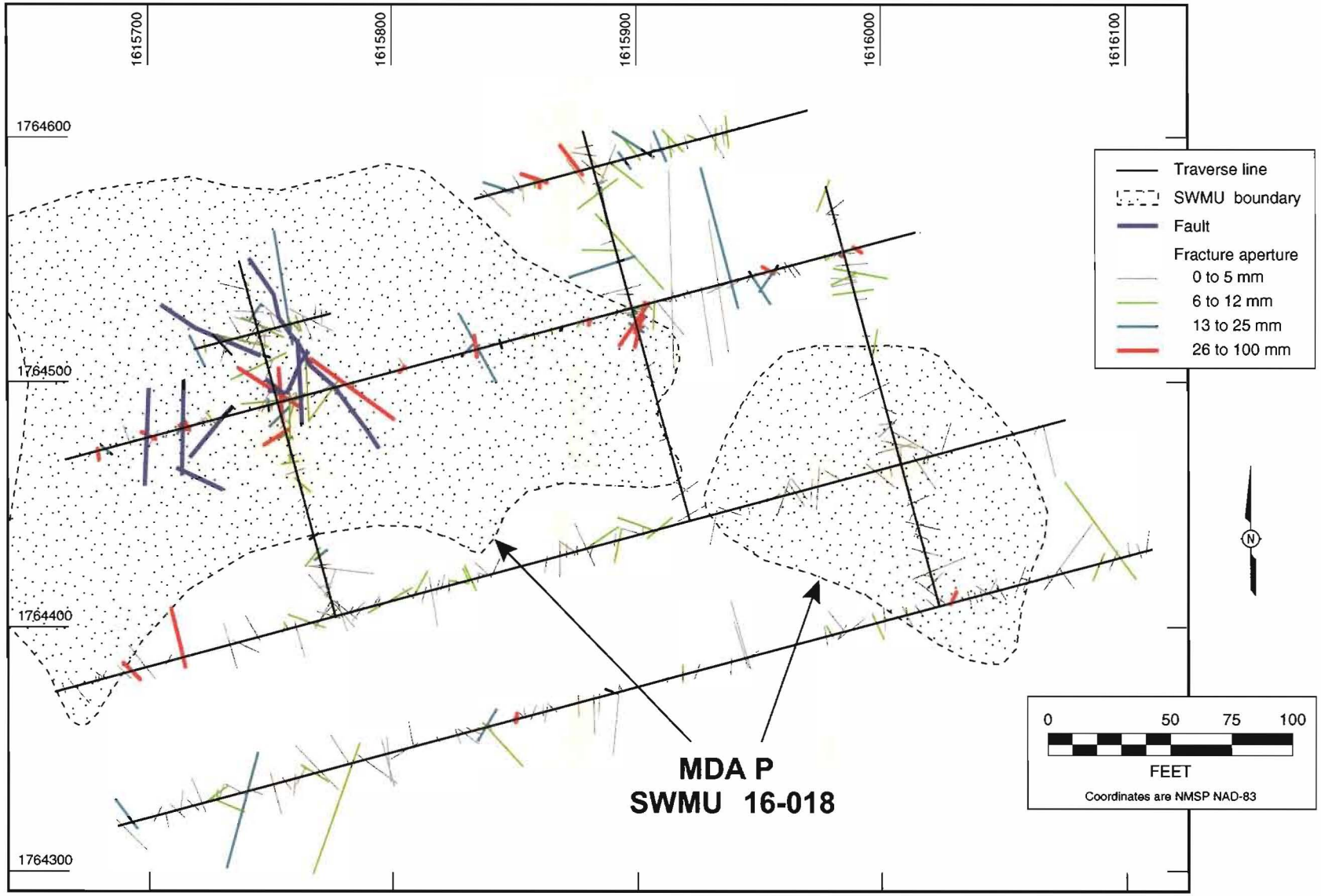

Sources: Fault, fracture & traverse lines, R. Channell (EES-9), 050802_Map R000001, MO, 111202_Rev. for MDA P Annex III, Phs II; 012603; cf

Figure 4.2-2. Map view of fracture apertures measured along traverses at MDA P (see Plate 1 for locations)

Table 4.2-1
Summary of Surface Fracture Density Measured at MDA P

Traverse Number	Orientation of Traverse	Fracture Density Number/ 100 ft	Stratigraphic Unit
1	N78E	20.7	4I
2	N77E	18.5	4I
3	N14W	17.4	4I/3T
4	N20W	18.8	4I/3T/3
5	N12W	26.7	4I/3T/3
6	N76E	31.1	3T/3
7	N78E	29.9	3
8	N80E	40.4	3

Note: Table extracted from Lewis et al. (2002, 73785)

4.3 Methods of Observations of Fractures in Core

Characteristics of fracture occurrences were recorded in the continuous cores from the 6 boreholes. The cores were examined for the presence and character of natural fractures, including frequency, dip, length, rubble zones, staining, and fracture-filling materials. Induced fractures were also examined, but are attributed to breakage during drilling and handling. The descriptions of the cores were made entirely by hand-specimen identification in a non-destructive manner. Information was recorded on the prepared logging forms in general accordance with Kulander et al. (1990, 73718).

Natural fractures are defined as those fractures that existed in the rock prior to drilling. They exhibit diagnostic characteristics, including irregular, open apertures that typically show evidence of solution dissolution and precipitation of minerals, such as staining, clay deposition and manganese oxide formation. Cataclastic zones are areas of fine-grained, granulated rock produced along fractures by shear forces. Secondary minerals, such as clays, oxides or gypsum may coat the fracture surface indicating eluvial transport of dissolved or suspended materials within the fracture system. In this study, rubble zones are considered indirect evidence of the presence of a fracture. Rubble in core is interpreted as evidence that a natural fracture is present, but the fracture itself is not visible in the core. The drill stem may have intercepted a nearby vertical fracture, but only rock fragments were recovered. This approach is considered conservative and is supported by the spatial relationships of the rubble zones to observed fractures.

Fractures that developed during drilling, coring, or handling are referred to as induced fractures. The induced fractures do not contribute to the understanding of the potential bedrock groundwater pathways, but are common in the cores recovered for this study. Induced fractures typically exhibit regular geometric relationships to the core. Because they may extend beyond the rock yet to be drilled, they may be present in the borehole wall. Coring induced fractures may develop anywhere along the core barrel, but typically form near the drill bit where pressures are the greatest.

Three types of induced fractures are recognized: disc fractures, torsion fractures, and petal-centerline fractures. Disc fractures are the most abundant induced fractures observed followed by torsion fractures. Disc fractures are coring-induced fractures that are recognized to be most prevalent in fine-grained rocks (Kulander et al. 1990, 73718) and are common in the non-welded parts of the MDA P cores. They primarily form in response to a vertically acting principal tension and are generally horizontal to subhorizontal in vertical cores. Torsion fractures are typically found at the base of the core runs. They typically develop when the driller twists off the core prior to extracting it from the borehole, but may develop when core fragments

are loose in the core barrel. Petal-centerline fractures are coring induced fractures that possess distinct morphologies that relate to the core axis. They have been observed to originate near the core boundary with vertically downward propagation paths parallel to the core axis. The surface morphology resembles a petal in the area of origin with fine, thin ridges that may curve to meet the core boundary or a pre-existing fracture. The fine ridges are referred to as hackle plumes. Arrest lines, or rib marks, may form closely spaced, concentric downcore arcs. The latter, in most cases indicates the direction of propagation, as the curvature is convex in the direction of propagation (Kulander et al. 1990, 73718). Hence, fractures induced by drilling typically possess features related to drilling stresses at the drill bit, core barrel, and core retrieval mechanism as well as core handling and boxing.

The fractures attributed to drilling are the most common type of fracture observed in the cores. It is possible that natural fractures with no evidence of staining or mineralization may have been interpreted as fractures induced by drilling, although it is unlikely, due to differences in morphology and texture. This does not change or alter the interpretations presented below.

4.3.1 Results of Observations of Fractures in Core

Natural fracture and rubble zones are present in all MDA P cores examined. Natural fracture and rubble zones are commonly associated with welded zones, as anticipated, although both are present in the partially welded Unit 4l and the upper, partially welded segment of Unit 3. Many fractures are high-angle, but subhorizontal fractures are very common in the upper parts of boreholes, probably due to weathering and unloading.

Fracture coatings consist of clays and manganese oxides that coat the fracture surfaces. Descriptions of selected fractures observed in cores are provided in Appendix B. These descriptions follow the hand lens methodology of Birkeland (1984, 44019) for the occurrences of clays and oxides on the fracture walls. Thickness, structure, luster, and Munsell color of clays are provided when observable. All clays were dry when inspected. Clays tend to be more common and thicker with darker hues on the west side of the MDA P footprint than on the east side. In the core from Borehole 526, colors range from 5YR 6/4 to 5YR 5/8 through the entire depth to 44 ft. In core from Boreholes 516 and 554 colors range from 5YR 3/3 to 5YR 3/4 at the 28- and 37-ft depths, respectively. Thicknesses of clay films or accumulations are also greater on the west side of the MDA P footprint than on the east side. Most clays are <1 mm in core from Borehole 526 (Photograph 4.3-1), with the greatest thickness of 5 mm at a depth of 28-ft. In Boreholes 554 and 557, thicknesses range up to 16 mm at the 75-ft depth (Photograph 4.3-2), and up to 15 mm at the 65-ft depth, respectively. Some of the variation may be due to sampling bias, as there are more and deeper boreholes on the west side.

The occurrence of manganese oxides appears to vary with depth. In the core from Borehole 526, these oxides are absent or have few occurrences at all depths. On the west side, in cores from Boreholes 554 and 557, oxides are more prevalent, exhibiting very few to few occurrences until the 75-ft depth in 554 where the material coating is continuous and has a measurable thickness. In core from Borehole 273, the oxides are absent until the 62-ft depth, becoming more common at the 116-ft depth.

Photograph 4.3-1. Natural fracture in core from Borehole 526 at 36.5-ft depth (center row of core)

The fractures that appear to be capable of conducting the largest volumes of water, as determined by the measurements of the heat pulse flowmeter (HPF) (discussed below) appear to have weak clay and manganese oxide accumulations, e.g., the fractures in Borehole 526 at 43- to 46-ft depths. The patterns of fracture density and apertures observed in the subsurface are similar to those in surface measurements. The darker colors of the clays observed suggest that these are translocated from surface soils, consistent with other studies (Vaniman and Chipera 1995, 54709). The larger fracture apertures on the west side would allow transport of these materials either as suspended or colloidal particles, whereas the fewer, tighter fractures on the east side may inhibit material transport.

Photograph 4.3-2. Natural fracture in core from Borehole 554 at 77.3-ft depth (top row of core)

4.4 Methods of Measurement of Fractures in Boreholes

Orientations of apparent fractures were made in the boreholes using Optical Televiewer, an Advances Logic Technologies OBI-40 Optical Televiewer Probe, Serial Number 2710. Optical borehole imaging (OBI) technology is based on direct optical observation of the borehole wall face. Precise measurements of dip angle and direction of bedding and joint planes, along with other geological analyses, are possible in both air and clear fluid filled boreholes. A ring of small lights illuminates the borehole wall, allowing a camera to directly image the borehole wall face. A conical mirror housed in a clear cylindrical window focuses a 360° optical "slice" of the borehole wall into the camera's lens. As the OBI probe is lowered down the borehole, the raw analog video signal from this camera is digitized and transmitted via wireline to the surface instrumentation. Orientation measurements are based on magnetic north and must be corrected for declination. Repeat logging of the Optical Televiewer is typically impractical due to the turbidity caused by logging down the borehole, or because the optical window becomes coated with mud when it reaches the bottom of the borehole.

The digitized signal captures 180, 360, or 720 pixels around a 1 mm ring from the conical image. The rings are stacked and unwrapped to a 2-D image of the borehole wall. A digital fluxgate magnetometer is used to determine the orientation of the digital image. The OBI image is an oriented, 2-D picture of the borehole wall unwrapped from north to north. Planar features that intersect the borehole appear to be sinusoids on the unwrapped image. To calculate the dip angle of a fracture or bedding feature the amplitude of the sinusoid (h) and the borehole diameter (d) are required. The angle of dip is equal to the arc tangent of h/d, and the dip direction is picked at the trough of the sinusoid.

4.4.1 Results of Measurement of Fractures in Boreholes

The OBI images generally appear to have a coating of fine drilling residues on the borehole walls. No attempt was made to mitigate this situation before the images were obtained due to the potentially large volumes of water that may have been needed to rinse the interior walls after drilling. The image in Borehole 273 has an image anomaly along the length of the images that partially block the view. Nonetheless, the images provide an in-situ view of the natural fractures. Sinusoidal features, interpreted as planer fracture surfaces that intersect the borehole walls were picked throughout boreholes by visual inspection of the digital images using interactive software. The software performed the orientation calculations and assigned depths to the fractures or bedding features at the inflection points (middle points) of the sinusoids.

The fracture tables for the five boreholes at MDA P are in Appendix C. The OBI images and fracture projections are included in the geophysical summary plots in Appendix D. Figure 4.4-1 provides a summary of the fractures in the surface measurements of Lewis et al. (2002, 73785), subsurface measurements from boreholes in this study, and the combined data sets. The subsurface borehole fracture data from the OBI was not available to Lewis et al. (2002, 73785). The fractures observed in the vertical borehole walls are biased toward subhorizontal orientations due to the low probability of intersecting more than one high-angle fracture in a borehole.

The orientations of fractures in Units 4I and 3T are largely unchanged or shifted slightly eastward, despite the low number of borehole fractures encountered. Most of the fractures measured in the boreholes were in Unit 3 due to stratigraphic thicknesses. The inclusion of subsurface fracture data in the entire data set appears to shift orientations of the preferred orientations in Unit 3 slightly westward from the surface measurements.

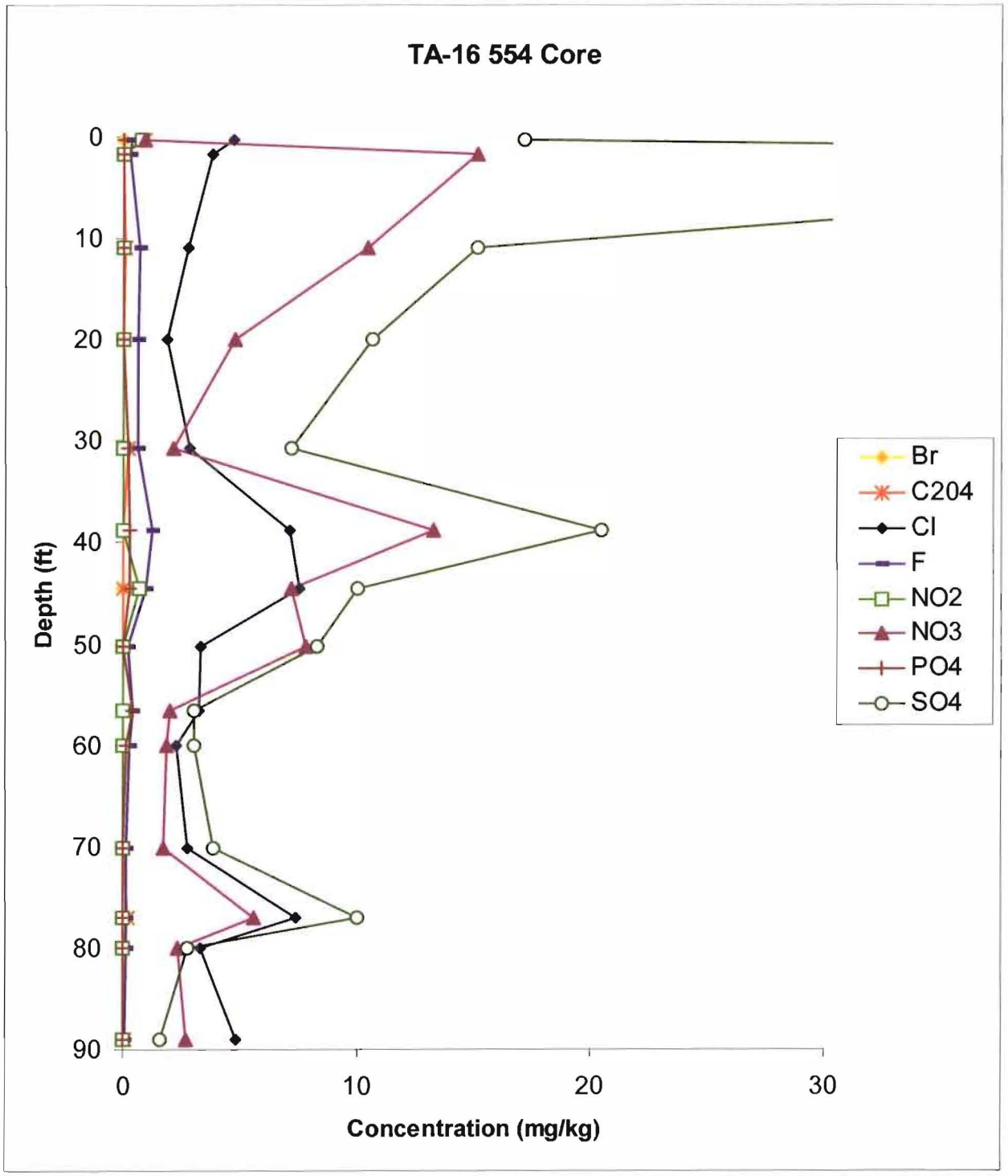

Figure 4.4-1. Plot of anion concentrations in core samples from Borehole 554

5.0 BOREHOLE GEOPHYSICS

A borehole geophysical investigation was conducted in the boreholes at the MDA P Site. Borehole geophysics provide measurements of the physical properties of the rocks and the fluids within them and have been successfully used to identify characteristics of flow in fractured bedrock, including alteration of the rocks as a result of those flows (Criswell and Bray 1994, 37382). Geophysical logs consist of the measurement of physical parameters plotted against depth. These data are used at MDA P to collect information concerning the lithology, porosity, conductivity, moisture contents of the rocks, and to identify any fluids in the boreholes. These data are used to identify characteristics of the fractures flow system, including specific zones of moisture and magnitude of flow associated with fractures and rubble zones observed in cores. Table 5.0-1 summarizes the geophysical logging suite performed in each borehole. The geophysical measurements were performed by Colog Geosciences, Inc., of Golden, Colorado, a Division of Layne-Christiansen Company.

Table 5.0-1
Summary of Borehole Geophysical Logging Suite

Type of Log	Borehole No. 257	Borehole No. 273	Borehole No. 516	Borehole No. 526	Borehole No. 554	Borehole No. 557
Caliper	X	X	—*	X	X	X
Natural gamma	X	X	—	X	X	X
EM conductivity	X	X	—	X	X	X
Optical televiewer	X	X	—	X	X	X
Neutron	X	X	—	X		X
HPF	X	X	—	X	X	

*— = no geophysical logging performed.

The borehole geophysical measurements performed included natural gamma, caliper, electromagnetic conductivity, neutron, HPF, and optical televiewer. The locations of the boreholes in which geophysical measurements were made are shown on Plate 1. With the exception of the HPF, the geophysical logs furnish a continuous digital record of the borehole conditions. The continuous logs were obtained by lowering the instruments into the boreholes to about 30-ft from the bottom, the lower 30-ft were logged as a quality check, and the borehole was logged completely from bottom to top to ensure constant speed and cable tension. The HPF measurements were conducted at selected depth intervals, and the results recorded digitally.

The measurements were performed September 10–12, 2001, in this order: caliper, optical televiewer, natural gamma, and electromagnetic induction. Due to the national events of September 11, 2001, the remaining measurements were not performed until October 1, 2001. The tool carrier for the neutron log was due to be shipped to the site on September 11, 2001, but all shipments were grounded. The second round of measurements were performed in the order of neutron and HPF. The neutron logs were run before the HPF, because the latter requires that the boreholes be filled with water and the neutron logs were planned for the boreholes in their natural state after boring. This tactic was to try to observe any natural water that may have been flowing through the fractures. Although planned, the neutron log was not performed in Borehole 554, because it was inadvertently filled with water before the test could be performed.

Additional measurements for the full-waveform sonic (FWS) log were planned in the deeper boreholes to investigate the fracture system. The FWS tool consists of a small diameter sonic probe that is approximately 10 ft long. The equipment is used to generate compression, shear and tube waves in a fluid-filled

borehole. The tube wave is a low frequency, broadband event that travels along the borehole wall at a predictable velocity close to that of the speed of sound in water. Tube wave energy is attenuated by fluid interaction between the borehole and the adjacent formation. Because permeable fractures or porous media provide a pathway for this interaction, these conditions reduce the energy of the transmitted wave, resulting lower energies in fractures rock. Boreholes 257 and 273 were drilled to depths of 180-ft to exploit this technique, but due to conditions at approximately 144- and 120-ft depths, respectively, would not hold water. The other boreholes did not have the depth to exploit the tool. These measurements were not performed.

5.1 Natural Gamma

The natural gamma log is a continuous record of the natural radioactivity of the formation. The radioactivity emanates from naturally-occurring uranium, thorium and potassium. Natural Gamma measurements were made at MDA P with a Mount Sopris Instruments HLP-2375/S Stratigraphic Gamma Probe, Serial Number 2022. Gamma radiation is measured with sodium-iodide scintillation detectors. The natural gamma log (also known as gamma or gamma ray log) provides a measurement recorded in counts per second that is proportional to the natural radioactivity of the formation. The depth of investigation for the natural gamma log is typically 10 to 12 in. Instrument calibration is performed with a source of known activity. All measurements at MDA P were made in dry, open boreholes.

5.1.1 Results and Discussion of Natural Gamma Logs

The natural gamma logs for the five boreholes at MDA P are shown in the geophysical summary plots in Appendix D. These data indicate little variability through Units 3 and 3T. Larger variations are observed between Units 4I and 3T in Boreholes 257 and 273. A marked increase in natural gamma activity occurs at 54- to 55-ft and 44- to 45-ft depths, respectively, that correlate with the lithologic changes from Unit 4I to 3T. This increase probably reflects the slight increases in uranium, thorium and potassium across the contact, but is interpreted to be due to the change in density due to welding in Unit 3T. In contrast, little or no change is observed at the contact of Unit 3T with Unit 3 in any boreholes. The lithologic changes from Unit 3T to 3 includes a slight increase in crystallinity and phenocryst contents with the latter being more porphyritic (Gardner et al. 2001, 70106; Lewis et al. 2002, 73785).

5.2 Caliper

The caliper tool measures borehole size and shape and provides a continuous record of the average borehole diameter determined by the extension of three spring-loaded arms. Caliper measurements were made at MDA P with a Mount Sopris Instruments CLP-2380 3-Arm Caliper Probe, Serial Number 2065. The measurement of the borehole diameter is determined by the change in the variable pot resistors in the probe, which are internally connected to the caliper arms. One important application of the caliper measurement is to identify intervals where rough borehole walls or washouts could have introduced large errors into such logs as neutron porosity and other measurements where log response is affected by borehole enlargement. All measurements at MDA P were made in dry, open boreholes.

Calibration of the probe was performed in the shop prior to commencement of logging operations. Calibration standards consist of rings of known diameters that are placed over the extended arms as the probe response at these diameters is recorded. Additionally, as with other geophysical measurements, a repeat section is collected and compared with original logs for consistency and accuracy. The stable caliper probe usually does not require frequent calibration, unless repeat logs show deviation from initial logs, or if measured borehole diameters do not match known drill bit sizes.

5.2.1 Results of Caliper Logs

The caliper logs for the five boreholes at MDA P are shown in geophysical summary plots in Appendix D. These data indicate that open borehole diameters generally range from just over 4 to over 8 in. The boreholes were cored with a diamond-tipped bit that had an outside measurement of a nominal 4-in. diameter. The borehole diameters in the nonwelded Unit 4I in Boreholes 257 and 273 are generally larger than the welded tuffs and taper to the contact with Unit 3T, a common phenomenon interpreted to be enlargement caused by drill steel whip. General downward increases in borehole diameters are observed in the partially welded Unit 3. This may be attributed to a general decrease in welding characteristics with depth, but this was not observed in the hand-specimen inspection of the core. Local borehole enlargement is apparent near fracture and rubble zones observed in all cores and local diameter peaks are superimposed on the general trends. Local borehole enlargement is interpreted to be due to local weathering at the rocks near fractures. The maximum diameters observed in Boreholes 526, 554 and 557 in Unit 3 are associated with fracture zones at 35- to 40-ft depths. In Borehole 257, local peaks are common in the nonwelded Unit 4I, but loss of core recovery in this unit limits correlations. In all boreholes, caliper diameters increase at observed fracture and rubble zones associated with increases in EM conductivity, discussed below.

The largest borehole diameters are measured at the 139- and 153-ft depths of Boreholes 273 and 257, respectively, where the diameters increase to over 8 in. These depths generally correspond to elevation 7314 ft above msl. An increase of less magnitude is observed at the similar elevation at the bottom of Borehole 554 (89-ft depth). A total loss of core recovery below this depth was experienced during drilling, and may be attributed to lithology rather than structural features such as fractures or cooling joints in the tuff. The rocks in this zone may consist of nonwelded tuffs and interbedded pyroclastic surge deposits. The latter are common in the Bandelier Tuff (Broxton and Reneau 1995, 49726) and could explain the loss of core recovery as they are generally poorly consolidated.

5.3 Electromagnetic Conductivity

The electromagnetic conductivity device is an induction tool that records the conductivity (inverse of resistivity) of rocks by inducing a current to flow in the rocks. In general, the induction tool signals come from deeper in the formation than those of any other borehole tool. Electromagnetic induction measurements at MDA P were made with a Mount Sopris Instruments Model EMP-2493/EM- 39 Induction Conductivity Probe, Serial Number 2033. The induction measurements are made by using a magnetic field to induce electric currents in the material being surveyed. Because the magnitude of these electric currents is proportional to the conductivity of the media being measured, the magnetic fields generated by the induced electric current are measured. The EMP-2493 probe is based upon the Geonics EM-39 probe, which is the industry standard for slimline induction probes. The probe is designed to measure formation conductivity in milliSiemens per meter. These are then converted to resistivity units.

The induction probe used contains a transmitter coil that emits a continuous wave of EM signal at 39.2 kHz, which produces a primary field in the formation around the borehole. A secondary field induced by the primary field is proportional to the conductivity of the formation and is sensed at the receiver coil located in the probe 20 in. (50 cm) from the transmitter coil. A second coil at 10 in. (25 cm) from the transmitter cancels the primary field in the vicinity of the borehole and allows horizontal focusing to reduce or eliminate borehole effects. Empirical evidence demonstrates that there are negligible borehole effects on the response for borehole diameters less than 9 in. Maximum depth of investigation is approximately 40 in. All measurements at MDA P were made in dry, open boreholes.

Calibration of the induction probe is performed by placing two loops of wire with known conductivity around the probe at a fixed distance and location. The two known values, compared to the counts per second that

they induce in the probe, provide the equation for a line. As the induction probe is temperature and humidity sensitive, this linear calibration was performed before logging in each of the boreholes at the Laboratory. Repeat logs are recorded to ensure data repeatability.

5.3.1 Results of Electromagnetic Conductivity Logs

The EM conductivity logs for the five boreholes at MDA P are shown in the geophysical summary plots in Appendix D. The depth of formation penetration tends to smooth the individual values measured and indicates that the rock matrices, not just fractures, are affecting the measurements. These data indicate that high conductivity zones of approximately 20-ft thickness occur at depths of 25 to 50 ft in all boreholes. Smaller, local zones are observed at shallower depths in boreholes 554 and 557, and at deeper depths in Boreholes 257, 273 and 554. In Boreholes 526, 554, and 557, the lower part of the zones of elevated conductivity are associated with changes of lithology, from partially welded tuff to welded tuff. In borehole 273, an upper zone of elevated conductivity is located across the contact of Unit 4I with Unit 3T, and a lower zone is located at 65- to 90-ft depths. In Borehole 257, a shallow zone of minor elevated conductivity is located entirely within Unit 4I, the deeper zone is located entirely within Unit 3. The conductivity highs in Borehole 257 are an order of magnitude less than those measured in other boreholes.

5.4 Neutron Logs

The neutron log provides a continuous record of the formation reaction to fast neutron bombardment. Rock formations absorb neutrons and attenuate fast neutrons rapidly when they contain abundant hydrogen nuclei, which are supplied by water in the geologic environment. The log is, therefore, principally a measure of the formation water content, whether it is mineralogically bound, water from crystallization, or free pore water.

Neutron porosity measurements were made at MDA P with a Mount Sopris Instruments LLP-2676 Neutron Logging Probe, serial number 2955. High-energy neutrons are generated by a 1 or 3 curie Am^{241}-Be radioactive source housed in the probe. These neutrons interact with the media that surround the probe, including any borehole fluid and formation water. The significant aspects of that interaction are the loss of energy due to collisions with hydrogen atoms and the subsequent capture of the neutrons by various nuclei (including hydrogen). The detector in the neutron probe is spaced 14 in. from the source and counts only the neutrons that have not been captured. Within a certain (unspecified) range the thermal neutron count rate is inversely proportional to the population of hydrogen atoms surrounding the probe. Therefore, for a constant borehole size, the neutron count rate can be related to total water content surrounding the probe, registering higher counts for lower water content. The inverse counts versus water content relationship can be explained in terms of the degree of neutron capture that occurs, because a lower water content captures fewer low energy neutrons and results in a higher neutron count rate at the detector.

No quantitative calibration is performed since the neutron log is a qualitative, relative measurement. However, the stability and repeatability of the neutron measurement is routinely checked by repeat logging a section of a borehole.

5.4.1 Results of Neutron Logs

The neutron logs for the 4 boreholes at MDA P are shown in the geophysical summary plots in Appendix D. Neutron log measurements were performed in Boreholes 257, 273, 526 and 557. Each of these measurements were made approximately one month after drilling completion, before the boreholes were filled with water for other measurements. These measurements were intended to measure the natural moisture contents of the boreholes. Borehole 554 was inadvertently filled with water in preparation for the

HPF tests before the neutron log could be performed, therefore no neutron measurements were made in this borehole.

Neutron logs indirectly measure the concentration of hydrogen ion in the vicinity of the borehole. It is interpreted that low neutron counts per second indicate high neutron porosity and that the hydrogen ion concentration is high. Low neutron counts are interpreted to indicate higher moisture contents. The interpretation of neutron counts for calculation of moisture content can be performed, but requires the use of calibration curves that consider the borehole diameter, as well as any liner materials.

Neutron counts are generally higher in all boreholes near observed fractures, rubble, and lost recovery zones, indicating that the fractures underlying MDA P are dry. While this may indicate areas of formation drying, neutron count data were not reproducible and are considered unreliable. The extreme and dry conditions of the boreholes were beyond the tolerance limits of the measurement instrumentation; thus, definitive conclusions of moisture at depth cannot be made based on the neutron logs.

5.5 HPF Measurements

HPF measurements were made with a Mount Sopris Instruments HPF-4293 Heat Pulse Flowmeter Probe, Serial Number 2656. The HPF is a high resolution device for measuring vertical fluid movement within the borehole. This flowmeter is based upon the proven US Geological Survey (USGS) design and works on the thermal fluid tracer concept. Borehole fluid is heated or thermally tagged by as much as 1°F with an electrical heater grid. The flow rate is determined by measuring the time between the grid discharge and the peak of the thermal pulse of water reaching an upper or lower thermistor sensor. The probe uses flow-concentrating diverters to direct fluid flowing in the borehole through the probe flow tube.

The flowmeter is calibrated in a flow chamber where flow rate can be controlled and measured. Values for response time are taken for a variety of flow rates and applied in an empirical curve-fit solution. The calibration coefficients are entered into the acquisition software to determine vertical flow rates in gallons per minute. Thermal buoyancy of the heat pulse imposes a small asymmetry on the flow calibration so that the device is slightly less sensitive to upflow than to downflow. A flow chamber calibration is performed each time repairs are made to the probe.

Presently the HPF measures flow from 0.01 to 1.3 gal./min with 0.005 gal./min resolution using a 1.125-in.-diameter flow tube and standard, multilayered flow diverter. The low-end flow limit of 0.01 gal./min is a function of the current calibration facility in which convective eddy currents as great as 0.01 gal./min are generated by differences between water temperature in the calibration device and surrounding air.

The HPF is run at discrete intervals within a borehole. Flow was measured at each interval and each test repeated until two or three measurements agree within given tolerances. The flow value was averaged from the multiple records. Time to collect flow data is subject to the flow rate and number of intervals tested. While the actual time to record a flow rate of 0.01 gal./min is less than 30 seconds, it was observed to up to 5 minutes per station for the borehole to stabilize and to obtain repeatable data. At higher flow rates, the borehole stabilizes more quickly and obtaining good data may take only a few minutes per station. Proper probe operation and repeatability is checked through the acquisition of multiple waveforms at each station.

At MDA P the HPF was used to measure flow rates in Boreholes 257, 273, 526, and 554. For Boreholes 526 and 554, water from the facility fire protection system was used to fill, or stem, the borehole with water from a 2000-gal. water truck. The flow was valved down to maintain a constant head at the top of the borehole. For these two boreholes the cumulative flow appeared to be greater than the HPF could measure, so the total flow inlet was measured by timing the filling of a 5-gal. bucket. The measured intervals were

selected upon review of the observed fractures in the cores. Three measurements were taken at each station by lowering the probe from the top to the bottom of the borehole.

In Boreholes 257 and 273, the boreholes could not be filled with water with the maximum output from the water source. The inlet flow was estimated to be approximately 10 gal./min with no evidence that the borehole was filling. Measurements were made in these 2 boreholes by metering the flow from the source down to approximately 2 gal./min, lowering the probe to the bottom of the boreholes, and withdrawing the probe and taking measurements in approximately 5-ft increments until the loss of water was identified.

5.5.1 Results of HPF Measurements

The HPF was used to measure the properties of induced water flow within Boreholes 257, 273, 526 and 557. The HPF data tables for the 4 boreholes at MDA P are included in Appendix E. Since all of the boreholes were dry, no measurements under ambient conditions were possible. All flow directions measured were downward.

What is apparent from the HPF data summary is the high flow rates observed in Boreholes 257 and 273. Flows greater than 10 gal./min were at the 7325- to 7330-ft elevation exceeded the 10 gal./min limits of our methodology. Additional measurements may have been possible with packers and other flow instruments, but this was beyond the scope of work. This loss of flow at the 7325-ft elevation in both of these boreholes suggests stratigraphic influences. This may be a layer of permeable pyroclastic rocks such as a surge or other well-sorted ash or lapilli layer that has relatively high permeability. No core recovery was possible at these depths, although the borehole remained open. The loss of core recovery is attributed to the non-welded and crystal-rich nature of the rocks in this zone. Below the 7325-ft elevation, measurements of flow were possible in both boreholes.

The HPF measures the flow properties of the boreholes and the fractures that intercept them. In Boreholes 526 and 557, flow rates decreased with depth. The flows measured by the HPF are cumulative, that is, the measurement of flow at the surface or any specific depth is an accumulation of all flows below that depth. The flow in Borehole 526 decreased much more rapidly with depth than Borehole 554. It is possible that the flow in Borehole 554 was influenced by whatever lithology is present at the 7325-ft elevation, but it is interpreted that the flows measured in each borehole are the result of the intersection of the boreholes with fractures. Individual fractures have specific influences on the flow properties of that borehole. The results of measurements in Boreholes 526 and 554 are consistent with observations of the surface fracture characteristics that indicate that an increase in fracture density and aperture occurs from east to west across the MDA P footprint. These data indicate that the larger, more frequent fractures in the western area are capable of transmitting larger volumes of water to greater depths under saturated conditions. Under unsaturated conditions that prevail naturally, the fractures with larger apertures or more densely fractures areas will have higher air permeability, which will enhance air movement.

For the summary plots described in Section 7, the HPF data are normalized by depth interval. This calculation derives the change in flow rate per interval between measurements. The integration of the resulting curve produces the cumulative measured flow.

6.0 GEOCHEMICAL PROFILES

As a result of the inspection of the EM conductivity data, samples were collected from selected cores for selected anion and cation analysis. It was suspected that some sort of weathering may be the cause of the EM conductivity variations observed. Samples were selected for determination of anion and cation concentrations from the entire length of cores from Boreholes 273, 526 and 554. Anion analytes included bromide, oxalate, chloride, fluoride, nitrite, nitrate, phosphate and sulfate. Cation analytes included sodium, magne-

sium, potassium, calcium and barium. Samples were collected systematically from the length of each core and augmented with biased samples from selected fracture zones. Nineteen samples were collected from core 273, 12 from core 526 and 14 from core 554. The anion and cation analyses were not originally planned and the core had not been moisture protected.

After removing samples from the core box they were placed in sample bags that were left open overnight in a fume hood. Since the cores had been air dried since boring, the samples were not oven dried prior to analysis. For each sample approximately 50 g of rock was crushed using a mortar and pestle. Crushed samples were placed in an Erlenmeyer flask with approximately 75 g of deionized water and the solutions were agitated for a minimum of 48 hr using a rotary mixer. After mixing, the solid material was allowed to settle for 24 hr before decanting the supernatant fluid. Prior to analysis the supernatant solutions were filtered through a 0.2µm nylon filter. Anion analyses were conducted using a Dionex Ion Chromatograph. Cation analyses were conducted by a Leeman sequential inductively coupled plasma emission spectrometer. Sample preparation and analyses were performed in the EES-6 geochemistry lab at Los Alamos National Laboratory. Anion and cation concentrations are reported as milligrams per kilogram (mg/kg). Analytical precision of the analyses are better than 5%.

6.1 Results of Geochemical Profiles

Results of the anion and cation analyses are included in Appendix F. The concentrations of all anions exhibit similar distribution patterns in cores 526 and 554 (Figure 4.4-1 and Appendix D). All anions in cores 526 and 554 exhibit a maximum at approximately 38-ft depths. With minor exceptions, bromide and nitrite concentrations in the cores were either very low or below detection limits. There are generally no significant differences between oxalate and phosphate concentrations in cores 273, 526 and 554. Core 526 exhibits higher concentrations of fluoride at shallower depths than those measured in cores 273 and 554. The highest concentration of sulfate measured is in core 554 at 1.75-ft depth. Nitrate concentrations were generally higher in cores 526 than cores 273 and 554. All nitrate concentrations are greatest at approximately 38-ft depths, with the exception of the near-surface samples in cores 526 and 554. Chloride concentrations are similar in cores 526 and 554, with concentrations in core 273 and order of magnitude higher at 62-ft depth.

With the exception of barium in core 526, concentrations of all cations measured exhibit similar distribution patterns. In core 526, barium concentration is 116 mg/kg at the sample mid-point of 0.3-ft depth. All other barium concentrations are near or less than 1 mg/kg in all other samples for all cores (Appendix D). Sodium exhibits the highest concentrations of all cations with similar concentrations in both cores. In core 526, sodium exhibits the highest concentrations from 26- to 56-ft depths. Calcium and magnesium in this core exhibit some variations with depth near the surface. Calcium has a broad increasing trend from the 36- to the 45-ft depth. In core 273, all cations exhibit a generally increasing concentration trend with depth, maximizing at the 62- and 80-ft depths (Appendix D). This trend mirrors the trend for chloride in the core. In core 554, calcium, sodium, and potassium exhibit some variation with depth near the surface, but exhibit secondary concentration maximums in the 30- to 44-ft depth range. Sodium exhibits the highest concentration at the 38-ft depth.

Because barium and nitrate are potential vadose zone contaminants (because of disposal of barium nitrate at MDA P), additional investigation was conducted to estimate the potential impact of barium and nitrate in the MDA P subsurface. Barium nitrate [$Ba(NO_3)_2$] is highly soluble, thus any significant flow of liquid water will dissociate the barium and nitrate, and the percolating water will cause relocation of the barium and nitrate to deeper parts of the vadose zone. The removal of large quantities of solid barium nitrate at MDA P (LANL 2003, 76054) is a good indicator that there has not been substantial percolation through the waste pile, consistent with the conceptual model of flow at MDA P described below. However, some of the solid barium nitrate that was removed appeared to show dissolution features, such as cavities and rounded

edges. Thus, even though substantial amounts of solid barium nitrate were removed from the waste pile, there was likely some dissolution and downward transport of barium and nitrate prior to its removal. When barium nitrate dissolves, the barium species in solution is dominantly Ba^{+2} (LANL 1998, 59891). Because it is a divalent cation, dissolved barium tends to adsorb or form precipitates such as barium carbonate or barium sulfate (LANL 1998, 59891). Conversely, the two nitrate molecules that are released when barium nitrate dissolves will be highly mobile anions (NO_3^-). Thus, it would be expected that nitrate would be transported further than barium.

The barium profiles for Boreholes 273, 554, and 526 show little indication of deep transport of barium. Nearly all values are less than 1 mg/kg and these values are likely controlled by the concentrations of naturally occurring barium in the tuff minerals. The 0.3-ft sample from Borehole 526 does have a concentration that indicates some barium contamination. However, barium concentrations drop dramatically below 2 ft, indicating minimal downward transport. The three barium profiles suggest that there has been little impact of barium contamination at depth at MDA P, and any contamination that is present is restricted to very shallow depths.

The impact of nitrate contamination on the subsurface at MDA P is harder to determine partly because it is more mobile than barium, and because nitrate can be both produced and destroyed by various natural biological processes in soil/vadose environments such as that of MDA P. All the boreholes show detectable nitrate concentrations. Borehole 526 has the highest nitrate concentrations and the elevated barium in the near surface, suggesting there may be an impact of nitrate contamination in the vicinity of this borehole. Nitrate in borehole 554 is intermediate between 526 and 273. Borehole 273 has only minor nitrate. Nitrate data from other boreholes at TA-16 (e.g., monitoring well R-25) show lower nitrate inventories than the 526 and 554 holes at MDA P (Broxton et al. 2002, 72640). However, examination of natural nitrate data from other mesa boreholes on the Pajarito Plateau (Newman 1996, 59372) and from other semiarid locations (Edmunds and Gaye 1997, 73714; Hartsough et al. 2001, 73713) indicates that the concentrations at MDA P (even those in Borehole 526) are not any higher than is observed under natural conditions elsewhere in semiarid environments. In addition, chloride inventories from the MDA P boreholes are similar to results from other boreholes at TA-16 (Broxton et al. 2002, 72640), suggesting there has not been substantial percolation through the MDA P vadose zone. Thus, while there may be some impact of nitrate in the shallow bedrock at 526, it is not a certainty that deeper nitrate at MDA P is from a contaminant source.

7.0 DISCUSSION

This section correlates the observations of lithology, fractures and geochemical data from the cores with the geophysical measurements from the boreholes. Descriptions of the eastern and western parts of the MDA P footprint are provided, as these areas have similarities and differences attributed to fracture density. A description of the bedrock characteristics near the watershed divide at Borehole 273 is provided because this area is located outside the MDA P footprint, but also exhibits similarities and differences attributed to its physical setting.

7.1 Characteristics of the Eastern Part of the MDA P Footprint

The characteristics of the fracture regime beneath the eastern part of the MDA P footprint are represented by Borehole 526. Characteristics of the bedrock in this area are defined by stratigraphic and fracture studies, augmented by hydrologic, geophysical, and geochemical measurements in the borehole. The methods and results of individual measurements are described in previous sections of this report. Figure 7.1-1 presents a correlation of stratigraphy, observed fractures, caliper and EM conductivity logs, selected anion and cation concentrations, and results of the HPF measurements. These data are plotted against both depth and elevation.

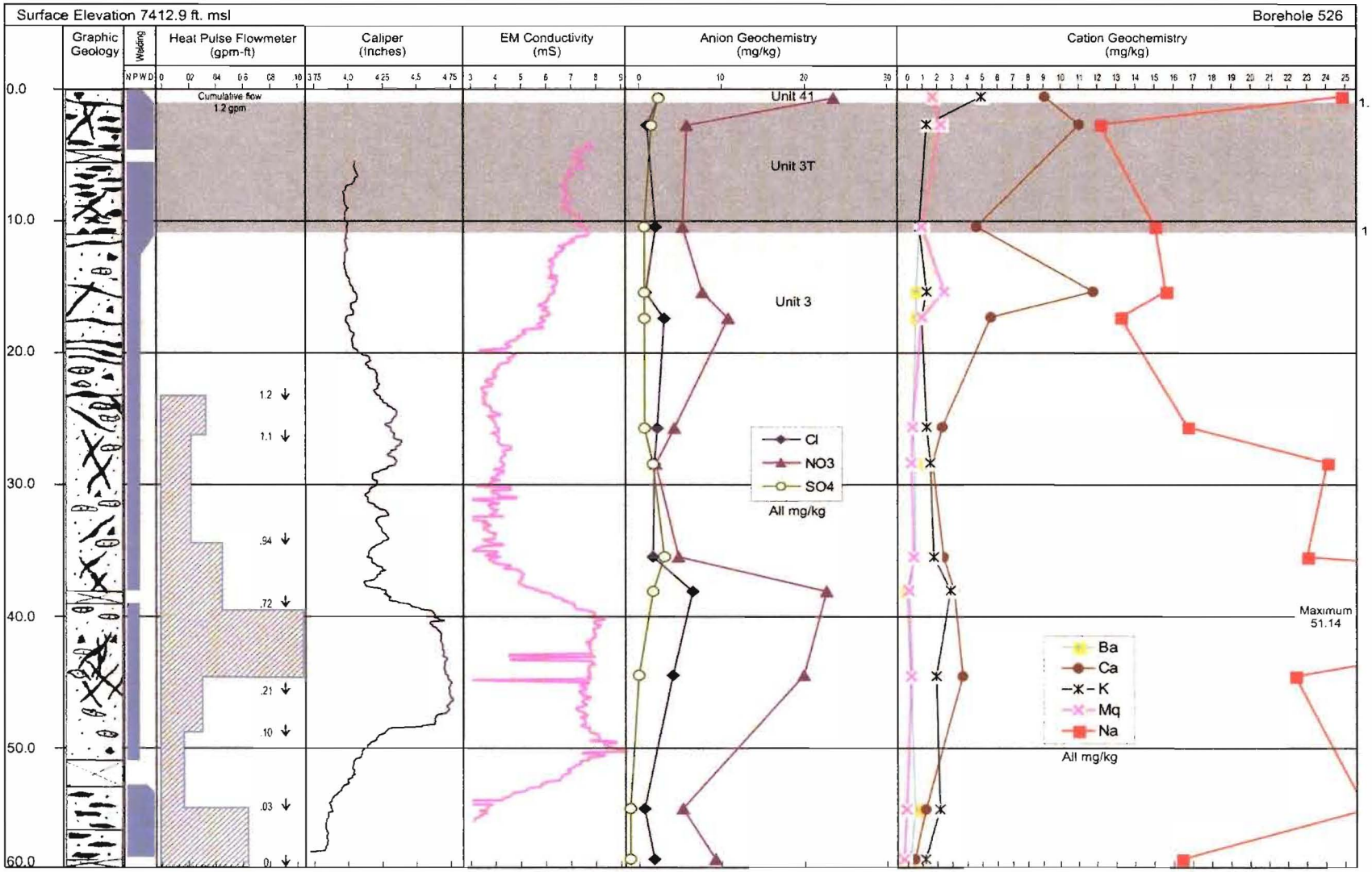

Figure 7.1-1. Empirical correlation diagram for Borehole 526, west side of the MDA P footprint

Borehole 526 was drilled to a total depth of 60 ft from a surface elevation of approximately 7420 ft above msl. The total depth is approximately the elevation of the stream in Cañon de Valle. The borehole was observed to be dry during and after drilling. The stratigraphic data indicate that the bedrock underlying the eastern part of the MDA P footprint consists of approximately 1 ft of nonwelded Unit 4l, 10-ft of the welded Unit 3T, and 42 ft of the partially welded Unit 3 that grades to approximately 8 ft of the welded Unit 3 in the bottom of the borehole. Unit 4l thickens southward from the borehole location due to topography. Fractures are observed throughout the core. Clay and manganese oxide accumulations observed in fractures in core are typically few to absent, although clays at 28-ft depth are commonly 5 mm thick (Appendix B).

Measurements with the HPF indicate that fractures above 24-ft depth contribute little to water flow within the borehole. The fracture group at 40- to 45-ft depths have the largest contribution to measured flow (Figure 7.1-1). This zone strongly correlates with a zone of high EM conductivity, maximum caliper radius, and maximum anion and sodium cation concentrations. The zone of high EM conductivity extends to a maximum depth of 54 ft where caliper, anion and measured induced water flows are minimized. The lower extent is characterized by an increase in welding of Unit 3.

These data are interpreted to indicate that an accumulation zone of surface salts exists from 36- to 52-ft depth below the current ground surface within the partially welded Bandelier Tuff Unit 3. The bottom of the accumulation zone lies approximately 20 ft above the active stream level. Fracture and rubble zones, or lost core recovery zones are associated with the extent of the zone. The accumulation zone is interpreted to be the result of vertical percolation of surface water through the bedrock, absorption into the matrix of Unit 3, followed by evaporation and accumulation of residual salts. Since the EM conductivity instrument detects matrix properties of the rocks, the salt accumulations appear to have penetrated the matrix of the Unit 3 rocks and affected some potential weathering, as suggested by the caliper logs. Since crystalline ionic solids do not conduct electric currents, moisture must be present in the rock matrices to produce high ionic strength solutions that result in the high EM conductivities measured. Depending on the actual moisture contents, the salts may occur as aqueous solutions or as actual precipitate minerals. Peaks of EM conductivity lows are superimposed across the highs. These may be local areas of moisture paucity where drying is enhanced by the larger fractures.

It is interpreted that the opening of the fractures at 36-ft depth facilitate a reduction in the water flux. The partially welded nature of Unit 3 facilitates absorption of water and dissolved species. The larger fractures serve as conduits of air flow, enhancing evaporation and precipitation. Evaporation is facilitated by the interconnection of the subsurface fractures with those exposed at outcrops along the south cliffs and benches of Cañon de Valle. Interconnection of these fractures may enhance response to changes in barometric pressure, humidity and local air temperatures that may affect the accumulation zone (Newman 1996, 59372; Kunkler 1969, 11671). The accumulation zone is interpreted to be the result of thousands of years of interaction of the fractured rock with the local climate. Salts of nitrates and chlorides are dissolved in surface waters and carried in the dissolved phase until precipitated at depth. The larger fractures represent the conduits of evaporation, whereas the smaller fractures, microfractures and rock pores represent the retention zones of residual moisture.

7.2 Characteristics of the Western Part of the MDA P Footprint

The characteristics of the fracture regime beneath the western part of the MDA P footprint are represented by Borehole 554. Figure 7.2-1 presents a correlation of selected data including stratigraphy, observed fracture and rubble zones, caliper and EM conductivity logs, anion and cation concentrations, and results of the HPF measurements. These data are plotted against both depth and elevation. There are many similarities with Borehole 526 on the east side, but there are some important differences attributed to the higher fracture density and larger apertures at Borehole 554.

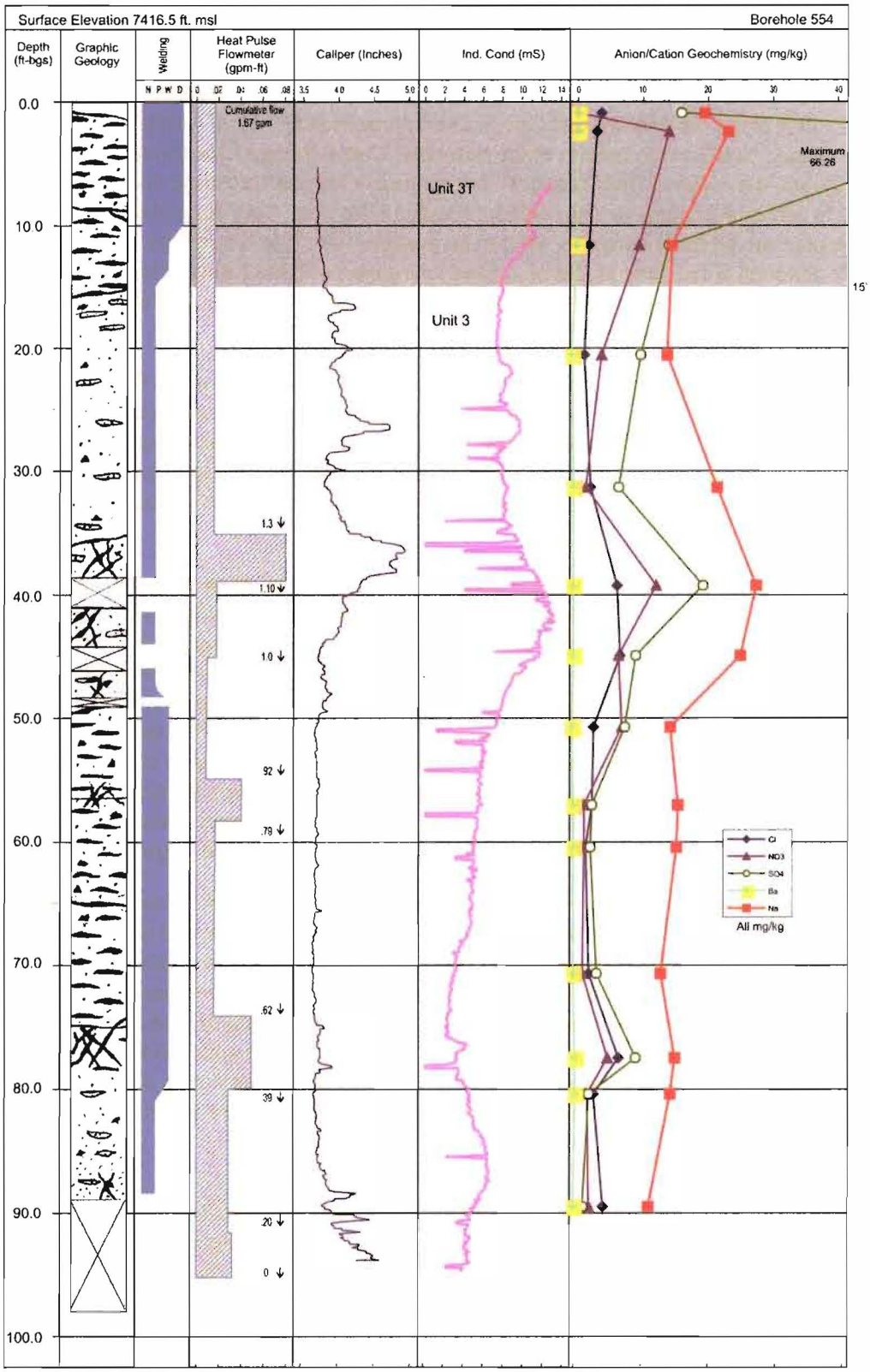

Figure 7.2-1. Empirical correlation diagram for Borehole 554, east side of the MDA P footprint

Borehole 554 was drilled to a total depth of 96 ft from a surface elevation of approximately 7422 ft msl, terminating approximately 36 ft below the elevation of the stream in Cañon de Valle. The borehole was observed to be entirely dry during and after drilling. The stratigraphic data indicate that the bedrock underlying the western part of the MDA P footprint consists of approximately 1 ft of nonwelded Unit 4l, 14 ft of the densely welded Unit 3T, 34 ft of the partially welded Unit 3, and approximately 32 ft of welded Unit 3 that grades to 8 ft of poorly welded Unit 3 in the bottom of the borehole. Unit 4l thickens southward from the borehole location. In outcrop, the rocks of Units 3 and 3T exhibit locally intense fracturing and local brecciation with apertures 20 to 30 cm. Fractures are observed throughout the core. Clay accumulations observed in fractures in core are typically common, tend to be massive, and 1 to 4 mm thick. Manganese oxides are typically few, although a thick accumulation occurs intergrown with the foliated clays in the high-angle fracture at 76-ft depth. White alteration halos occur around mafic phenocrysts and lithic fragments (Appendix B).

Measurements of the HPF indicate that fractures above 35-ft depth contribute little to water flow within the borehole. The fracture group at 35- to 38-ft depths have the largest contribution to measured flow (Figure 7.2-1). This zone strongly correlates with maximum caliper radius, the top of a zone with high EM conductivity, and maximum anion concentrations. The zone of high EM conductivity extends to a maximum depth of 50 ft where caliper, anion and measured induced water flows are minimized. The lower extent is characterized by an increase in welding of Unit 3.

As with Borehole 526, these data are interpreted to indicate that an accumulation zone of surface salts and residual moisture exists in a zone from 35- to 49-ft depth below the current ground surface within the partially welded Bandelier Tuff Unit 3. The bottom of the accumulation zone lies approximately 20 ft above the stream level. Fracture and rubble zones, or lost core recovery zones are again associated with the extent of the zone. What is apparent in Borehole 554 is that smaller EM conductivity highs are present in addition to the primary zone at 35- to 50-ft depths. Shallow anomalies are present at 21- and 25-ft depths, with a deeper zone possible from 78- to 90-ft depths. The shallow zones are not associated with observed fractures or anion concentration increases. The deeper zone is associated with observed fractures and an increase in the anion and cation concentrations. Local EM conductivity lows are again associated with larger fractures across the EM conductivity high, emphasizing the association with the larger fractures.

The similarities of the accumulation zone beneath the east and west parts of the MDA P footprint indicate that similar processes have been active over some period of geologic time. The extent and degree of accumulations of surface salts in a accumulation zone approximately 35 to 50 ft below ground surface is similar in both settings. The differences between the fracture densities and apertures, however, between the east and west sides suggest that differences should exist in potential hydraulic conductivity. The similarities indicate that the limiting factor is probably climate and annual precipitation, not the ability to transmit water. The apparent occurrences of thicker, more extensive clay accumulations on the west side are interpreted to indicate a greater capacity to transmit suspended solids through the larger fracture apertures.

7.3 Characteristics of Flash Pad 387 at the Watershed Divide

The characteristics of the fracture regime beneath the flash pad at the watershed divide are represented by Borehole 273. Figure 7.3-1 presents a correlation of selected data including stratigraphy, observed fracture zones, caliper and EM conductivity logs, and anion and cation concentrations. These data are plotted against both depth and elevation. Measurements with the HPF were not possible in Borehole 273 due to the high flow rates of induced water at the 125-ft depth.

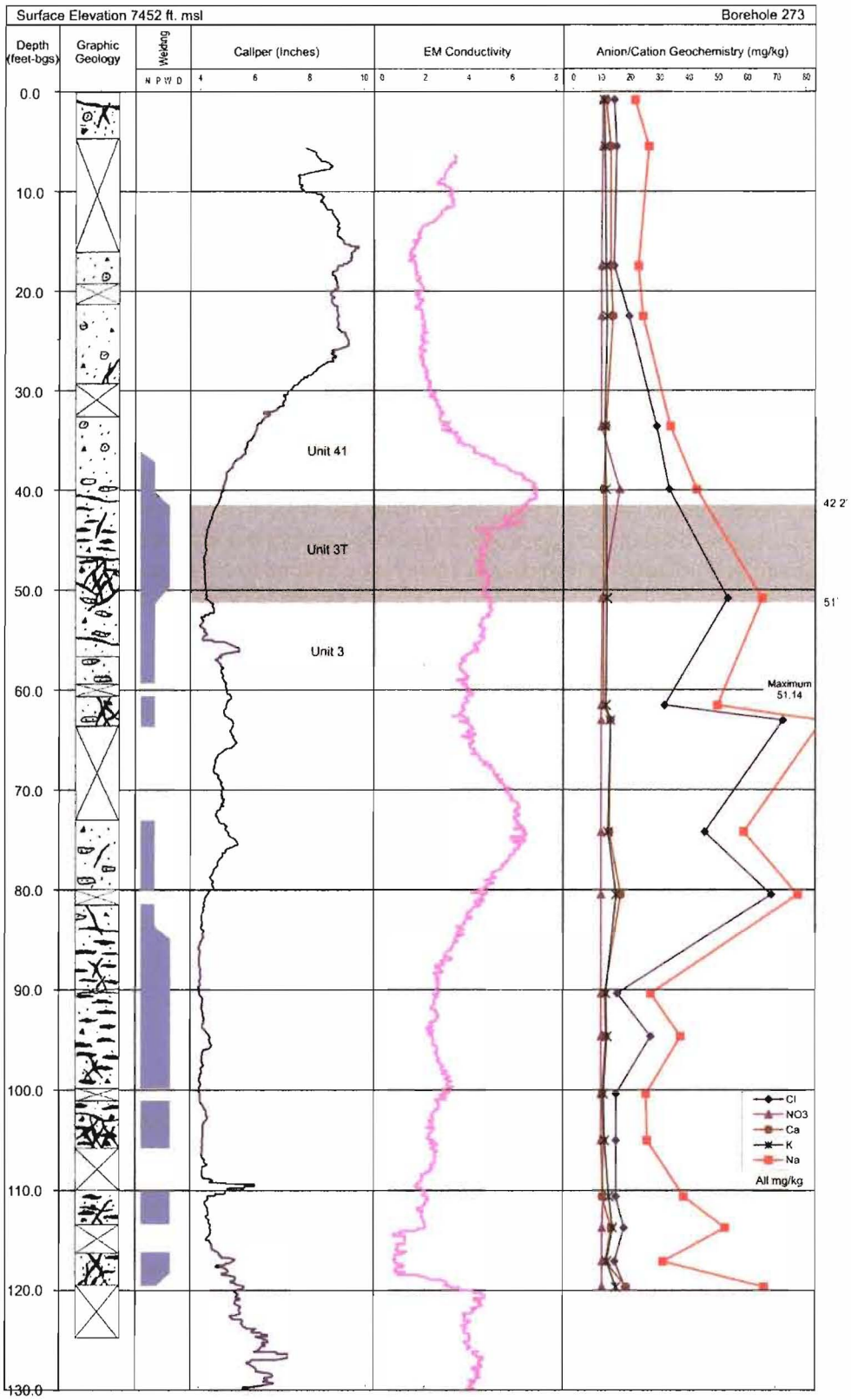

Figure 7.3-1. Empirical correlation diagram for Borehole 273 and Flash Pad 387 at the watershed divide

Borehole 273 was drilled to a total depth of 170 ft from a surface elevation of approximately 7452 ft msl, terminating approximately 80 ft below the elevation of the stream in Cañon de Valle. No core was retrieved from the last 50 ft drilled, and the lower 35 ft of the borehole collapsed after drilling. The borehole was observed to be entirely dry during and after drilling. The stratigraphic data indicate that the bedrock underlying the flash pad at the watershed divide consists of 42 ft of nonwelded Unit 4I, 9 ft of the densely welded Unit 3T, approximately 34 ft of poorly welded Unit 3, and approximately 35 ft of welded Unit 3 that is interpreted to grade to nonwelded Unit 3 in the bottom of the borehole. Fractures are observed throughout the core. Clay accumulations observed in fractures in core are typically continuous with the exception of the fracture at the 48-ft depth where they are few. Clays tend to be massive to foliated and 1 to 12 mm thick. Manganese oxides are typically few, although a thick accumulation occurs intergrown with the foliated clays in the high-angle fracture at the 117-ft depth (Appendix B).

EM conductivity highs are measured from 35- to 45-ft and 65- to 90-ft depths. In contrast to Boreholes 526 and 554, the caliper log does not mirror the trend of the shallow EM conductivity high, but does exhibit a weak increase from 55- to 85-ft depths. The EM conductivity high from 35- to 45-ft depth is located across the welded contact of Units 4I and 3T (Figure 7.3-1). Fracture zones are present immediately above and below the anomaly. Nitrate concentrations increase slightly across this interval, but other anions and cations do not have local concentration peaks at 50-ft depth. The zone at 65- to 90-ft depth is located in the partially welded Unit 3. Approximately 10 ft of the upper part of this interval suffered lost core recovery, so no core is observable. A fracture at 62-ft depth is observed to have many foliated to massive clays with few manganese oxide stains and clay intergrowths. Chloride and all cations exhibit local peaks in samples collected at 62- and 80-ft depths (Appendix F).

These data are interpreted to indicate that a broad zone of surface salt accumulation is present from approximately 35- to 90-ft depths below the current ground surface within the partially welded Bandelier Tuff Unit 3. The upper portion of this zone exhibits a small nitrate concentration increase. Most of the zone exhibits high chloride and sodium concentrations with local concentration lows of these species at 61- and 74-ft depths. These local lows are correlated with either a fracture zone or lost core, respectively. Similar relationships are observed in Boreholes 526 and 554 at 45-ft depths. The fractures are interpreted to act as conduits for both water and air flow. As with the other boreholes, the bottom of the zone is marked by the presence of welded tuff, suggesting that the partially welded matrix is acting as an absorbent that has the ability to absorb and release moisture in response to atmospheric changes. The bottom of the accumulation zone in Borehole 273 remains above the stream level of Cañon de Valle.

8.0 CONCEPTUAL MODEL OF THE FRACTURE FLOW SYSTEM AT MDA P WATERSHED

The rocks of the Tshirege Member of the Bandelier Formation form the bedrock in the small watershed that contains the MDA P Site. These rocks are composed of welded to nonwelded ashflow deposits from the Valles Caldera. Most studies of hydrologic characteristics of the Bandelier Tuff attribute water movements to diffusion, capillarity and gravity drainage through the porous tuff (Abraham 1963, 08149; Brown et al. 1988, 06871). In studies at nearby Pajarito Mesa, Vaniman et al. (2002, 73280) found the evaporite minerals halite and gypsum in fracture-filling materials, suggesting that evaporation processes were effective near the mesa margins. Vaniman and Chipera (1995, 54709) found clays from surface soils had been translocated to at least 25-m (80-ft) depths in vadose zone fractures. Studies of the geology and hydrology at MDA P recognized the regional setting within the Pajarito Plateau (Brown et al. 1988, 06871), but attributed hydrologic characteristics of the tuff to the degree of welding, with porosity and hydraulic conductivity decreasing with the increasing degree of welding. Rogers et al. (1996, 55543) analyzed the available data at MDA P and concluded that no saturation was apparent, and that a downward decrease in head was apparent that indicated a downward flow of water.

The flow of water through unsaturated, fractured rock is affected by the lithologic and structural characteristic, including porosity, degree of welding, density and apertures of fractures, infiltration, percolation, as well as precipitation, runoff and evaporation. This report correlates and augments the surface fracture characterization measurements at MDA P reported by Lewis et al. (2002, 73785) with geophysical measurements taken in the boreholes and observations of fractures and geochemical data from cores to create a conceptual model of fracture transport of shallow groundwater in the bedrock beneath the MDA P watershed. The conceptual model developed is empirical and qualitative in nature (Figure 8.0-1). The conceptual model of recharge and localized flow through fractures developed for the MDA P watershed provides site-specificity to the TA-16 hydrogeologic conceptual model presented by the Laboratory (1998, 59891).

MDA P lies on the south rim of Cañon de Valle in a transition zone in which fracture density and apertures decrease from west to east. The site is underlain by Units 3 and 4 of the Bandelier Tuff. The partially to densely welded Units 3 and 3T form the cliffs and benches of the canyon walls, respectively (Figure 8.0-1). The non-welded Unit 4l forms the gentle slopes from the topographic bench southward to the surface of former Flash Pad 387 at the watershed divide. The partially welded to welded Unit 4u (not shown) forms the caprock of the highlands west of the MDA P watershed, but is not present within the MDA P watershed. The establishment of the MDA P waste pile and Flash Pad 387 resulted in the removal of the natural vegetation, soil, and unconsolidated surface deposits. The removal of the waste pile resulted in exposure of the bedrock with only local unconsolidated deposits remaining, either as residual veneers or as reclaimed soils. The southern part of the watershed toward the divide [(at locations of Flash Pad 387 and SWMU 16-016(c)-99] are now dominated by thin reclaimed soil and gravel veneer over bedrock.

There are no springs, seeps, ponds, or other natural perennial water sources contained within the small MDA P watershed. The semi-arid climate provides the area with approximately 18.7 in. of average annual precipitation as both winter snowfall and warm-season thunderstorms in approximately equal proportions. As a result of the waste pile removal, precipitation in this watershed provides runoff to two ephemeral arroyos that cross the western and eastern margins of MDA P. The central portion of the watershed and the MDA P footprint receives overland flow only from direct precipitation.

Infiltration in the conceptual model is the entry of water into the soil or rock from the surface. It is controlled by the annual precipitation, soil storage capacity and hydraulic conductivity. Winter snowmelt is probably the more efficient source due to lower evapotranspiration demands and slower release rates. Field measurements by Flint et al. (2001, 73716) indicated that fracture flow is best initiated when water is ponded on exposed bedrock, or when the soil-bedrock contact reaches near-saturation conditions. Thicker soils tend to have a higher storage capacity, so that water is held in the root zone, and removed by evapotranspiration. Thinner soils do not have sufficient storage capacity so that near-saturation conditions can occur at the soil-bedrock contact (Flint et al. 2001, 73716). At MDA P, the soils and colluvium on the gently sloping mesa top from the watershed divide at Flash Pad 387 northward to the cliffs along Cañon de Valle would have had a relatively high water-holding capacity. Interflow of water may have occurred within the El Cajete pumice on the west side, as this unit consists of well-sorted, coarse pumiceous ash, and as such possesses a high permeability in contrast with the thick, underlying clay soil. Topography on the non-welded Unit 4l would have promoted subsurface ponding of water and facilitated infiltration. The surface fractures in Unit 4l, however, exhibit small apertures suggesting low infiltration rates.

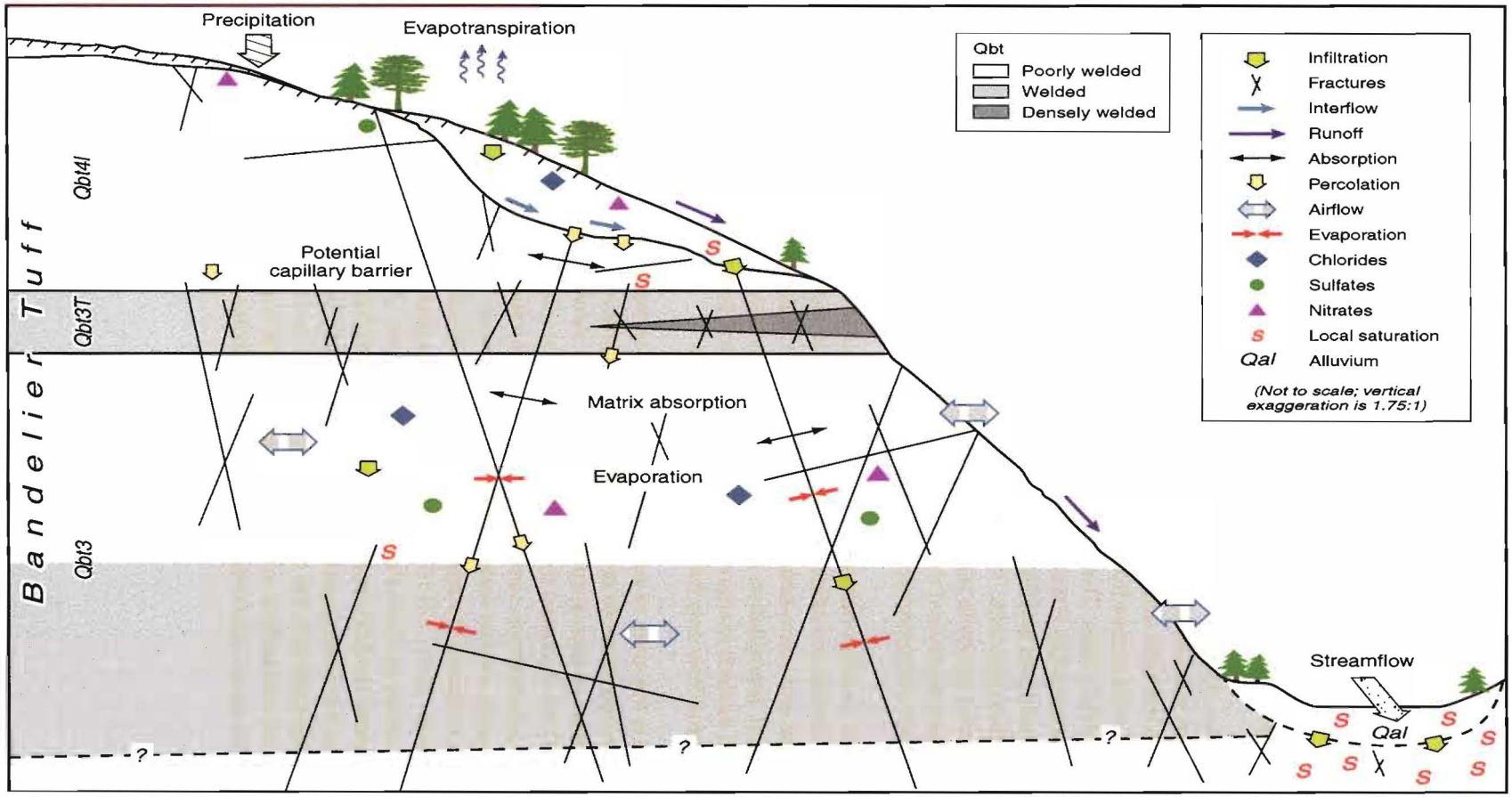

Source: Shaw_Rev. for MDA P Area Closure Certification Report; Annex III, Phase II; 012703; cf

Figure 8.0-1. Conceptual model of fracture flow in bedrock at MDA P

Percolation in the conceptual model is defined as the vertical flow of water within the bedrock. Percolation will occur in the rock matrix of nonwelded to partially welded Units 4I and 3, but is exceedingly slow in the welded matrix of Units 3 and 3T (Figure 8.0-1). Percolation of water in through-penetrating fractures may act as preferential flow paths (Su et al. 2000, 73717). Flow in fractures is controlled by capillary forces that act against gravity due to surface tension pressures. Large fracture apertures lose saturation first due effectively to drainage. Fracture segments with rough surfaces or thin apertures may remain saturated due to tension forces. Fractures with large apertures tend to remain dry. Water may occur in isolated, thin films along grain boundaries, in thin or rough fracture apertures, or in local ponds of water trapped in discontinuous vertical fractures. Increased saturation from increased infiltration may result in coalescence of isolated occurrences of water in fractures to form sinuous channels down the fracture wall (Tsang et al. 2001, 73716).

Capillary barriers may exist across the lithologic boundaries from the nonwelded Unit 4I to the densely welded Unit 3T and the poorly welded Unit 3 to the welded Unit 3 (Figure 8.0-1) due to changes in porosity, fracture density and aperture. Experimental evidence indicates that flow across such boundaries in fractured rock will be intermittent. In conditions of low water flow, pulses of water may be induced into the fractures of the underlying welded units as the forces of gravity momentarily exceed capillarity. Higher flow rates may induce steady flow along dynamic channels (Su et al. 1999, 63765; Tsang et al. 2001, 73716) as the water seeks the paths of least resistance. Through-penetrating fractures mitigate the effects of capillarity and will promote percolation across lithologic contacts. Segments along the fracture trace may experience drying while other segments remain moist.

Water carried by fractures may be absorbed or imbibed into the rock matrix at depth, depending on relative moisture contents and matrix porosity, a process termed *matrix suction* by some authors. Robinson and Bussod (2000, 73717) observed that water residing in fractures tends to absorb into nonwelded tuffs, causing a transition to matrix flow. They did not observe fractures within nonwelded tuff to enhance flow through the unit. In the conceptual model for MDA P, the non-welded Unit 4I and partially welded Unit 3 may absorb or imbibe water that is percolating through nearby fractures. This suggests that percolation through the fractures of Unit 4I will be more effective in the thinner parts near the canyon wall (Figure 8.0-1). The welded Units 3T and lower part of Unit 3 have little storage capacity and little ability to absorb water transmitted through them. It is assumed in the conceptual model that water entering the fractures at the tops of these welded units passes through the fractures with no matrix absorption.

Evaporation is believed to remove moisture from the porous matrices near the fracture walls in the partially welded Unit 3, as well as cause drying of water films along fractures in the welded portions (Figure 8.0-1). The evaporation is enhanced by air circulation in fractures in the unsaturated zone, a process recognized at many other arid and semi-arid sites across the western US and the Pajarito Plateau (Kunkler 1969, 11671; Newman 1996, 59372). In a similar setting, Weeks (2001, 73716) reported substantial air exchange through fractured welded tuffs at Yucca Mountain. In summer, instrumented wells were observed to alternately intake and exhaust air, and in winter were observed to exhaust air nearly continuously. Purtymun et al. (1974, 05477) similarly measured cycles of air intake and exhaust in boreholes at TA-49 and correlated these with atmospheric pressure changes and water level variations. Pruess (2001, 73716) reported that barometric pumping causes exchange of dryer atmospheric air with moister soil gas resulting in evaporation and drying. Hence, in the conceptual model, the larger fractures promote exchange of atmospheric gases, the smaller fractures promote retention of moisture, and provide the initial paths of re-wetting.

Neeper and Gilkeson (1996, 56025) and Newman (1996, 59372) suggested that a hydraulic barrier is formed by the removal of moisture from within a mesa based on data at other sites at Los Alamos. Only those percolation events that have sufficiently sustained flow to survive the effects of matrix absorption and evaporation will be available to percolate to greater depths. It has long been recognized that rapid infiltra-

tion rates, small matrix permeability, and small matrix moisture capacity enhance deep fracture flow (Montazer and Wilson 1984, 73715). It is postulated that within the MDA P watershed, low infiltration rates and moderate matrix moisture capacity of Unit 4l, potential capillary barriers, and evaporation within Unit 3 have served in concert to severely limit the supply of water that was available for percolation into the welded Unit 3. Since the upper parts of the welded Unit 3 are also exposed along Cañon de Valle, atmospheric evaporation will be an effective barrier to deeper fracture flow.

The matrix absorption and evaporation processes at the MDA P watershed are observed to result in the accumulation of salts in the bedrock matrix, in a zone that ranges from 30 to 90 ft below the mesa surface (Figure 8.0-1). The salts are interpreted to result from dissolution of surface salts, including nitrates, chlorates, and sulfates, and subsurface redistribution during percolation. Salt accumulation is believed to be an interplay among many variables including solution chemistry, bedrock porosity and structure. Most of the salts, including nitrates, chlorides, and sulfates are contained within the partially welded Unit 3 tuff. In Borehole 273, accumulation appears to start within the basal portion of Unit 4l, then decreases with a maximum in the partially welded Unit 3. Matrix absorption of dissolved species is enhanced by the porosity of the partially welded Unit 3. Precipitation of salts may occur on the rough fracture walls of Unit 3T, but not enough data is available to assess this situation. The lower limit of the accumulation zone appears to represent the decrease in matrix porosity represented by an increase in welding in Unit 3. The zone of salt accumulation appears to exist entirely above the stream level, where fractures are open to the atmosphere along the canyon walls. The evaporation processes may be most efficient nearest the canyon walls and may decrease in efficacy into the mesa away from the walls. The presence of the broad zone in Borehole 273 (near the watershed divide) suggests that evaporation is still effective at this distance from the canyon. Subsequent percolation events may actually dissolve some of the accumulated salts near major fractures. MDA P chloride inventories are similar to those of other TA-16 boreholes (Broxton et al. 2002, 72640), which suggests that the downward percolation rates are similar. The chloride data suggest that residence times in the MDA P vadose zone may be hundreds to thousands of years.

The similarities of salt accumulation across the small MDA P watershed suggest that the fracture zone on the west side has little influence on the response of the system compared to the east side. This suggests that the availability of water is the limiting factor of subsurface flow. The fracture zone on the west side of the MDA P footprint may be able to pass more water, but the data demonstrating this is simply not available. The larger apertures of fractures on that side of the watershed appear to have allowed more transport of suspended materials, however, as evidenced by thicker, more abundant clays than observed on the east side.

The evaporation zone is interpreted to be essentially climatically controlled. The zone represents the balance of precipitation, infiltration, percolation and evaporation in the semi-arid climate of the Pajarito Plateau. The zone has probably been in existence long before the construction of the TA-16 Burning Ground and the MDA P waste pile, perhaps tens of thousands of years, or longer. The natural processes are probably still at work in undisturbed areas adjacent to the MDA P watershed. The removal of all soils and unconsolidated cover across the MDA P footprint results in promotion of runoff and elimination of saturated soils or surface ponding of water that promotes infiltration. The results should be a reduction of the subsurface moisture regime and increased drying of the bedrock at the MDA P footprint. In the conceptual model, the current conditions at MDA P are represented by the fractures that intersect the surface at barren surface locations (Figure 8.0-1).

9.0 REGIONAL SETTING OF MDA P

The regional setting of MDA P is defined by the Pajarito Fault Zone. The Pajarito Fault Zone is a bounding fault of the Rio Grande rift. Numerous studies of the fault zone have been performed, the salient features

of the fault zone and the associated deformation zone are reviewed by Gardner et al. (2001, 70106). The main escarpment of the Pajarito fault lies west of the TA-16 administrative area along NM Highway 501 (Figure 1.0-1). Faulting and related deformation extend approximately 5000 ft east of the main escarpment to the approximate location of the fracture zone at MDA P. Within the Pajarito Fault Zone, graben and monoclinal folds are common. Open-fissure networks are typically associated with the tensional upper hinge zones of the monoclines (Gardner et al. 2001, 70106; Lewis et al. 2002, 73785).

MDA P lies on the southern rim of Cañon de Valle at the transition from a graben structure to the west and a bedrock promontory to the east. Lewis et al. (2002, 73785) define the TA-9 graben (labeled G2 on Figure 9.0-1) just west of MDA P by a series of north-trending faults. The eastern boundary of the graben is defined by a pair of faults (labeled F2 on Figure 9.0-1) with down-to-the-west displacement. The western boundary is defined by a fault with down-to-the-east displacement (labeled F4 on Figure 9.0-1). Springs within the graben feed the Cañon de Valle stream. At MDA P, five small faults were identified in associated with the fracture zone on the west side. The lack of stratigraphic markers prevented an estimate of the displacement along these faults, but it was thought to be small because the fault traces were only about 16 ft (5 m) on the average. The locally high fracture density on the west side of MDA P suggested a small amount of horizontal extension over possible deep-seated normal faults (Lewis et al. 2002, 73785).

10.0 DISCUSSION OF MDA P AND THE CAÑON DE VALLE STREAM

The Cañon de Valle stream trends east-northeast to form the northern boundary of the MDA P watershed (Figure 1.1-1). The stream does have a perennial flow, fed by upstream springs and seeps; hence, input to the stream system includes both subsurface (e.g., spring flow) and overland flow. Ephemeral streams on the eastern and western margins of the MDA P watershed drain to the stream when fed by precipitation or snowmelt. No springs or seeps have been observed in the MDA P watershed. The lack of water observed in Boreholes 554 and 557 indicates that there is not a perched water table beneath MDA P related to the Cañon de Valle alluvial water system.

The structural features observed at MDA P may have an effect on the stream morphology and behavior. The stream gradient may be affected by the fracture system observed at MDA P. The fracture zone on the west side suggests that this area should be more brecciated and hence more permeable due to fracture interconnection. These conditions may allow the rocks to be more easily eroded, and may decrease the stream gradient through this reach, allowing for the accumulation of sediments and creating a swampy area, as is observed along this reach of the stream to the northwest of MDA P. The lower fracture density and smaller apertures of the east side of MDA P should result in decreased interconnection of fractures, suggesting that infiltration and saturation will be reduced along this reach of the stream to the northeast of MDA P.

The subsurface flow in the fracture system beneath the stream would be largely affected by gravity and capillarity, due to the interconnection of fractures, and the porosity of the nonwelded portion of Unit 3. Downward advective flow driven by gravity is likely to dominate the saturation profile along the stream axis (Figure 8.0-1). The fracture zone on the west side of MDA P may represent the eastern termination of structures farther to the west, so subsurface saturation of the stream north of MDA P is likely to decrease from west to east at the toe of the waste pile. Lateral flow away from the stream axis would be controlled by the inability of water to flow downward; therefore, the shallow saturation front should decay laterally away from the stream axis, probably in a convex pattern. As the volume of the source varies, the saturation front may expand and contract laterally, depending on the balance of inflows and outflows to the fracture system beneath the stream. Interception of the fractures beneath the footprint of MDA P is unlikely, as they lie entirely above stream levels. The presence of a weak accumulation zone at 78-ft depth in Borehole 554 suggests that this area has not been saturated.

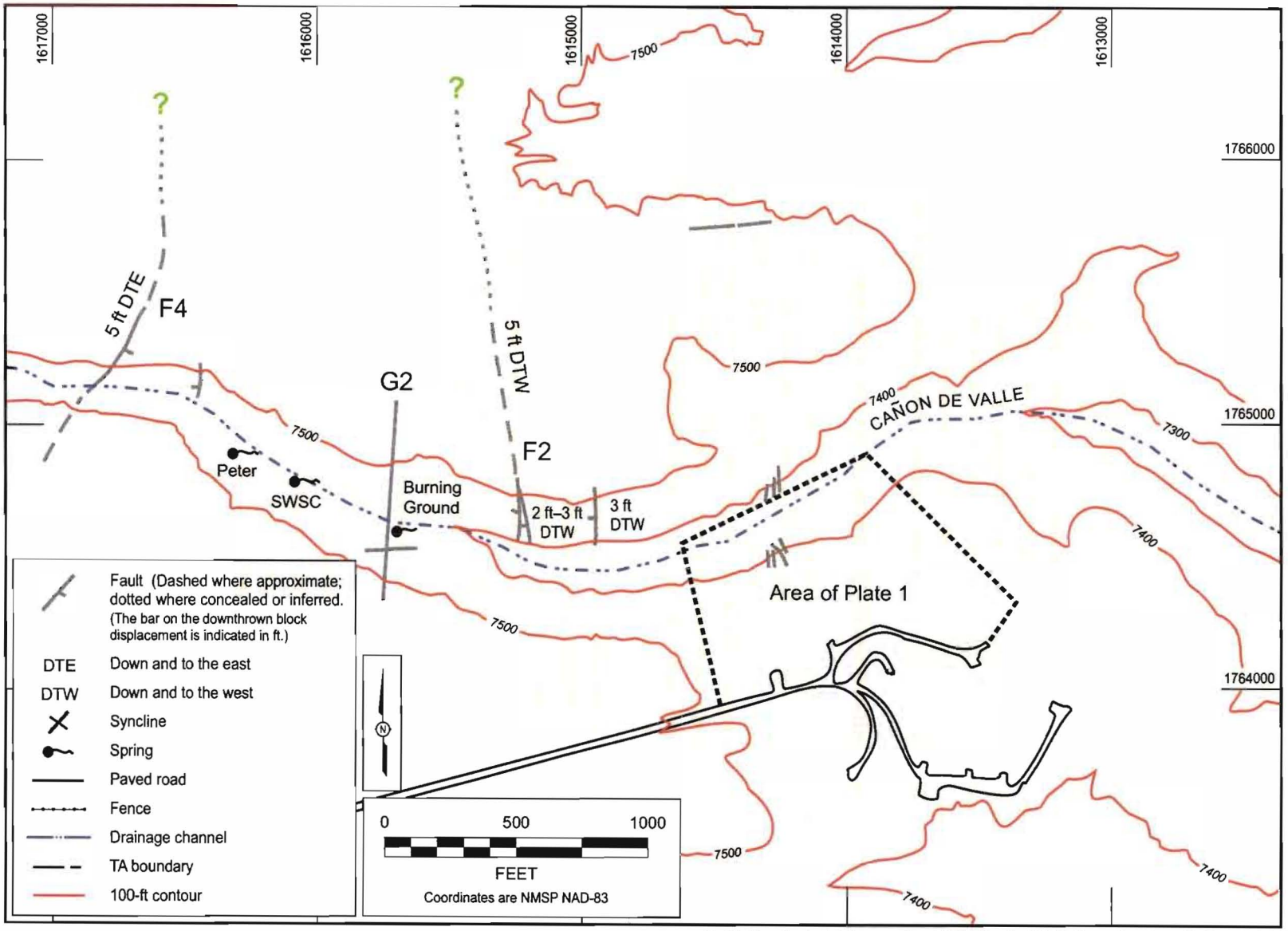

Modified from Lewis et al, in preparation, 111402_Rev. for MDA P Closure Rpt.; Annex III, Phase II; 012603; cf

Figure 9.0-1. Generalized regional structure map of the MDA P Site

The only viable mechanism by which contaminants from the MDA P watershed would affect surface waters is by overland flow. It is possible that surface runoff from the MDA P watershed carried particulate and chemical contaminants to the stream historically due to erosion of the waste materials, but the impact on the stream appears to be very small (LANL 1998, 59891). The removal of most unconsolidated deposits across the watershed has resulted in the elimination of all potentially near-saturated and ponded water sources at the surface, so that current conditions promote runoff and inhibit infiltration. In addition, the removal of the waste materials has resulted in the elimination of contaminant sources to the surface waters of Cañon de Valle.

11.0 IMPLICATIONS FOR THE TA-16 CONCEPTUAL MODEL

The processes of surface water infiltration, percolation, matrix absorption and evaporation provide site specificity to the hydrogeologic conceptual model of TA-16 (LANL 1998, 59891). The TA-16 conceptual model is complex due to mesa and canyon conditions, geological units with varying properties, multiple flow paths, types of flow behavior and multiple source areas. Saturated flow systems within the area included the alluvial aquifer of Cañon de Valle, springs within the canyon, and surface water ponds and water sources. Recharge areas included known or suspected transient sources, as well as diffuse infiltration and fracture flow. The saturated systems that feed the springs in the canyons were hypothesized to be ribbon-like structures within the mesa. The TA-16 conceptual model was described to extend eastward to the confluence of Cañon de Valle and Water Canyon; thus, the MDA P watershed is located in the eastern portion of this area.

At the MDA P watershed, there is no evidence of springs, seeps, or other evidence that would indicate that the ribbon-like structures extend as far east as MDA P. The contact of Bandelier Tuff Unit 4l and Unit 3T is consistently dry, including outcrops of this contact in the undisturbed areas to the west of the MDA P footprint along the access road cuts. The evidence of matrix absorption and evaporation indicate that the processes of recharge through diffuse infiltration and recharge through fractures will be highly inefficient. The suggestions by Neeper and Gilkeson (1996, 56025) and Newman (1996, 59372) that the process of removing moisture from within the mesa by evaporation through barometric or topographic pumping effects form a hydraulic barrier are supported by the data in this report. The similarities of the salt accumulation zone beneath the eastern and western parts of the MDA P footprint, despite the differences between the fracture densities and apertures, suggest that the limiting factor to infiltration on mesa tops is probably climate and annual precipitation, not the ability to transmit water.

As discussed in section 10.0, the fracture zone observed on the western side of MDA P should have a significant impact on the ability of the bedrock fracture flow system to transmit under saturated conditions. The increased interconnection of fractures is postulated to result in an increase in depth of saturation with less fractured areas experiencing less interconnection and less saturation. Structural elements related to the Pajarito Fault Zone which intersect Cañon de Valle may have unanticipated influences if not identified. The fracture zone observed on the west side of MDA P may not have been identified without the exposures that resulted from the entire waste pile removal, as vegetation and colluvial cover in adjacent areas have prohibited detailed examination (Lewis et al. 2002, 73785).

12.0 CONCLUSIONS

This report correlates and augments the fracture characterization measurements at MDA P that were reported by Lewis et al. (2002, 73785) with geophysical measurements taken in 6 boreholes, observations of fractures, and geochemical data from cores to create an initial conceptual model of fracture transport of shallow groundwater in the bedrock beneath MDA P.

The MDA P Site is located within a small open watershed with no springs, seeps, ponds, or other natural source of water. Excavation and removal of the waste pile and adjacent contaminated soil as part of the Phase I Closure activities resulted in removal of most of the unconsolidated, surficial materials and exposure of the bedrock surfaces at MDA P and Flash Pad 387. The resulting bedrock exposures provide excellent exposures for surface mapping of stratigraphy and fractures.

The geologic mapping delineates the stratigraphy of the Tshirege Member of the Bandelier Tuff at the MDA P Site. Tshirege Member stratigraphic units that were exposed at MDA P include Units 3, 3T, and 4l, from bottom to top, respectively. Within the regional structure, the MDA P Site is within the deformation zone of the Pajarito Fault Zone, and lies on the southern rim of Cañon de Valle at the transition from a graben structure to the west and a bedrock promontory to the east.

Fracture densities and apertures studies indicate that both increase from east to west across the MDA P footprint. The addition of subsurface fractures in this report to the data set analyzed by Lewis et al. (2002, 73785) do not change the orientations or conclusions. The fractures that appear to be capable of conducting the largest volumes of water, as determined by the measurements of the HPF appear to have weak clay and manganese oxide accumulations. Under unsaturated conditions that prevail naturally, the fractures with larger apertures or more densely fractured areas are interpreted to have the greatest capabilities to circulate air and promote drying and evaporation, resulting in the accumulation of surface salts. The concentrations of the anions nitrate and chloride are generally mirrored with those of the cations sodium and potassium. These data strongly correlate with caliper and EM conductivity logs at similar depths. The EM conductivity highs are interpreted to result from local high, ionic strength solutions within the rock matrices. Examination of natural nitrate data from other mesa boreholes on the Pajarito Plateau and from other semiarid locations (Edmunds and Gaye 1997, 73714; Hartsough et al. 2001, 73713) indicates that the concentrations at MDA P are not any higher than is observed under natural conditions elsewhere in semiarid environments.

A conceptual model is developed from the empirical data that states that the fracture flow system is unsaturated, with local infiltration of precipitation and downward percolation, but dominated by matrix absorption and evaporation. The suggestions by Neeper and Gilkeson (1996, 56025) and Newman (1996, 59372) that the process of removal of moisture from within the mesa by evaporation through barometric pumping effects form a hydraulic barrier is supported by the data in this report. An accumulation zone of surface salts of nitrate, chloride and sulfate is present at 30- to 90-ft depths below the current mesa surface and is attributed to evaporation. The zone is apparent in all boreholes, and is located entirely above the stream level of Cañon de Valle. The evaporation zone is interpreted to represent the response of the fracture system to the semi-arid climate and probably required thousands of years to develop. It is postulated that the removal of all surface soils and unconsolidated deposits will result in a reduction of the subsurface moisture regime and increased drying of the subsurface bedrock under the MDA P footprint.

The lack of water observed in any boreholes during or after drilling suggests that the saturated conditions along the Cañon de Valle alluvial aquifer do not extend laterally to produce a perched water table beneath the MDA P footprint.

13.0 REFERENCES

Abrahams, J., Jr., January 1963. "Physical Properties of and Movement of Water in the Bandelier Tuff, Los Alamos and Santa Fe Counties, New Mexico," US Geological Survey Administrative Release, Albuquerque, New Mexico. (Abrahams 1963, 08149)

Birkeland, P., 1984. *Soils and Geomorphology*, Oxford University Press, Inc., New York, 372 p. (Birkeland 1984, 44019)

Brown, F., W. Purtymun, A. Stoker, and A. Barr, February 1988. "Site Geology and Hydrology of Technical Area 16, Area P," Los Alamos National Laboratory report LA-11209-MS, Los Alamos, New Mexico. (Brown et al. 1988, 06871)

Broxton, D., and S. Reneau, August 1995. "Stratigraphic Nomenclature of the Bandelier Tuff for the Environmental Restoration Project at Los Alamos National Laboratory," Los Alamos National Laboratory report LA-13010-MS, Los Alamos, New Mexico. (Broxton and Reneau 1995, 49726)

Broxton, D., R. Ryti, D. Carlson, R. Warren, E. Kluk, and S. Chipera, March 1996. "Natural Background Geochemistry of the Bandelier Tuff at MDA P," Los Alamos National Laboratory document LA-UR-96-1151, Los Alamos, New Mexico. (Broxton et al. 1996, 54948)

Broxton, D. E., R. Warren, P. Longmire, R. Gilkeson, S. Johnson, D. Rogers, W. Stone, B. Newman, M. Everett, D. Vaniman, S. McLin, J. Skalski, and D. Larssen, 2002. "Characterization Well R-25 Completion Report," Los Alamos National Laboratory report LA-13909-MS, Los Alamos, New Mexico. (Broxton et al. 2002, 72640)

Criswell, C., and A. Bray, October 1994. "Integrated Approach for Characterization of Bedrock Fracture Flow System, Mound Plant, Miamisburg, Ohio," in *Abstracts with Programs, Geological Society of America, 1994 Annual Meeting,* published by the Geological Society of America, Seattle, Washington. (Criswell and Bray 1994, 37382)

Carey, W., and G. Cole, January 2002. "Description of the Cerro Grande Fire Laser-Altimetry (LIDAR) Data Set," Los Alamos National Laboratory report LA-13892-MS, Los Alamos, New Mexico. (Carey and Cole 2002, 73784)

Cross, S., September 1997. "Biological and Water Quality Assessments for the Material Disposal Area P Project Area, March 1995–August 1997," Los Alamos National Laboratory document LA-UR-97-3844, Los Alamos, New Mexico. (Cross 1997, 59096)

Edmunds, W., and C. Gaye, 1997. "Naturally High Nitrate Concentrations in Groundwaters from the Sahel," *J. Environ. Qual.,* Vol. 26, pp. 1231–1239. (Edmunds and Gaye 1997, 73714)

Flint, A., L. Flint, J. Hevesi, and D. Hudson, 2001. "Characterization of Arid Land Water-Balance Processes at Yucca Mountain, Nevada," in *Flow and Transport Through Unsaturated Fractured Rock*, D. Evans, T. Nicholson, and T. Rasmussen (Eds), Geophysical Monograph 42, 2nd ed., American Geophysical Union, Washington, D.C., pp. 135–149. (Flint et al. 2001, 73716)

Gardner, J., S. Reneau, C. Lewis, A. Lewis, D. Krier, G. WoldeGabriel, and G. Guthrie, July 2001. "Geology of the Pajarito Fault Zone in the Vicinity of S-Site (TA-16), Los Alamos National Laboratory, Rio Grande Rift, New Mexico," Los Alamos National Laboratory report LA-13831-MS, Los Alamos, New Mexico. (Gardner et al. 2001, 70106).

Hartsough, P., S. Tyler, J. Sterling, and M. Walvoord, 2001. "A 14.6 KYr Record of Nitrogen Flux from Desert Soil Profiles as Inferred from Vadose Zone Pore Waters," *Geophysical Research Letters,* Vol. 28, pp. 2955–2958. (Hartsough et al. 2001, 73713)

Kulander, B., S. Dean, and B. Ward, Jr., 1990. *Fractured Core Analysis: Interpretation, Logging, and Use of Natural and Induced Fractures in Core,* AAPG Methods in Exploration Series, No. 8. The American Association of Petroleum Geologists, Tulsa, Oklahoma. (Kulander 1990, 73718)

Kunkler, J., 1969. "The Sources of Carbon Dioxide in the Zone of Aeration of the Bandelier Tuff near Los Alamos, NM," US Geological Survey Professional Paper 650-B, US Department of the Interior Geological Survey, pp. 184–188. (Kunkler 1969, 11671)

LANL (Los Alamos National Laboratory), February 1995. "TA-16 Material Disposal Area P Closure Plan, Revision 0," Los Alamos National Laboratory document, Los Alamos, New Mexico. (LANL 1995, 58713)

LANL (Los Alamos National Laboratory), 1998. "RCRA Facility Investigation Report for TA-16, PRS 16-021(c)," Los Alamos National Laboratory document LA-UR-98-4101, Los Alamos, New Mexico. (LANL 1998, 59891)

LANL (Los Alamos National Laboratory), June 2003. "Material Disposal Area P Site: Phase I Closure Implementation Report," Los Alamos National Laboratory document LA-UR-02-7002, Los Alamos, New Mexico. (LANL 2003, 76054)

Lewis, C., A. Lavine, S. Reneau, J. Gardner, R. Channel, and C. Criswell, 2002. "Geology of the Western Part of Los Alamos National Laboratory (TA-3 to TA-16), Rio Grande Rift, New Mexico," Los Alamos National Laboratory report LA-13960-MS, Los Alamos, New Mexico. (Lewis et al. 2002, 73785)

McLin, S., August 18, 1989. "Vadose Zone Monitoring Observations at the TA-16, Area P Landfill," draft, Los Alamos National Laboratory Group HSE-8 document, Los Alamos, New Mexico. (McLin 1989, 11718)

Montazer, P., and W. Wilson, 1984. "Conceptual Hydrologic Model of Flow in the Unsaturated Zone, Yucca Mountain, Nevada," *U.S. Geological Survey Water Resources Inv.*, report 84-5345, US Geological Survey, Lakewood, Colorado. (Montazer and Wilson 1984, 73715)

Neeper, D., and R. Gilkeson, 1996. "The Influence of Topography, Stratigraphy, and Barometric Pumping on the Hydrology of Unsaturated Bandelier Tuff," in *The Jemez Mountains Region,* F. Goff, B. Kues, M. Rogers, L. McFadden, and J. Gardner (Eds), New Mexico Geological Society Forty-Seventh Annual Field Conference, September 25–28, 1996, pp. 427–432. (Neeper and Gilkeson 1996, 56025)

Newman, B., 1996. "Vadose Zone Water Movement at Area G, Los Alamos National Laboratory, TA-54: Interpretations Based on Chloride and Stable Isotope Profile," Los Alamos National Laboratory document LA-UR-96-4682, Los Alamos, New Mexico. (Newman 1996, 59372)

Nyhan, J., March 1989. "A Hydrologic Modeling Study of Water Balance Relationships at the Area P Landfill in Los Alamos, New Mexico," Los Alamos National Laboratory report LA-11521-MS, Los Alamos, New Mexico. (Nyhan 1989, 06890)

Pruess K., 2001. "Two-Phase Unsaturated Flow at Yucca Mountain, Nevada: A Report on Current Understanding," in *Flow and Transport Through Unsaturated Fractured Rock,* D. Evans, T. Nicholson, and T. Rasmussen (Eds), Geophysical Monograph 42, second edition, American Geophysical Union, Washington, D.C. pp. 113–133. (Pruess 2001, 73716)

Purtymun, W., F. Koopman, S. Barr, and W. Clements, October 1974. "Air Volume and Energy Transfer Through Test Holes and Atmospheric Pressure Effects on the Main Aquifer," Los Alamos National Laboratory report LA-5725-MS, Los Alamos, New Mexico. (Purtymun et al. 1974, 05477)

Robinson, B., and G. Bussod, 2000. "Radionuclide Transport in the Unsaturated Zone at Yucca Mountain: Numerical Model and Preliminary Field Observations," in *Dynamics of Fluids in Fractured Rock,* B. Faybishenko, P. Witherspoon, and S. Benson (Eds), Geophysical Monograph 122, second edition, American Geophysical Union, Washington, D.C., pp. 323–336. (Robinson and Bussod 2000, 73717)

Rogers, D., B. Gallaher, and E. Vold, 1996. "Vadose Zone Infiltration Beneath the Pajarito Plateau at Los Alamos National Laboratory," in *The Jemez Mountains Region,* F. Goff, B. Kues, M. Rogers, L. McFadden, and J. Gardner (Eds), New Mexico Geological Society Forty-Seventh Annual Field Conference, September 25–28, 1996, pp. 413–420. (Rogers et al. 1996, 55543)

Su, G., J. Geller, K. Pruess, and J. Hunt, 2000. "Overview of Preferential Flow in Unsaturated Fractures," in *Dynamics of Fluids in Fractured Rock*, B. Faybishenko, P. Witherspoon, and S. Benson (Eds), Geophysical Monograph 122, second edition, American Geophysical Union, Washington, D.C., pp. 147–155. (Su et al. 2000, 73717)

Su, G., J. Geller, K. Pruess, and F. Wen, 1999. "Experimental Studies of Water Seepage and Intermittent Flow in Unsaturated, Rough-Walled Fractures," *Water Resources Research,* Vol. 35, pp.1019–1037. (Su et al. 1999, 63765)

Tsang, C., Y. Tsang, J. Birkholzer, and L. Morena, 2001. "Dynamic Channeling of Flow and Transport in Saturated and Unsaturated Heterogeneous Media," in *Flow and Transport Through Unsaturated Fractured Rock*, D. Evans, T. Nicholson, and T. Rasmussen (Eds), Geophysical Monograph 42, second edition, American Geophysical Union, Washington, D.C., pp. 33–44. (Tsang et al. 2001, 73716)

Vaniman, D., S. Chipera, D. Bish, M. Duff, and D. Hunter, 2002. "Crystal Chemistry of Clay-Mn Oxide Associations in Soils, Fractures, and Matrix of the Bandelier Tuff, Pajarito Mesa, New Mexico," *Geochemica et Cosmochemica Acta*, Vol. 66, No. 8., pp. 1349–1374. (Vaniman et al. 2002, 73280)

Vaniman, D., and S. Chipera, 1995. "Mesa-Penetrating Fractures, Fracture Mineralogy, and Projected Fault Traces at Pajarito Mesa," in *Geological Site Characterization for the Proposed Mixed Waste Disposal Facility, Los Alamos National Laboratory,* S. Reneau and R. Raymond, Jr. (Eds), Los Alamos National Laboratory report LA-13089-MS, Los Alamos, New Mexico, pp. 71–85. (Vaniman and Chipera 1995, 54709)

Weeks, E., 2001. "Effect of Topography on Gas Flow in Unsaturated Fractured Rock: Concepts and Observations," in *Flow and Transport Through Unsaturated Fractured Rock*, D. Evans, T. Nicholson, and T. Rasmussen (Eds), Geophysical Monograph 42, second edition, American Geophysical Union, Washington, D.C., pp. 53–59. (Weeks 2001, 73716)

Appendix A

Field Boring Logs, Lithologic Field Logs

BORING LOG

SITE ID: 273-GP

CLIENT: LANL
SITE NAME: MDA-P Landfill
PROJECT NO.: PHASE II
DRILLING CO.: BMS Drilling
LOGGED BY: Gary Steopes

ELEV. (GRND): 7,400 (TOC):
NORTHING:
EASTING:
DEPTH TO WATER (bgs):
TOTAL BORING DEPTH (bgs): ~~2 in.~~ Initial 170' Final
DRILL METHOD: CORE
SITE TYPE: Well ( ) Boring (X) Pipe ( ) Other:
Page 1 of 3
DATE:

Hole collapsed Final T.D. = 145.8'

	SAMPLE INTERVAL (ft) FROM	TO	RECOVERY (in)	BLOWS	GRAPHIC COLUMN	XRF ppm	HE TEST KIT	LITHOLOGIC DESCRIPTION & COMMENTS
8/7/01	0	9.5	55					QTB-4. lt. BRN to TAN SOFT non-welded
								Tuff. Dull Red pumice evident, Horizontal
								to High angle Fractures 1-4' BRNish
								Residue on Fracture surfaces. @ ~4.9-5.0'
								andesitic lithic got caught in core barrel
								and Recovery was lost 5-9.5'
8/8/01	9.5	19.6	30					V. SOFT NON-welded Tuff only 30%
								Recovery core Broken up by Drilling
								Dull yellow weathering Rinds evident.
	19.6	29.6	70					AS Above, Better Recovery
	29.6	39.6	60					SOFT NON-welded Tuff lt pinkish BRN
								to TAN yellowish-white weathering Rinds
								Numerous Drilling Breaks
	39.6	49.8	100					STARTS NON-welded Tuff ~39.6'
								Transitions to welded Tuff @ ~42'
								welded Tuff DK Red BRN
	49.8	60	90					Less welded Than above from 50'
								High angle foot long Fracture @~50-51'
								welding/Hardness varies

LEGEND

Graphic	Soil Type

WESTON
MANAGERS DESIGNERS/CONSULTANTS

BORING LOG

SITE ID: 273-GP

Page 1 of 3

CLIENT: LANL
SITE NAME: MDA-P Landfill
PROJECT NO.: Phase II
DRILLING CO.: BMS Drilling
LOGGED BY: Gary Stoopes

ELEV. (GRND): 7,400 (TOC):
NORTHING:
EASTING:
DEPTH TO WATER (bgs):
TOTAL BORING DEPTH (bgs): ~~2 in.~~ 170'
Initial

DATE:
DRILL METHOD: CORE 2 in
SITE TYPE: Well ( ) Boring (X) Piezo ( ) Other:

	SAMPLE INTERVAL (ft) FROM	TO	RECOVERY (%)	BLOW COUNTS	GRAPHIC DESCRIPTION	XRF ppm	HE TEST KIT	LITHOLOGIC DESCRIPTION & comments
8/8/01	60	70	30					Soft, Fractured Non welded Tuff, High
								Angle Fracture 60.5 - 62'. No Recovery
								62-70'
	70	79.6	70					Non welded Tuff Brn Gray, No Recovery
								70-72.8' Drilling Breaks throughout
								core
								START 81.1
8/9/01	79.6	89.6	72					@ 80 ft Transition to welded Tuff lost
			85					core 79.6-~~82.4~~' of Transition zone @
								~~82.4~~-83' welded Reddish brn Tuff, Hard
								with increase in xtals. Numerous Drilling
								Breaks especially below 85'
	89.6	99.5	95					Dense, Hard xtals rich Tuff reddish
								brn welded
	99.5	109.5	45					As above High angle Fracture filled with
								clayey material 103.8 - 105'
8/14/01	109.5	119.0	70					welded xtals rich Red brn Tuff, Large
								Fracture 112 - 116' No Recovery 113.3-
								115.7' clayey material abundant @ end of
								Fracture ~ 115.9'

LEGEND

Graphic	Soil Type

WESTON
MANAGERS DESIGNERS/CONSULTANTS

BORING LOG

SITE ID: 273-GP

Page 3 of 3

CLIENT: LANL
SITE NAME: MDA-P Landfill
PROJECT NO.: Phase II
DRILLING CO.: BMS Drilling
LOGGED BY: Gary Steopes

ELEV. (GRND): 7,400 (TOC):
NORTHING:
EASTING:
DEPTH TO WATER (bgs):
TOTAL BORING DEPTH (bgs): ~~210~~ 170' Ad.

DATE: 8/15/01
DRILL METHOD: CORE 2in
SITE TYPE: Well ( ) Boring (X) Piezo ( ) Other:

Initial

	SAMPLE INTERVAL (ft) FROM	TO	RECOVERY DEPTH (ft) (ft)	(ft)	GRAPHIC COLUMN	XRF PPM	HE TEST KIT	LITHOLOGIC DESCRIPTION & comments
8/15/01	119.0	129.0	0					No Recovery Drilled 10' very easily possible surge Beds (?)
	129	139.5	0					No Recovery, Possible unconsolidated material or soft unwelded Tuff
	139.5	149.5	0					No Recovery, as above
	149.5	159	0					No Recovery, as above
	159	170	0					No Recovery as above. Got stuck @ ~ 170' Also got stuck @ ~80-75' when pulling drill stem, Decided to stop drilling @ 170' will not risk getting stuck for extra 10'.

LEGEND

Graphic	Soil Type

WESTON
MANAGERS DESIGNERS/CONSULTANTS

SENT 1 7-17- 1 14:23

BORING LOG

Page 1
DATE: 8

	SAMPLE INTERVAL (ft) FROM	TO	RECOVERY (ft)	BLOWS (ft)		ppm		LITHOLOGIC DESCRIPTION & comments
8/17/01	0	9.5	5		QTB-4			V little Recovery core Barrel clogged air circulation cutoff. Soft non welded Tuff
	9.5	19.5	95					Soft non to partially welded Tuff Dull Reddish pumice, Gray lithics evident Tan to lt brn. Natural Fractures @ 10.5 13.5; 13.7 & 17.2'
	19.5	29.5	~50					Soft non-welded Tuff lt brn to TAN Dull red pumice
	29.5	39.5	0					No Recovery, Assume as above.
8/20/01	39.5	49.5	35					Soft non to partially welded Tuff QTB-4 yellowish brn Halos evident by lithic Fragments to gray to red brn pumice. only 35% Rec. lost on Ground up last 6ft.
	49.5	59.5	68					Tuff as above To 56.0' Then QTB-3T dense Hard welded Tuff.
				55	QTB-3T			

LEGEND

Graphic	Soil Type

WESTON
MANAGERS DESIGNERS&CONSULTANTS

BORING LOG

SITE ID: 257-GP

Page 2 of 3

CLIENT: LANL
SITE NAME: MDA-P Landfill
PROJECT NO.: phase II
DRILLING CO.: BMS Drilling
LOGGED BY: Gary Stoopes

ELEV. (GRND): 7,400 (TOC):
NORTHING:
EASTING:
DEPTH TO WATER (bgs):
Initial TOTAL BORING DEPTH (bgs): 180
Final T.D. = 158?

DATE: 8/21/01
DRILL METHOD: CORE
SITE TYPE: Well ( ) Boring (X) Piezo ( ) Other:

	SAMPLE INTERVAL ON FROM	TO	RECOVERY INFER ON %	▲	GEOLOGIC UNIT	XRF ppm	HE TEST KIT	LITHOLOGIC DESCRIPTION & comments
8/20/01	59.5	69.5	28		QTB-3T			Dense Hard welded Tuff QTB-3T only 28% recovery. Lost most in first part
				66				of drilling and last. Drilled easy
					QTB-3			last few feet. Probably Transition to QTB-3
8/21/0	69.5	79.5	80					DK Gray Partially welded Tuff. QTB-3
	79.5	89.5	80					DK gray Partially welded Tuff QTB-3
								Increase in mafic xtals Abundant Sanidine
	89.5	99.5	85					As above to ~ 93 ft Transition to
				96				more Densely welded Tuff 93-95'
					QTB-2			Becoming Hard, dense Reddish Brn by
								~ 96 ft.
	99.5	109.5	90					QTB-2 Dense Hard welded Tuff
01	109.5	119.5	91					As above Some lithics evident ~ 119'
								Fracture @ ~ 114.5 with Clayey filling
	119.5	129.8	100					Dense Hard welded Tuff Reddish gray,
								few lang lithics

LEGEND

Graphic	Soil Type

WESTON
MANAGERS DESIGNERS/CONSULTANTS

SENT

BORING LOG

SITE ID: 257-GP

Page 3 of 3

CLIENT: LANL
SITE NAME: MDA-P Landfill
PROJECT NO.: phase II
DRILLING CO.: BMS Drilling
LOGGED BY: Gary Stoopes

ELEV. (GRND): 7,400 (TOC):
NORTHING:
EASTING:
DEPTH TO WATER (bgs):
Initial TOTAL BORING DEPTH (bgs): 180
Final T.D = 158.7

DATE: 8/23/01
DRILL METHOD: CORE
SITE TYPE: Well ( ) Boring (X) Piezo ( ) Other:

	SAMPLE INTERVAL (ft) FROM	TO	RECOVERY (ft)	DEPTH (ft)		XRF PPM	HE TEST KIT	LITHOLOGIC DESCRIPTION & comments
8/23/01	129.8	139.9	100		CRB-2			Dense Hard welded Tuff As above to ~ 132.5 Then gradually becomes less welded. @ ~ 134' only partially welded 135' ~ Non welded Tuff Color change Through Transition Zone from Med. Gray to Reddish gray - Red brn
	139.9	149.5	25					Non welded Tuff becoming Softer Xtals Rich mafic xtals evident dominant gray pumice.
					?			
	149.5	160						No Recovery U. Soft Rock
	160	170			?			No Recovery U. Soft Rock
	170	180						No Recovery Drilled to ~180'
								Measured Borehole 8:50 on 8/24/01 T.D. = 158.7' 22 feet of Hole collapsed

LEGEND

Graphic	Soil Trac

WESTON MANAGERS DESIGNERS/CONSULTANTS

SENT BY 7- 1 14:23

BORING LOG

SITE ID: S16-BH

CLIENT: LANL
SITE NAME: MDA-P Landfill
PROJECT NO. PHASE II
DRILLING CO.: BMS Drilling
LOGGED BY: Gary Stoopes

ELEV. (GRND): 7,400 (TOC):
NORTHING:
EASTING:
DEPTH TO WATER (bgs):
TOTAL BORING DEPTH (bgs): 33.7
Initial TD = 32.0 8/30/01

Page 1 of 1
DATE: 8/27/01
DRILL METHOD: CORE
SITE TYPE: Well ( ) Boring (X) Piezo ( ) Other:

SAMPLE INTERVAL (ft) FROM	TO	RECOVERY (%)	DEPTH (ft)	GRAPHIC DESIGN	XRF ppm	HE TEST KIT	LITHOLOGIC DESCRIPTION & comments
0	3	80		QTB-4			STARTS NON to partially welded Tuff
			1.3				Fairly soft pinkish TAN gray pumice
				QTB-3T			evident, QTB-4 @ ~ 1-1.5' Transition
							to QTB-3T welded dense Hard Tuff
							DK reddish brown.
3.0	9.8	95					QTB-3T As above probable large
							Fracture ~8' no recovery 7.3-8.6
							Fracture @ ~ 9.5' with clayey filling.
9.8	15	100					QTB-3T As Above numerous Fractures
15	19.8	85					QTB-3T As Above Good Fracture
							@ ~16.5' filled with clayey material,
							Tuff becoming softer less welded ~18.0'
			18	QTB-3			QTB-3 @ ~18'
19.8	29.9	100					NON to partially welded Tuff Fracture
							@ 29.5' filled with clayey material
29.9	33.7	100					Soft QTB-3 Fracture Along entire length
							To 33.6' TD 33.7

LEGEND

Graphic	Soil Type

WESTON
MANAGERS DESIGNERS/CONSULTANTS

BORING LOG

SITE ID: 526

CLIENT: LANL
SITE NAME: MDA-P Landfill
PROJECT NO.: PHASE II
DRILLING CO.: BMS Drilling
LOGGED BY: Gary Stoopes

ELEV. (GRND): 7,400 (TOC):
NORTHING:
EASTING:
DEPTH TO WATER (bgs): DR
TOTAL BORING DEPTH (bgs): ~~2~~ 59.4

Page 1 of 2
DATE: 7/18/01
DRILL METHOD: USCD Foam/water core 2 in
SITE TYPE: Well ( ) Boring (X) Piezo. ( ) Other:

	SAMPLE INTERVAL (ft) FROM	TO	RECOVERY (cm)	SAMPLE NO.	GRAPHIC DESCRIPTION	XRF PPM	HE TEST KIT	LITHOLOGIC DESCRIPTION & COMMENTS
7/18/01	0	1	100	1				Soft non welded pinkish Red Bandelier
								Tuff QTB-4 Fracture at .9' mm
								wide filled with DK brn-black material.
	1	3.2	100	3.2				Hard welded Tuff @ ~ 2' Fractures @
								1.9' & 2.4' QTB-3
	3.2	5.2		5.2				DK Reddish brn welded Tuff. No Recovery
								4.8-5.2' core broken by Drilling.
	5.2	7.2		7.2				No Recovery 4.8-5.7. Tuff as above.
	7.2	8.3	100	8.3				Tuff As Above
	8.3	10.2	100	10.2				Tuff As Above
	10.2	20.2	100	20.2				Dense Hard welded Tuff Red brn.
								Numerous fractures mm wide filled with
								material
	20.2	26.7	100	26.7				Mod welded Red brn Tuff Fractures @
								20' / 23.5' / 24.9' / 25.7 cm wide
								Fracture at 25.7' filled with Brn material
7/20/01	26.7	30.2	100	30.2				Med-welded Red brn Tuff Steep angle
								Fracture 27.5-28.4' Tuff becoming
								less welded Dense

LEGEND

Graphic	Soil Type

WESTON
MANAGERS DESIGNERS/CONSULTANTS

BORING LOG

SITE ID: 526

CLIENT: LANL
SITE NAME: MDA-P Landfill
PROJECT NO.: Phase II
DRILLING CO.: BMS Drilling
LOGGED BY: Gary Steepes

ELEV. (GRND): 7,400 (TOC):
NORTHING:
EASTING:
DEPTH TO WATER (bgs): 2nd.
TOTAL BORING DEPTH (bgs): ~~39.7~~ 59.4

Page 2 of 2
DATE: 7/20/01
DRILL METHOD: CORE 2 inch
SITE TYPE: Well ( ) Boring (X) Piezo. ( ) Other:

	SAMPLE INTERVAL (ft) FROM	TO	RECOVERY (%)	BLOW COUNTS	GRAPHIC COLUMN	XRF PPM	HE TEST KIT	LITHOLOGIC DESCRIPTION & COMMENTS
7/20/01	30.2	38.5	100					Red brn. mod to slightly to non welded Tuff.
								Tuff becoming less welded, dense past ~30'
								Gradual color change from Red brn to
								Med Gray ~ 36'
8/1/01	38.5	45.5	90					Partially to non welded Med Gray Tuff
								soft, fractured ~ 39' Poor to no Recovery
								Small fracture with drillfilling material
								@ ~ ~~45~~ 44.8'
	45.5	55	50%					Partially to mod to welded Tuff.
								Transition zones ~ 45'/@ 53-54' Tuff
								Becomes Hardest welded @ ~ 54'. less
								pumice more xtalline at ~ 45-46'. less
								Recovery at Transition zones
	55	59.4	90					Hard welded Tuff all "Fractures" due to
								drilling

LEGEND

Graphic	Soil Type

WESTON
MANAGERS DESIGNERS/CONSULTANTS

SENT B

BORING LOG

SITE ID: 554-BH

Page 1 of 2

CLIENT: LANL
SITE NAME: MDA-P Landfill
PROJECT NO.: phase II
DRILLING CO.: BMS Drilling
LOGGED BY: Gary Stoopes

ELEV. (GRND): 7,400 (TOC):
NORTHING:
EASTING:
DEPTH TO WATER (bgs):
TOTAL BORING DEPTH (bgs): 100'
Initial T.D.= 96.5' measured 8/30/01

DATE: 8/28/01
DRILL METHOD: CARE
SITE TYPE: Well ( ) Boring (X)
Piezo ( ) Other:

SAMPLE INTERVAL (ft) FROM	TO	RECOVERY (%)	DEPTH (ft)	GRAPHIC COLUMN	XRF PPM	HE TEST KIT	LITHOLOGIC DESCRIPTION & comments
0	9.6	100		QTB-4			QTB-4 first ~1.5' Partially welded
			1.5				Tuff pink TAN @ ~1.5 welded Tuff
				QTB-3T			Reddish Gray Hard Dense Fractures @
							1.7' and 8.4'
9.6	19.7	100					QTB-3T As above Fracture @ 15.7'
							Tuff becomes less welded past 16'
			17				@ ~17' partially to non-welded Tuff
				QTB-3			QTB-3 More lithics gray pumice
19.7	39.7	100					QTB-3 partially welded To non-welded Tuff DK reddish brn.
39.7	39.1	95					QTB-3 non welded Tuff. lithics
							evident, Fractures with filling @ 37.5'
							38 - 39'
39.1	49.5	65					QTB-3 As above Becoming more vitric
							Rich Large Fracture with clayey
			46				Filling @ 44.3 - 44? feet Lost recovery
				QTB-2			Tuff harden more welded by ~46.5'
							Brittle? broken core by drilling 46 - 49.0'
							QTB-2 Large lithic @ ~47'

LEGEND

Graphic	Soil Type

WESTON
MANAGERS DESIGN&CONSULTANTS

SENT B

BORING LOG

SITE ID: 554-BH

Page 1 of 2

CLIENT: LANL
SITE NAME: MDA-P Landfill
PROJECT NO.: Phase II
DRILLING CO.: BMS Drilling
LOGGED BY: Gary Stoopes

ELEV. (GRND): 7,400 (TOC):
NORTHING:
EASTING:
DEPTH TO WATER (bgs):
Initial TOTAL BORING DEPTH (bgs): 100'

DATE: 8/29/01
DRILL METHOD: CORE
SITE TYPE: Well ( ) Boring (X) Piezo. ( ) Other:

SAMPLE INTERVAL (ft) FROM	TO	RECOVERY (ft)	BLOW COUNTS	GRAPHIC COLUMN	XRF ppm	HE TEST KIT	LITHOLOGIC DESCRIPTION & comments
8/29/01 49.5	59.4	95		QTB-2			Partially welded Tuff Med Gray to Med Reddish Gray lithics evident. Grayish green pumice More mafic xtals than QTB-3 Fractures, one @ ~52.5' has some clayey filling/residue
59.4	69.6	100					QTB-2 partially to fully welded Tuff. Some cm size lithics, pumice Numerous drilling Fractures.
69.6	79.7	100					QTB-3 welded Tuff As above wide High angle clay filled Fracture ~76-78'
79.7	89.5	98					Tuff as Above to ~ 85.5' Then Tuff becomes gradually softer NON-welded @ 87' V. Soft xtals Rich Tuff mafic xtals Abundant
89.5	99.5	0					No Recovery Very easy drilling.
							T.D = 96.5 measured on 8/30/01 ~ 3.5' of Hole collapsed.

LEGEND

Graphic	Soil Type

WESTON MANAGERS DESIGNERS/CONSULTANTS

BORING LOG

SITE ID: 557

CLIENT: LANL
SITE NAME: MDA-P Landfill
PROJECT NO.: PHASE II
DRILLING CO.: BMS Drilling
LOGGED BY: Gary Steepes

ELEV. (GRND): 7,400 (TOC):
NORTHING:
EASTING:
DEPTH TO WATER (bgs): DR
TOTAL BORING DEPTH (bgs): ~~71~~ 69.5'
DRILL METHOD: AIR ONLY CORE
SITE TYPE: Well ( ) Boring (X) Piezo ( ) Other:

Page 1 of 2
DATE: 9/2/01

SAMPLE INTERVAL (ft) FROM	TO	RECOVERY (ft)	RECOVERY (%)	GRAPHIC COLUMN	XRF PPM	HE TEST KIT	LITHOLOGIC DESCRIPTION & COMMENTS
0	9.7	100					Soft NON to partially welded pinkish
							Tuff 0 - ~ 1 foot Transition To
							Darkish Gray mod welded Tuff (QTB-3)
							Fractures @ .3' and @ 8.6' 0 - ~1ft
							QTB-4 1.5 → 9.7 QTB-3
9.7	19.4	100					QTB-3 mod to partially welded Tuff becomes
							softer @ ~ 15'. Fracture @ 12.1' & 15.5'
							Probable Fracture(s) @ ~ 19.4'
19.4	29.4	100					QTB-3 partially to NON welded Tuff
29.4	39.5	90					Partially To NON welded Tuff V soft
							Broken/Fracture 37 - 38' 37.4 - 38.4
							little to no Recovery.
39.5	49.5	90					NON welded Tuff To partially weld Tuff
							39.5 - ~47 Tuff Becomes harder more
							welded 47 - 49'

LEGEND

Graphic	Soil Type

WESTON
MANAGERS DESIGNERS/CONSULTANTS

BORING LOG

SITE ID: 557

CLIENT: LANL
SITE NAME: MDA-P LANL II
PROJECT NO.: Phase II
DRILLING CO.: BMS Drilling
LOGGED BY: Gary Stoopes

ELEV. (GRND): 7,400 (TOC):
NORTHING:
EASTING:
DEPTH TO WATER (bgs): NA
TOTAL BORING DEPTH (bgs): ~~71m~~ 69.5'
DRILL METHOD: CORE
SITE TYPE: Well ( ) Boring (X) Piezo. ( ) Other:

Page 2 of 2
DATE: 8/2/01

	SAMPLE INTERVAL (ft) FROM	TO	RECOVERY INTERVAL (ft) %		GRAPHIC COLUMN	XRF PPM	HE TEST KIT	LITHOLOGIC DESCRIPTION & comments
8/2/01	49.5	60	80					partially welded to welded Tuff
								soft @ 50 becoming harder more
								welded @ 55 - 60 Broken/Fractured
								56 - 58'
	60	69.5	70					Partially welded To mod welded Tuff
								DK Gray, xtals. Rich Tuff natural
								Fracture 60.9', 64.1' - 64.6 number
								of Fractures. Transition To Red brn
								Matrix in Tuff @ ~ 65'. Natural Fracture
								@ ~ 66' with clay filling. Last ~ 3 ft
								broken up Fractured No real recovery.

LEGEND

Graphic	Soil Type

WESTON
MANAGERS DESIGNERS/CONSULTANTS

SENT BY

BORING LOG

SITE ID:

CLIENT: LANL
SITE NAME: MDA-P Landfill
PROJECT NO.: Phase II
DRILLING CO.: BMS Drilling
LOGGED BY: Gary Stoopes

ELEV. (GRND): 7,400 (TOC):
NORTHING:
EASTING:
DEPTH TO WATER (bgs):
TOTAL BORING DEPTH (bgs):

Page of
DATE:
DRILL METHOD: CORE
SITE TYPE: Well ( ) Boring (X) Piezo. ( ) Other:

SAMPLE INTERVAL (ft) FROM	TO	RECOVERY (%)	INTERVAL (ft)	GRAPHIC COLUMN	XRF PPM	HE TEST KIT	LITHOLOGIC DESCRIPTION & comments

LEGEND

Graphic	Soil Type

WESTON
MANAGERS DESIGNERS/CONSULTANTS

SENT BY 7-17 14:23

BORING LOG

SITE ID:

CLIENT: LANL
SITE NAME: MDA-P Landfill
PROJECT NO.: phase II
DRILLING CO.: BMS Drilling
LOGGED BY: Gary Stoopes

ELEV. (GRND): 7,400 (TOC):
NORTHING:
EASTING:
DEPTH TO WATER (bgs):
TOTAL BORING DEPTH (bgs):

Page of
DATE:
DRILL METHOD: CORE
SITE TYPE: Well ( ) Boring (X) Piezo. ( ) Other:

SAMPLE INTERVAL (ft) FROM	TO	RECOVERY (ft)	DEPTH (ft)	GRAPHIC COLUMN	XRF ppm	HE TEST KIT	LITHOLOGIC DESCRIPTION & comments

LEGEND

Graphic	Soil Type

WESTON
MANAGERS DESIGNERS/CONSULTANTS

BORING LOG

SITE ID:

CLIENT:
SITE NAME:
PROJECT NO.:
DRILLING CO.:
LOGGED BY:

ELEV. (GRND): (TOC):
NORTHING:
EASTING:
DEPTH TO WATER (bgs):
TOTAL BORING DEPTH (bgs):

Page of
DATE:
DRILL METHOD:
SITE TYPE: Well ( ) Boring ( )
Piezo ( ) Other:

SAMPLE INTERVAL (ft)		RECOVERY DEPTH (ft)		GRAPHIC COLUMN	REMARKS	COLOR	LITHOLOGIC DESCRIPTION
FROM	TO	(ft)	%		PID		

LEGEND

Graphic	Soil Type

WESTON
MANAGERS DESIGNERS/CONSULTANTS

BMS Drilling Co.
Daily Billing and Tracking Sheet
For Roy F. Weston Inc.
Contract 2982-U0017
MDA-P Closure Phase II Sampling

Driller: **Equipment:** **Date:**
Helper: **Comments:**

Field Use Only

No.	Grid ID	Vert. Setup	Core LF	Angle Setup	Core LF	Grout LF
1						
2						
3						
4						
5						
6						
7						
8						
9						
10						
11						
12						
13						
14						
15						
Subtotal						
Other						
Standby	St. Time		End Time			
					Hours	

Comments: _____

BMS Site Rep. _____ **Date:** _____

RFW Site Rep. _____ **Date:** _____

Field Totals						
Contract Rate		$	$	$	$	$
SUBTOTAL		$	$	$	$	$
Other					$	$
Standby				Hrs @	$	$

TOTAL $

Prepared by: _____ **Date:** _____

Accepted by: _____ **Date:**

Areap\BMS Drilling1.doc page __ of rev.06/18/01

BMS Drilling Co.
Daily Billing and Tracking Sheet
For Roy F. Weston Inc.
Contract 2982-U0017
MDA-P Closure Phase II Sampling

Driller: Equipment: Date:
Helper: Comments:

Field Use Only

No.	Grid ID	Vert. Setup	Core LF	Angle Setup	Core LF	Grout LF
1						
2						
3						
4						
5						
6						
11						
12						
13						
14						
15						
	St. Time		End Time			
					Hours	

Comments: _____

BMS Site Rep. _____ Date: _____

RFW Site Rep. _____ Date: _____

Administrative Use Only

Field Totals						
Contract Rate		$	$	$	$	$
SUBTOTAL		$	$	$	$	$
Other					$	$
Standby				Hrs @	$	$

TOTAL $

Prepared by: _____ Date: _____

Accepted by: _____ Date

Areap\BMS Drilling1.doc page of rev.06/18/01

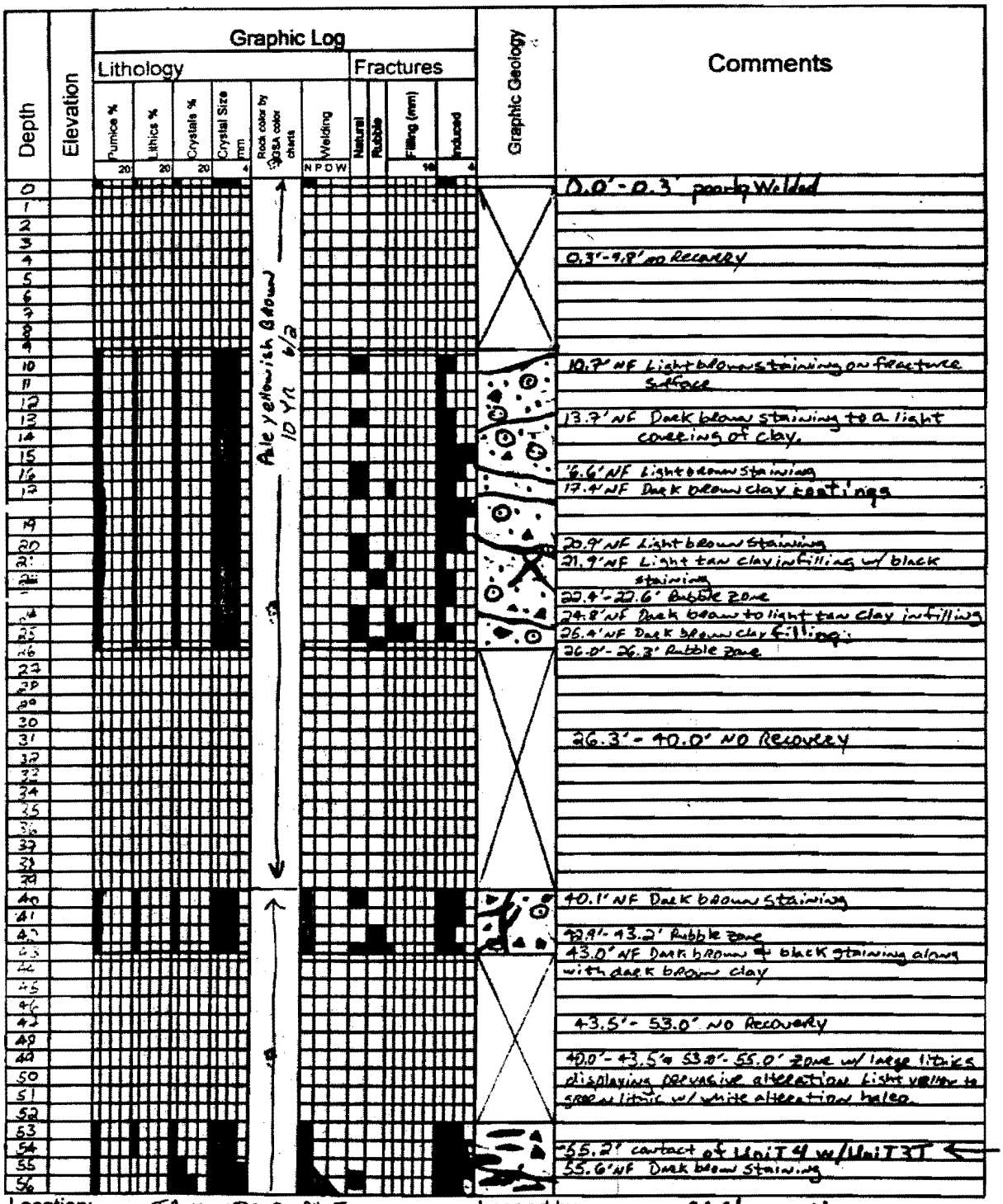

Location: TA-16 MDA-D PH II
Borehole No.: 257-GP
Total depth: 180'
Surface elevation: 7464.2

Logged by: RAChennell
Reviewed by: CWCriswell
date: 9/6/01

Page 1 of 3.

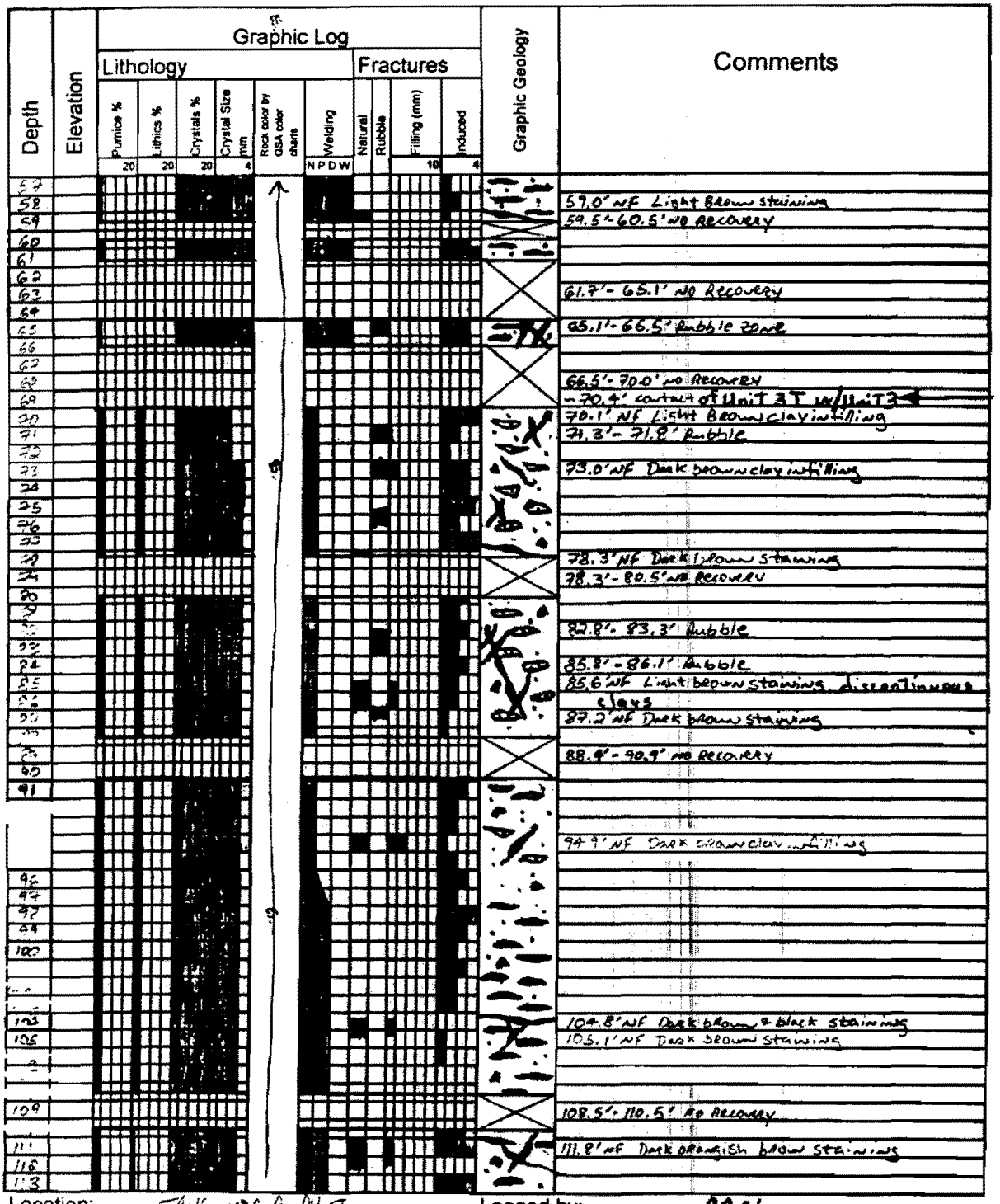

Location: TA-16 MDA-P PH II
Borehole No.: 257-GP
Total depth: 180'
Surface elevation: 7464.2

Logged by: RAGhonnell
Reviewed by: CW Criswell
date: 9/6/01

Page 2 of 3.

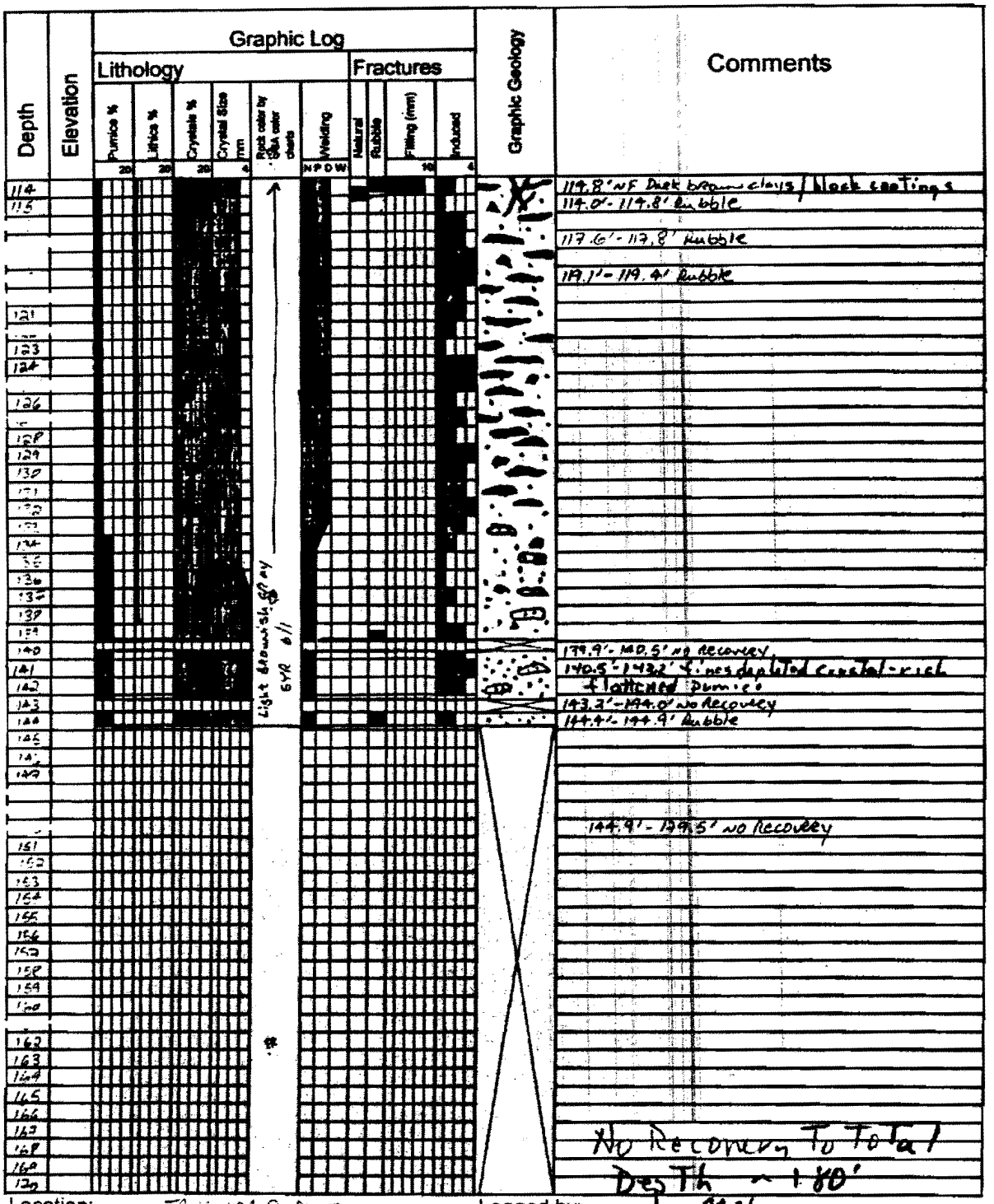

Location: TA-16 MDA-P PH I
Borehole No.: 257-GP
Total depth: 180'
Surface elevation: 7464.2

Logged by: RAChannell
Reviewed by: CW/Criswell
date: 9/6/01

Page 3 of 3.

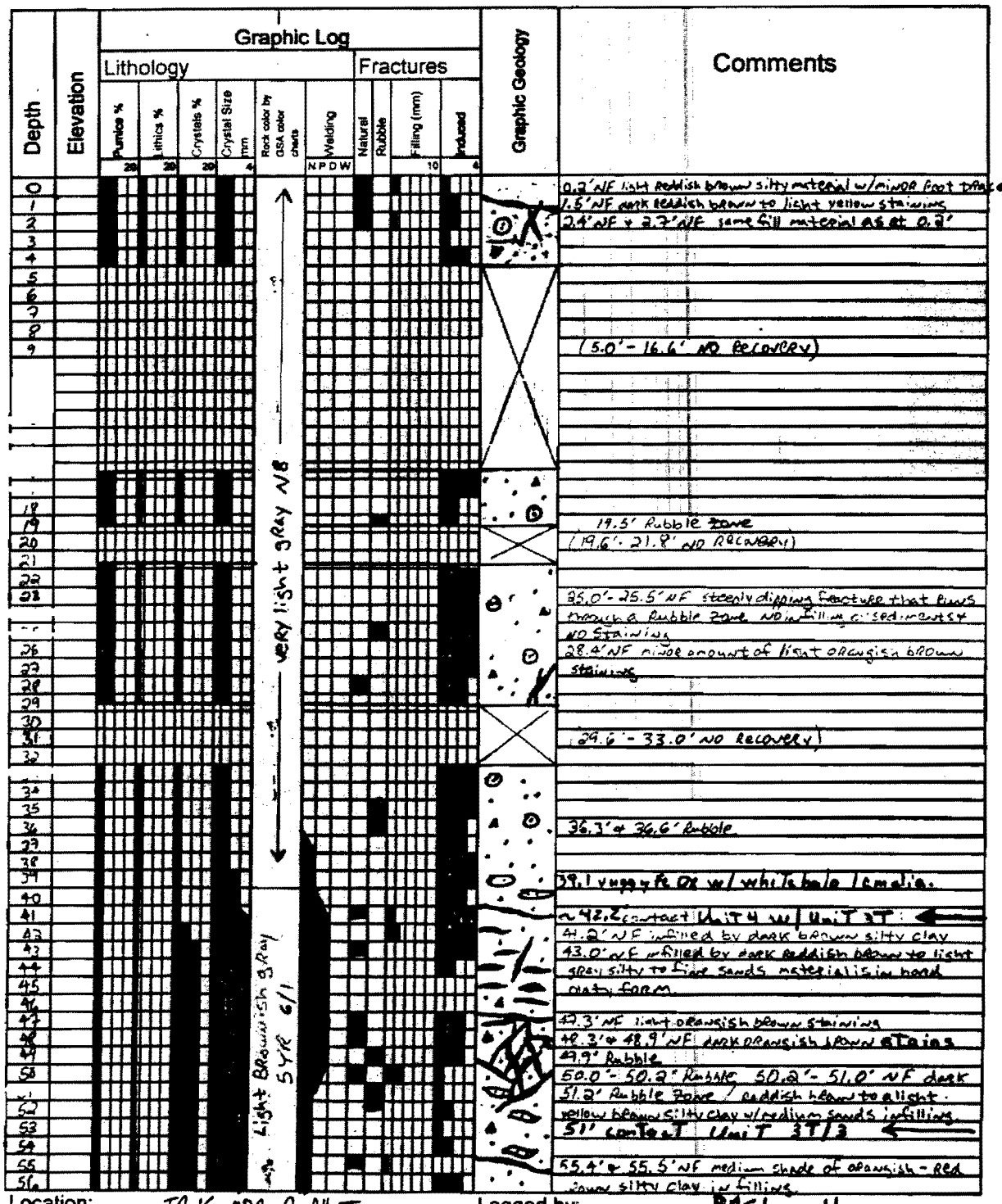

Location: TA-16 MDA-P PH II
Borehole No.: 273-GP
Total depth: 120'
Surface elevation: 7452.8'

Logged by: RAChannell
Reviewed by: PWRapison II
date: 9/20/01

Page 1 of 3

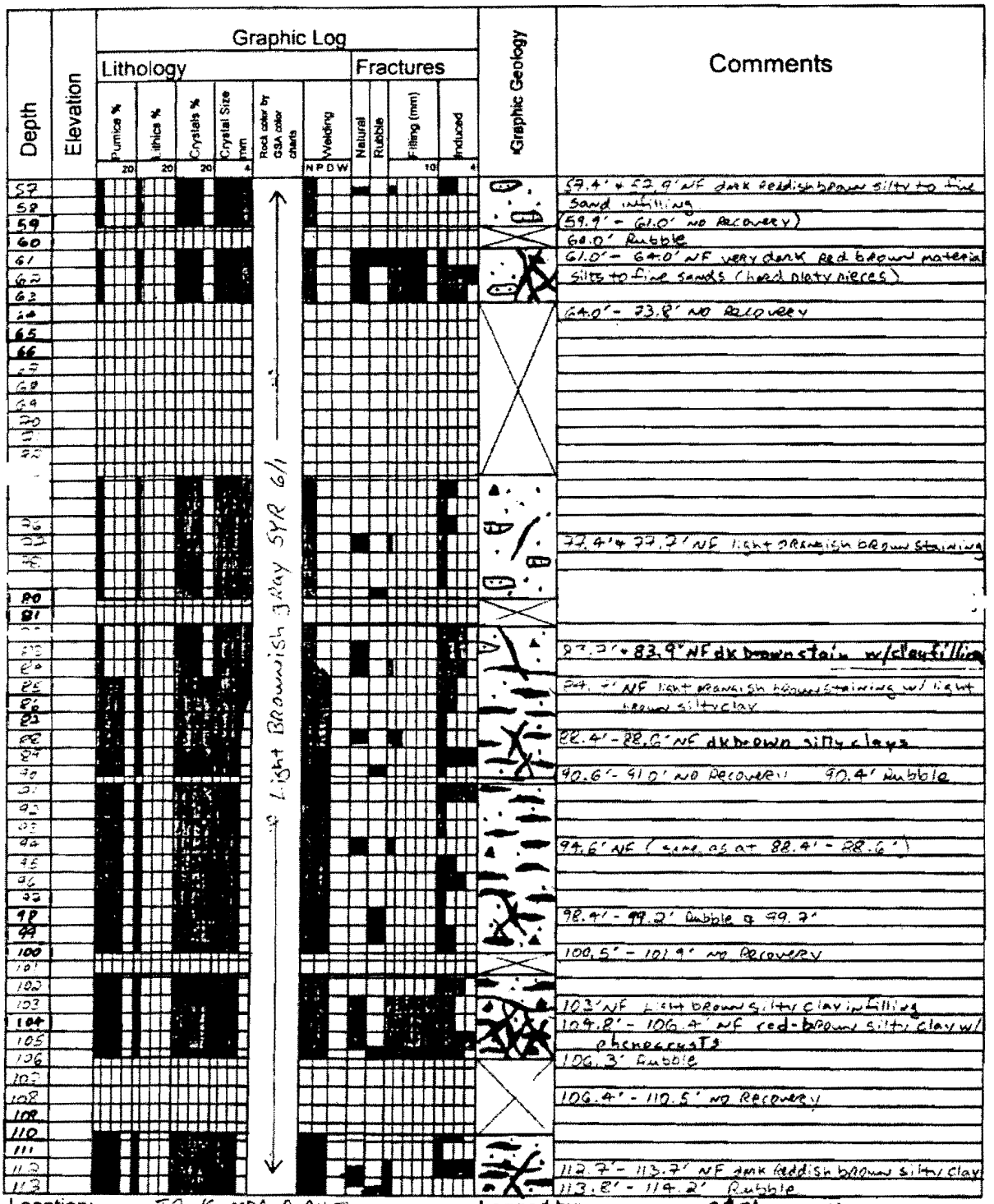

Location: TA-16 MDA-P PH II
Borehole No.: 273-GP
Total depth: 120'
Surface elevation: 7452.8'

Logged by: RAChanne II
Reviewed by: CWPrisnell
date: 9/20/01

Page 2 of 3

Depth	Elevation	Graphic Log: Lithology: Pumice % (20)	Lithics % (20)	Crystals % (20)	Crystal Size mm (4)	Rock color by GSA color charts	Welding (N P O W)	Fractures: Natural	Rubble	Filling (mm) (10)	Induced (4)	Graphic Geology	Comments
114													(114.3' - 116.9' NO RECOVERY)
115													116.9' - 117.4' NF dk brown silty clay
						Light Brownish Gray 5YR 6/1							117.6' NF dark brown silty clay coating
													119.5' - 120.0' Rubble - crystalinity increasing - fines decreasing
119													
120													

Location: TA-16 MDA-P PH II
Borehole No.: 293-GP
Total depth: 120'
Surface elevation: 7452.8'

Logged by: RAChennell
Reviewed by: CWCriswell
date: 9/20/01

Page 3 of 3

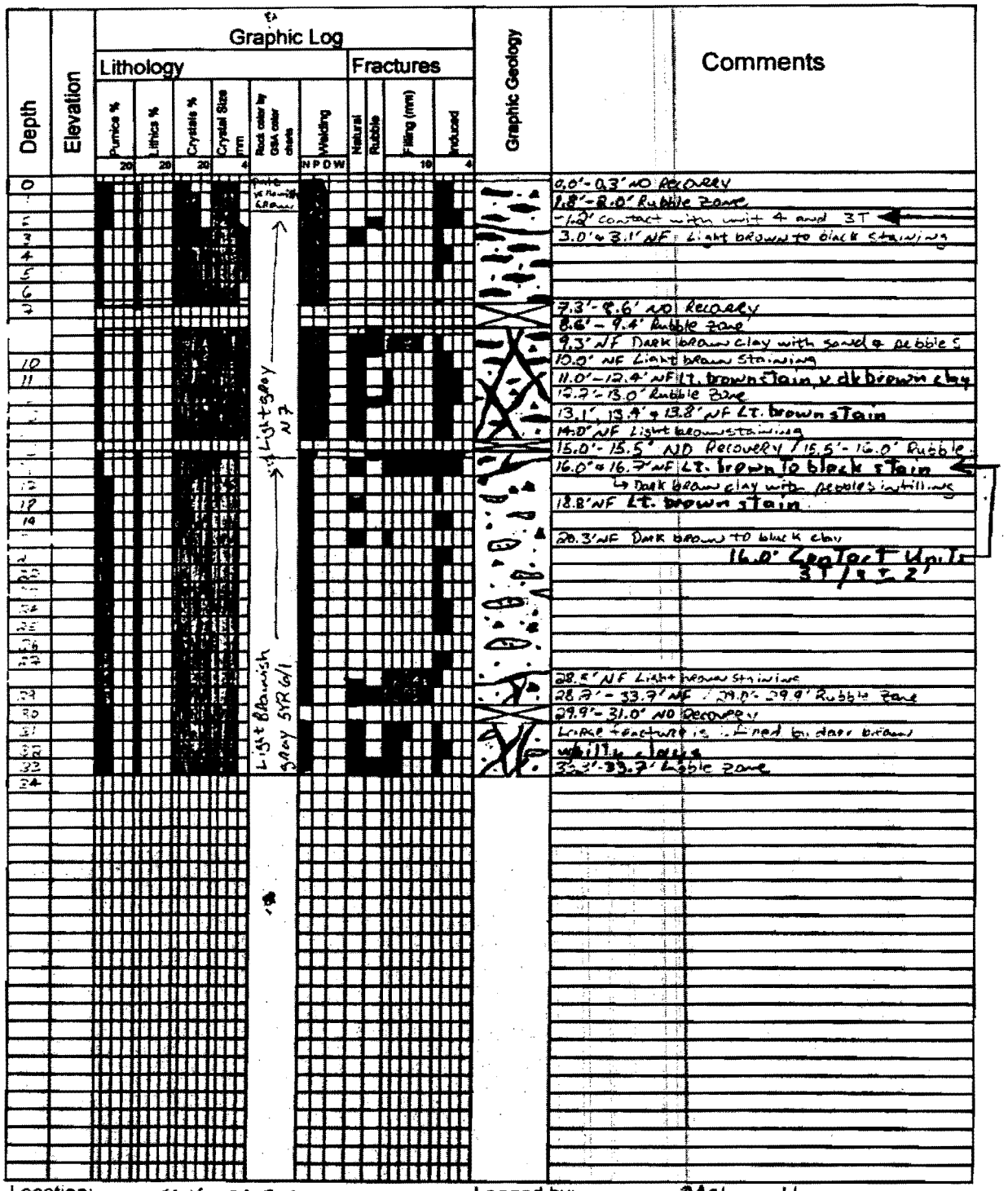

Location: TA-16 MDA-P PH II
Borehole No.: 516 BH
Total depth: 33.7'
Surface elevation: 7419.9

Logged by: RAChannell
Reviewed by: C.W. Reischell
date: 9/5/01

Page 1 of 1.

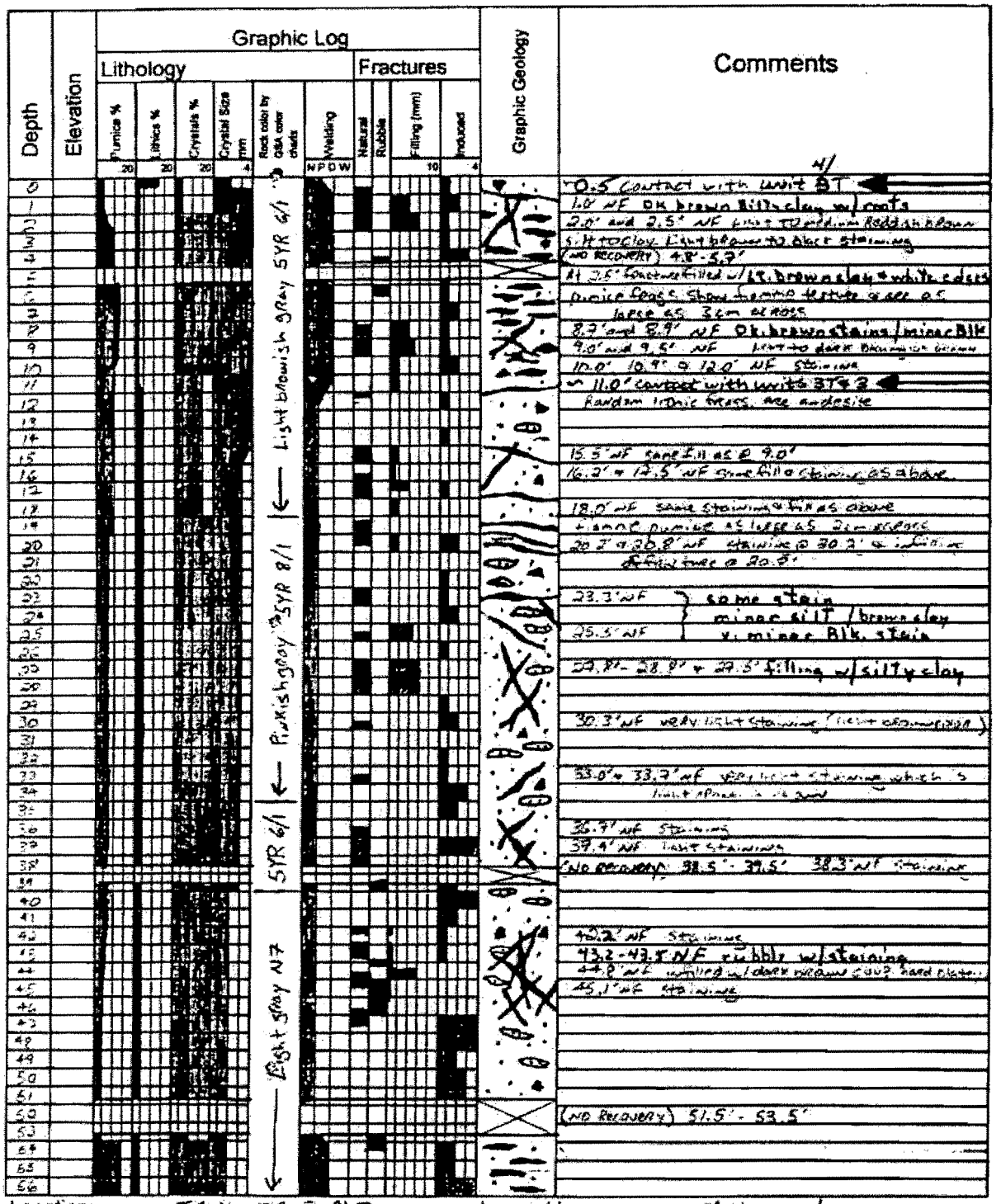

Location: TA-16 MW-F Alt II
Borehole No.: 526
Total depth: 60'
Surface elevation: 7412.9

Logged by: RAGhanem
Reviewed by: CW Criscum II
date: 8/21/01

Page 1 of 2

Depth	Elevation	Graphic Log: Lithology: Pumice % (20)	Lithics % (20)	Crystals % (20)	Crystal Size mm (4)	Rock color by GSA color charts	Welding (N P D W)	Fractures: Natural	Rubble	Filling (mm) (10)	Induced (4)	Graphic Geology	Comments
57						Light gray							
58													
59													(NO RECOVERY) 59.4' - 60.0'
60													

Location: TA-16 MDA-P PH II
Borehole No.: 5-26
Total depth: 60'
Surface elevation: 7412.9

Logged by: RAChannell
Reviewed by: CWCriswell
date: 8/21/01

Page 2 of 2

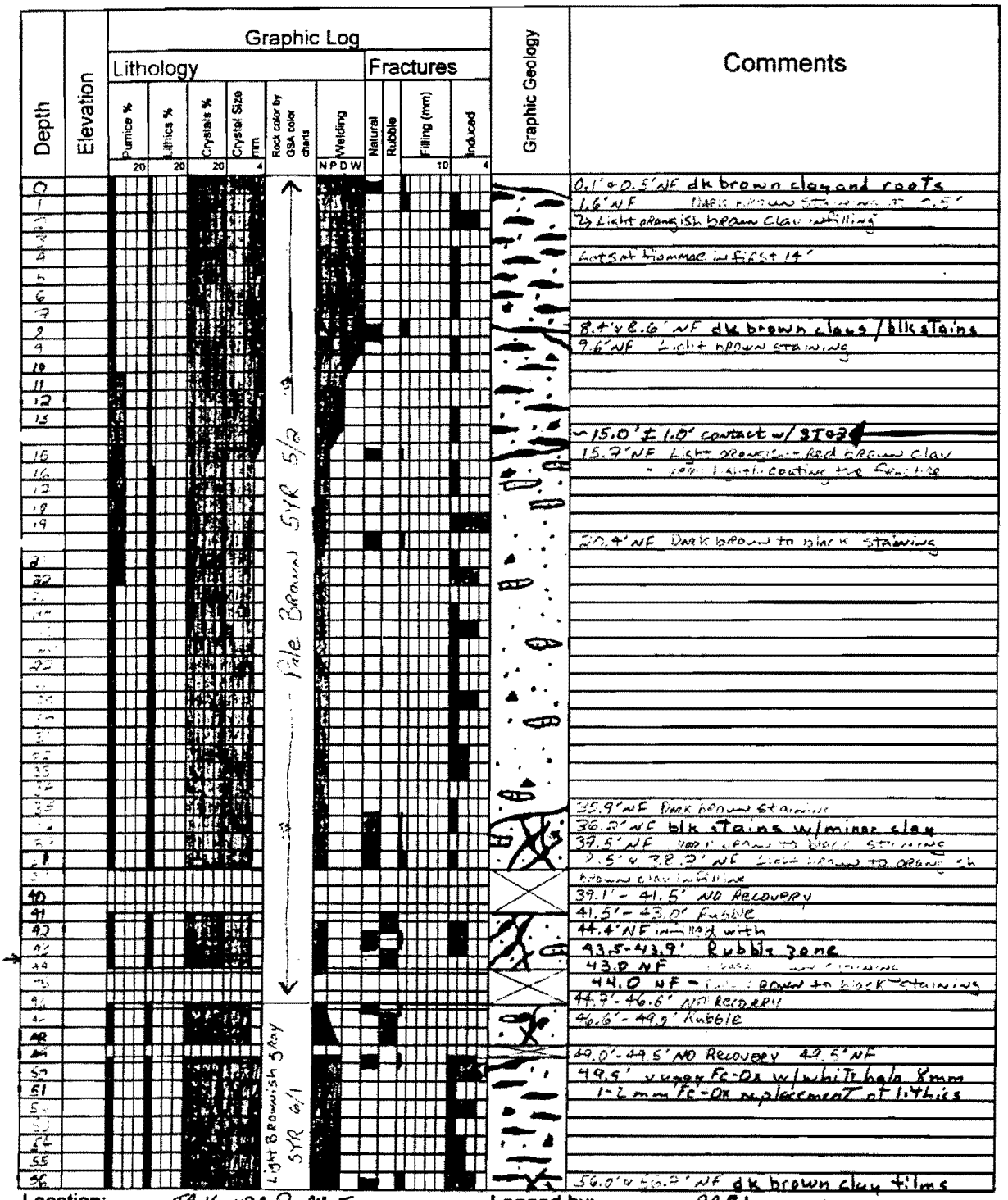

Location: TA-16 MDA-P PH I
Borehole No.: 554-BH
Total depth: 100'
Surface elevation: 7416.5

Logged by: RA Channell
Reviewed by: CW Criswell
date: 8/29/01

Page 1 of 2.

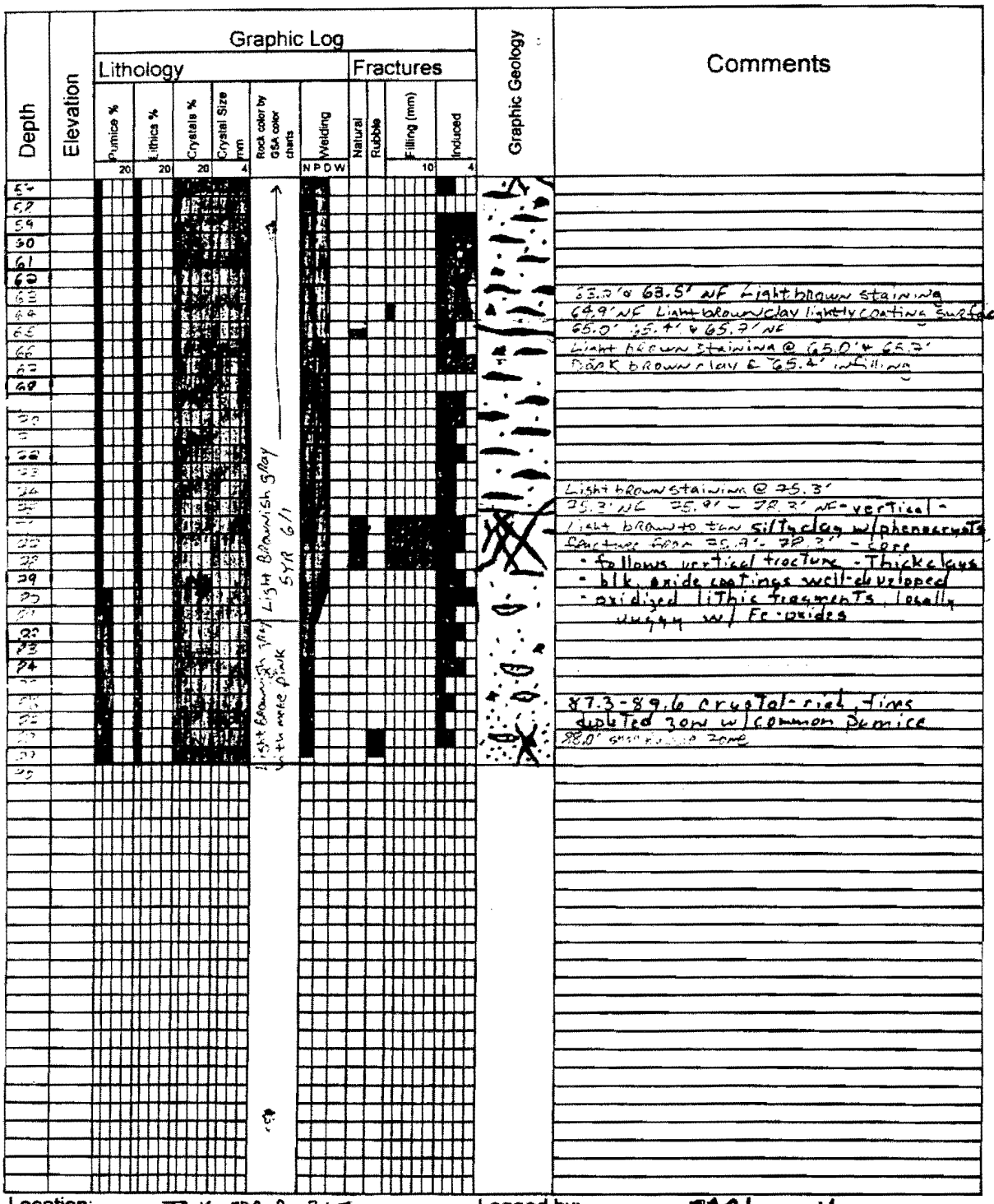

Location: TA-16 MDA-P PH II
Borehole No.: 554 - BH
Total depth: 100'
Surface elevation: 7916.5

Logged by: RA Channell
Reviewed by: CW Criswell
date: 8/29/01

Page 2 of 2.

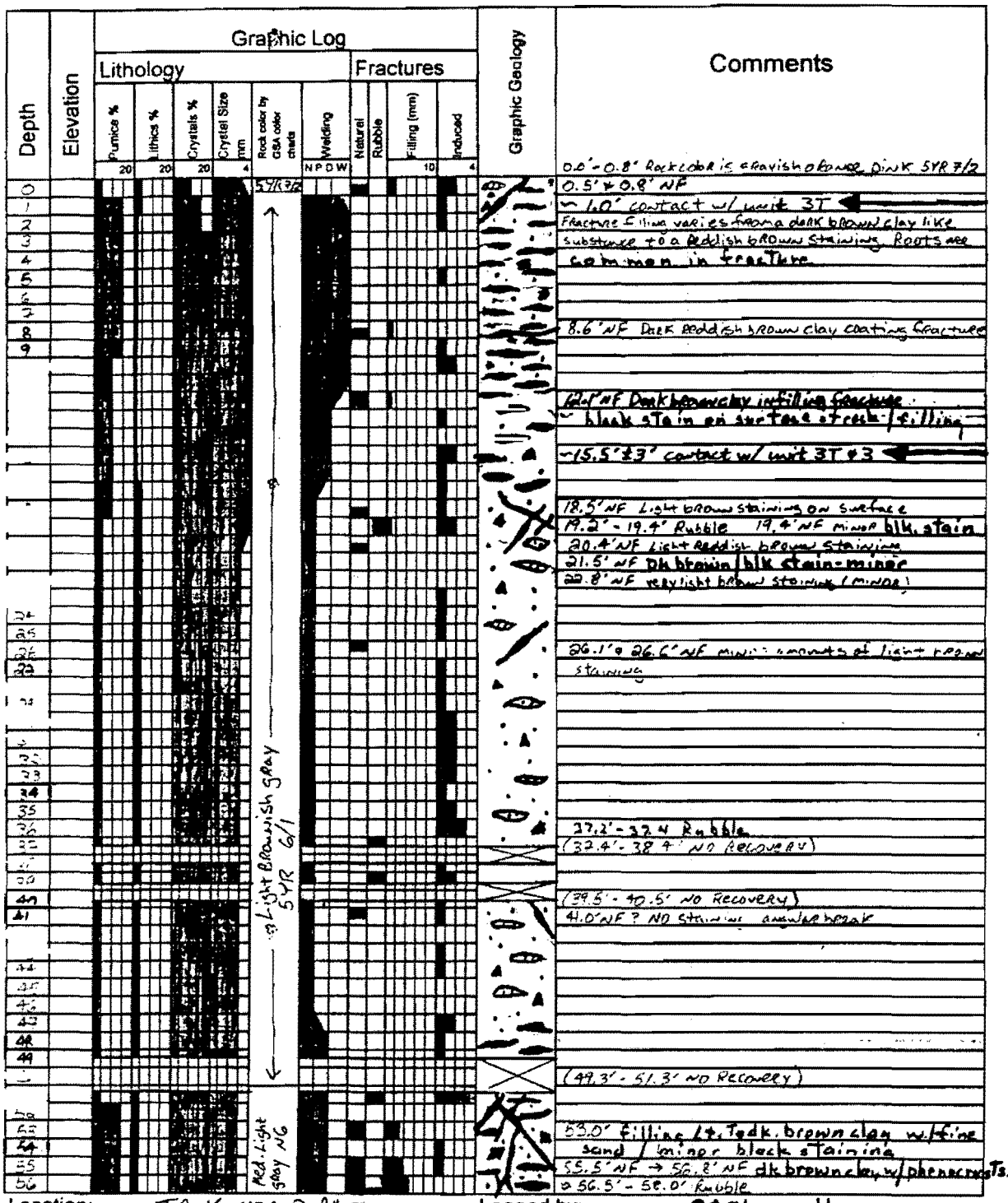

Location: TA-16 MDA-D PA II
Borehole No.: 557
Total depth: 70'
Surface elevation: 7415.5

Logged by: RAChannell
Reviewed by: CW Criswell
date: 9/10/01

Page 1 of 2.

file Code 6.19.5

Depth	Elevation	Graphic Log: Lithology: Pumice % (20)	Lithics % (20)	Crystals % (20)	Crystal Size mm (4)	Rock color by GSA color charts	Welding (N P D W)	Fractures: Natural	Rubble	Filling (mm) (10)	Induced (4)	Graphic Geology	Comments
57						Med. Light Gray N6							(58.0'-58.2' NO RECOVERY)
58													58.2' NF steeply dipping fracture no staining
59													
60													60.0' NF fracture is not through core completely
61													no visible staining
62													
63													
64													64.1' NF 64.9' NF dk brown clays/minor Blk.
65						Pale Red 10R 6/2							65.3' NF massive clay filling 2-12mm
66													& 66.4'-69.5' Rubble 66.0' NF
67													Light reddish brown to pink very fine sands
68													to silt infilling fracture.
69													
70													

Location: TA-16 MDA-P PH II
Borehole No.: 557
Total depth: 70'
Surface elevation: 7415.5

Logged by: RACbannell
Reviewed by: C.W. Reiswell
date: 9/10/01

Page 2 of 2.

Appendix B

Surface Fracture Data Tables
and
Subsurface Fracture Data Tables Generated
from Borehole Optical Televiewer

B-1.0 SURFACE FRACTURE DATA TABLES

MDA P Surface Fracture Data

fracture no.	Position (ft)	Unit	Strike	Dip	Aperture (mm)	fracture filling	Trace length (ft) S	Trace length (ft) N	Total length (ft)	Termination Type S	Termination Type N
Traverse 1, N78E Trend, Grid origin 421, 60' long						***Start 421***	**1616107.68**	**1764430.1**			
						End 419	**1616049.75**	**1764414.6**			
1-1	3.0	4	7	73	1	C	1.3	8.6	9.9	Te	Sp
1-2	4.5	4	343	43	1	C/R	1.1	4.1	5.2	Tr	Tr
1-3	9.5	4	352	69	1	C/R	1.2	5.3	6.5	Tr	C
1-4	13.1	4	313	80	10	C/R	10.7	38	48.7	Sp	C
1-5	16.4	4	202	48	>10	C/R/OX	4.7	4.1	8.8	Tr	Tr
1-6	22.1	4	204	63	10	C/R	8.8	5.2	14.0	Tr	Tr
1-7	36.3	4	323	60	3	C/R	7.8	2.7	10.5	C	Tr
1-8	40.6	4	216	79	5	C/R	8.3	26.6	34.9	Sp	Tr
1-9	44.7	4	348	80	1	C/R	2.4	0.55	3.0	Tr	Tr
47' - 50' Covered											
1-10	51.2	4	100	63	2	C/R/OX	2	4.4	6.4	C	C
1-11	53.1	4	202	74	2	C/R	3.2	1	4.2	Tr	Tr
1-12	56.6	4	22	78	2	C/R	4.6	9.4	14.0	C	Tr
Traverse 1, N78E Trend, Grid origin 421, 60' long						***Start 419***	**1616049.75**	**1764414.6**			
						End 417	**1615991.9**	**1764399**			
1-13	4.9	4	150	58	3	C/R	4.7	2.6	7.3	C	Tr
1-14	8.9	4	28	76	2	C	1.0	6.0	7.0	Tr	C
1-15	9.9	4	303	75	5	C	5.4	4.9	10.3	C	Tr
1-16	12.5	4	349	90	2	C	1.8	2.4	4.2	Tr	Tr
1-17	13.5	4	338	90	2-4	C	1.8	2.4	4.2	Tr	Tr
1-18	17.5	4	345	56	2	C	2.7	3.1	5.8	Tr	Tr
22.3' - 34.5' Covered											
1-19		4	23	50	2-3	C	0.6	5.7	6.3	C	Tr
1-20	31.8	4	16	43	5	C/R	0.2	4.2	4.4	Tr	Tr
1-21	31.9	4	131	84	4	C/R	0.0	4.6	4.6	C	Tr
34.6'-36.8' Covered											
1-22	38.6	4	140	53	1	C	3.2	3.3	6.5	Tr	C
1-23	43.5	4	332	85	10	F/C/B	5.8	3.8	9.6	C	Tr
1-24	44.1	4	174	83	5	C/R	0.0	3.6	3.6	C	Tr
44.4'-51.7' Covered											
1-25	51.7	4	300	80	2	C	0.0	1.5	1.5	Tr	Te
1-26	53.9	4	173	69	3	C/R	4.4	5.1	9.5	C	Tr
53.9'-56.5' Covered and likely brecciated											
1-27	56.5	4	334	88	10	F/OT	7.0	4.5	11.5	C	Tr
Traverse 1, N78E Trend, Grid origin 421, 60' long						***Start 417***	**1615991.9**	**1764399**			
						End 415	**1615933.89**	**1764383.5**			
1-28	8.4	4	51	90	1	C	6.2	7.3	13.5	Tr	C
1-29	10.8	4	322	90	1	C	1.3	10.7	12.0	Tr	Tr
1-30	10.9	4	210	86	1	C	3.5	3	6.5	Tr	C
12.3'-14.5' Covered											
1-31	15.7	4	149	77	10	F/C/R	0.6	4.4	5.0	Tr	Tr
1-32	18.0	4	80	90	3	C	2.7	0.5	3.2	Tr	Tr
1-33	18.8	4	173	88	5	C	3.8	4.1	7.9	Tr	Tr
1-34	50.1	4	59	76	1	C	0.0	4.8	4.8	Tr	Tr
1-35	50.4	4	163	83	1	B/C/F	4.8	24.3	29.1	Tr	Sp
1-36	52.0	4	162	86	2	B/C	3.8	15.2	19.0	C	Tr
1-37	58.6	4	6	70	5	C/B/F	4.9	0.9	5.8	Tr	Tr
Traverse 1, N78E Trend, Grid origin 421, 60' long						***Start 415***	**1615933.89**	**1764383.5**			
						End 413	**1615875.85**	**1764367.9**			
5'-12.6' Covered											
1-38	13.3	4	199	63	3	C/R	3.3	3.4	6.7	C	Tr
14.2'-18.0' Covered											
1-39	25.8	4	8	90	5	C	2.0	1.1	3.1	Tr	Tr
1-40	27.3	4	na	na	10	C	2.8	5.4	8.2	Sp	Tr
34.3'-41.3' Covered											
1-41	44.9	4	132	88	3	C	0.8	2.4	3.2	Tr	Tr
1-42	46.5	4	187	87	2	C/F	26	3.8	29.8	C	Tr
1-43	48.0	4	97	78	15	C	1.5	4.2	5.7	Tr	Tr
1-44	54.8	4	4	90	4	F/C	7.8	0.9	8.7	Te	Tr
1-45	57.3	4	359	90	1	C	14.2	2.55	16.8	Tr	Tr

Traverse 1, N78E Trend, Grid origin 421, 60' long						***Start 413***	**1615875.85**	**1764367.9**			
						End 411	**not surveyed**				
1-46	3.3	4	2	72	2	C	5.5	2.6	8.1	Tr	Sp
1-47	14.2	4	133	63	1	C/R	1.9	3.0	4.9	Tr	Tr
1-48	18.3	4	10	80	1	C/R	3.6	2.5	6.1	Tr	C
1-49	18.5	4	175	64	2	C/R	1.8	2.0	3.8	Tr	C
1-50	24.3	4	19	60	1	C/R	1.3	3.8	5.1	T	Tr
1-51	26.2	4	170	79	1	C/R	1.8	4.2	6.0	Tr	Tr
1-52	26.8	4	128	70	1	OX/R	0.7	3.3	4.0	Tr	Tr
1-53	29.4	4	339	90	50	B/C	0.7	2.3	3.0	Sp	Tr
1-54	30.6	4	175	71	1	C	0.4	2.5	2.9	Tr	Tr
1-55	31.1	4	10	76	1	C	0.8	1.3	2.1	Tr	Tr
1-56	41.2	4	158	76	1	C	1.9	1.8	3.7	Tr	Tr
1-57	42.6	4	138	65	10	C/F	22.4	0.2	22.6	Tr	Tr
1-58	43.0	4	29	75	22	F/C/B	6.5	9.2	15.7	Tr	Tr
1-59	48.0	4	115	80	2	C	3.4	3.2	6.6	Tr	Tr
1-60	51.6	4	125	70	4	C	7.2	3.1	10.3	Sp	C
1-61	53.8	4	160	82	1	C	3.8	1.9	5.7	Tr	Tr
Traverse 1, N78E Trend, Grid origin 421, 60' long						***Start 411***	**not surveyed**				
						End 409	**1615760.01**	**1764336.8**			
1-62	2.3	4	332	78	2	C/R	1.2	0.9	2.1	Tr	Tr
	3.1'-9.4' Covered										
1-63	12.6	4	240	69	2	C	10.9	1.6	12.5	Tr	C
1-64	14.1	4	170	67	1	C/B	0.9	9.9	10.8	Tr	Tr
1-65	24.6	4	174	71	1	C/R	11.9	6.7	18.6	Sp	Tr
1-66	25.3	4	345	90	1	C	14.0	6.4	20.4	Sp	Tr
1-67	34.4	4	125	85	1	C	16.7	3.4	20.1	Tr	Tr
1-68	39.6	4	20	90	12	C/B	49.0	11.7	60.7	Sp	Sp
1-69	40.5	4	145	8	2	C	0.7	14.0	14.7	Tr	Tr
1-70	52.8	4	135	77	1	C	10.4	15.3	25.7	Tr	Sp
1-71	55.6	4	121	72	6	C	7.0	5.9	12.9	Tr	C
1-72	61.7	4	150	89	1	C	4.1	4.5	8.6	Tr	Tr
1-73	63.9	4	187	83	4	C	7.4	1.6	9.0	Tr	Te
Traverse 1, N78E Trend, Grid origin 421, 80' long						***Start 409***	**1615760.01**	**1764336.8**			
						End 407+20'	**not surveyed**				
1-74	8.2	4	143	74	1	C/R	4.5	1.3	5.8	C	Te
1-75	13.5	4	165	72	1	C	13.0	4.7	17.7	C	Sp
1-76	22.9	4	341	74	1	C	5.5	1.0	6.5	Sp	Tr
1-77	24.2	4	15	90	22	C/R/F	32.7	16.1	48.8	Tr	Tr
1-78	27.0	4	297	90	1	C/R	2.5	7.0	9.5	Tr	Tr
1-79	37.0	4	20	78	4	C/R	0.6	6.0	6.6	Tr	Tr
1-80	37.8	4	5	83	6	C	0.3	3.5	3.8	Tr	Tr
1-81	38.2	4	292	90	8	C/F	14.0	2.0	16.0	Tr	Tr
1-82	42.1	4	54	90	8	C/R	0.2	12.0	12.2	Tr	C
1-83	42.4	4	155	80	2	C/R	3.2	11.6	14.8	Tr	C
1-84	46.8	4	132	67	1	R	3.0	3.3	6.3	Tr	Tr
1-85	53.0	4	190	71	1	C	1.5	8.7	10.2	Tr	C
1-86	54.5	4	309	84	4	C	4.7	3.5	8.2	Tr	Tr
1-87	58.7	4	348	70	2	C	5.9	0.7	6.6	Tr	Tr
1-88	62.9	4	25	72	4	C/F	3.1	2.9	6.0	Sp	Tr
1-89	73.0	4	322	90	16	C/R	3.7	11.7	15.4	Tr	Tr
1-90	77.3	4	310	84	1	C	15.5	2.7	18.2	Tr	C
END	**440' total**			**mean**	**4**			**mean**	**11.0**		
				max	**50**			**max**	**60.7**		
				min	**1**			**min**	**1.5**		

fracture density = 20.7 fractures / 100 ft

fracture no.	Position (ft)	Unit	STrike	Dip	Aperture (mm)	fracture filling	TraCe length (ft) S	TraCe length (ft) N	Total length (ft)	Termination Type S	Termination Type N
Traverse 2, N77E Trend, Grid origin 478, 90' long						***Start 478***	**1615657.57**	**1764371.4**			
						End 481	**1615744.51**	**1764394.8**			
2-1	4.5	4	341	90	1	C	1.1	2.2	3.3	Tr	C
5.0'-8.3' Covered											
2-2	8.7	4	320	81	1	C	9.7	4	13.7	Sp	C
2-3	18.2	4	340	80	2	C/R	0.5	2.6	3.1	Tr	C
2-4	18.6	4	0	61	1	C/R	0.7	2	2.7	Tr	Tr
2-5	19.7	4	40	70	1	C	0.9	4.2	5.1	Tr	C
2-6	20.9	4	122	66	1	C	2	4	6.0	Tr	C
2-7	30.0	4	314	80	2	C/B	3.7	4	7.7	C	C
2-8	32.6	4	137	72	32	C/R	5.1	5	10.1	C	C
2-9	39.2	4	322	90	2	C	5.8	11.3	17.1	C	C
2-10	48.6	4	150	76	1	C	1.5	2.8	4.3	Tr	Tr
2-11	54.5	4	166	85	40	C/R	4.3	21	25.3	Sp	C
2-12	75.1	4	164	66	3	C	10.1	9.2	19.3	Sp	C
2-13	77.1	4	115	90	2	C	9.8	1.1	10.9	C	Tr
2-14	86.3	4	150	85	1	C	2	10.2	12.2	C	Tr
Traverse 2, N77E Trend, Grid origin 478, 79' long						***Start 481***	**1615744.51**	**1764394.8**			
						End 483+19'	**1615802.37**	**1764410.3**			
0'-6' Covered											
2-15	7.6	4	19	72	2	C/R	1.4	1.6	3.0	C	Tr
2-16	8.9	4	151	70	8	C/F	0.7	3.2	3.9	C	C
2-17	13.3	4	165	90	1	C	13	2	15.0	Te	Sp
2-18	18.6	4	109	73	10	C/R	8	9.4	17.4	C	Tr
2-19	23.5	4	30	90	1	C	3	9.7	12.7	Tr	Tr
2-20	32.5	4	161	71	1	C/R	7.5	6	13.5	Tr	Tr
2-21	35.4	4	308	80	2	C	5.2	7.5	12.7	Tr	Tr
2-22	36.3	4	140	76	1	C/R	0.5	2	2.5	Tr	Tr
2-23	39.4	4	128	74	1	C	3.1	4.7	7.8	Tr	C
2-24	42.1	4	140	84	2	C	6.5	0.6	7.1	Tr	C
2-25	47.4	4	150	81	2	C/R	1.5	3.6	5.1	Tr	Tr
2-26	48.0	4	147	74	1	C	1.7	2.9	4.6	Tr	Tr
2-27	51.0	4	60	90	12	C/R	8.1	12.9	21.0	Sp	Sp
2-28	61.7	4	314	88	1	C	1.7	3.7	5.4	Tr	Tr
2-29	64.2	4	150	80	10	C/R	1.9	11	12.9	Tr	Tr
2-30	68.8	4	15	90	1	C	5.6	1.1	6.7	Tr	Tr
2-31	70.9	4	170	73	1	C	15	5.6	20.6	Tr	Tr
2-32	73.8	4	169	77	3	C	2.4	2.9	5.3	C	Tr
2-33	75.7	4	15	90	1	C	1.2	5.1	6.3	Tr	Tr
Traverse 2, N77E Trend, Grid origin 478, 41' long						***Start 483+19'***	**1615744.51**	**1764394.8**			
						End 485	**1615802.37**	**1764410.3**			
2-34	78.8	4	178	83	1	C	3.3	2.9	6.2	C	Sp
2-35	82.2	4	276	85	8	C/F?	4.8	3.5	8.3	Tr	Tr
2-36	86.7	4	339	90	10	C	0.3	5.3	5.6	Tr	Tr
2-37	86.9	4	155	82	10	C	5.6	6	11.6	Tr	C
2-38	91.1	4	170	74	1	C	2.3	1.1	3.4	Tr	Tr
2-39	93.7	4	270	90	1	C	0.8	3.7	4.5	Tr	C
2-40	94.2	4	133	76	1	C	1.8	7	8.8	Tr	Tr
2-41	97.6	4	25	90	2	C	2.4	6.3	8.7	Tr	C
98.3'-117.4' Covered											
2-42	119.7	4	171	61	na	na	5.2	1.2	6.4	C	C
Traverse 2, N77E Trend, Grid origin 478, 60' long						***Start 485***	**1615860.37**	**1764425.9**			
						End 487	**1615918.37**	**1764441.4**			
2-43	124.8	4	0	74	1	C	11.3	5.7	17.0	Tr	Tr
2-44	128.5	4	176	76	1	C	0.9	4.3	5.2	Sp	Tr
2-45	131.3	4	305	63	1	C	0.8	7.5	8.3	Tr	C
2-46	131.5	4	25	44	1	C	0.8	1.7	2.5	Tr	C
2-47	132.8	4	175	40	1	C	0.9	2.6	3.5	Tr	C
2-48	136.2	4	336	90	4	C	8	11.3	19.3	C	Te
2-49	137.2	4	234	81	10	C	1.4	15	16.4	Tr	Tr
2-50	139.6	4	20	69	2	C	3.6	2	5.6	Tr	Tr
2-51	149.7	4	172	86	1	C	2.9	2.2	5.1	Tr	Te
2-52	150.2	4	169	75	8	C/R	9.8	4.6	14.4	C	Sp
2-53	158.3	4	286	77	2	C	2	7.5	9.5	Tr	Tr
2-54	160.4	4	5	77	1	C	1.2	2.5	3.7	Tr	Tr
2-55	164.0	4	290	90	10	C	2.2	15.4	17.6	Tr	Tr
2-56	167.3	4	230	71	10	C	7	6.7	13.7	Tr	Te

Traverse 2, N77E Trend, Grid origin 478, 30' long						***Start 487***	**1615918.37**	**1764441.4**		
						End 488	**1615947.24**	**1764449.3**		
2-57	11.8	4	11	90	1	C	13	1.6	14.6 C	Tr
2-58	14.6	4	178	71	1	C	3	0.5	3.5 Te	Tr
2-59	15.8	4	290	70	1	C	6.3	3.7	10.0 Sp	Tr
2-60	25.3	4	349	43	1	C	4.2	2.4	6.6 Tr	C
Traverse 2, N77E Trend, Grid origin 478, 60' long						***Start 488***	**1615947.24**	**1764449.3**		
						End 490	**1616005.23**	**1764464.7**		
2-61	9.2	4	57	50	2	Ca	3.3	3	6.3 Te	Tr
2-62	13.0	4	303	30	2	C/r	0.7	2.6	3.3 Tr	Tr
2-63	15.1	4	325	50	2	C/r	6	4.8	10.8 Tr	Tr
2-64	12.0	4	19	90	1	Ca/r	9.2	7.4	16.6 Tr	Tr
2-65	17.8	4	323	50	2	C/r	4.6	6.6	11.2 Tr	Tr
2-66	23.3	4	3	90	2	f/b	4.7	3.9	8.6 Tr	C
2-67	25.4	4	3	90	1	C	9.3	8	17.3 Tr	Tr
2-68	33.6	4	303	90	2	C/r	0.6	6.5	7.1 Tr	Tr
2-69	38.3	4	50	58	1	C/r	2.4	0.6	3.0 Tr	Te
2-70	48.2	4	310	63	4	f/b	10.6	4	14.6 C	Te
2-71	56.1	4	350	54	4	C/r	3.6	1.6	5.2 C	C
59'-60' Covered										
Traverse 2, N77E Trend, Grid origin 478, 60+' long						***Start 490***	**1616005.23**	**1764464.7**		
						End 492+	**not surveyed**			
0'-2' Covered										
2-72	6.0	4	326	90	2	f	15	2	17.0 Tr	Tr
2-73	10.9	4	23	62	1	r	3	2.4	5.4 Tr	Tr
2-74	11.8	4	18	90	1	r	3.1	1.8	4.9 Tr	Tr
2-75	14.2	4	300	80	2	C	3	20	23.0 Tr	Sp
2-76	17.3	4	18	90	2	C	0.4	13.3	13.7 Tr	
20'-34' Covered										
40'-41' Covered										
45'-56' Covered										
2-77	58.2	4	27	66	2	C/r	2.5	1.3	3.8 C	Tr
2-78	60.6	4	347	84	5	f/b	20	0.6	20.6 Tr	C
END	**390' total**			**mean**	**4**			**mean**	**9.7**	
				max	**40**			**max**	**25.3**	
				min	**1**			**min**	**2.5**	
fracture density =		**20 fractures / 100 ft**								

Traverse 3, N14W Trend, Grid origin 418, 30' long						***Start 418***	**1616020.78**	**1764406.9**		
						End 454	**1616013.01**	**1764435.8**		
3-1	4.1	4	309	90	4	C/R/F	3	9.7	12.7 Te	Sp
3-2	9.5	4	44	90	2	C/R	7	3.6	10.6 C	Tr
3-3	12.0	4	305	65	1	C/R	2.4	2.3	4.7 Tr	Tr
3-4	14.7	4	67	90	1	C	14.3	7.1	21.4 Tr	Tr
3-5	22.9	4	284	64	1	C/R	5.3	6.5	11.8 Sp	Sp
3-6	27.2	4	148	36	2	R	2.4	1.4	3.8 C	Tr
3-7	30.1	4	116	60	2	C	3.7	3	6.7 Tr	C
Traverse 3, N14W Trend, Grid origin 418, 90' long						***Start 454***	**1616013.01**	**1764435.8**		
						End 562	**1615989.62**	**1764522.7**		
3-8	0.4	4	11	59	1	C/R	4.8	0.6	5.4 Tr	Tr
3-9	4.2	4	15	48	1	R	1.4	4	5.4 Tr	Tr
3-10	5.5	4	101	80	1	C	9.3	5.2	14.5 C	Sp
3-11	9.7	4	22	53	3	C/R	2.5	4.3	6.8 Tr	Tr
3-12	13.9	4	65	90	1	C	8.1	1.9	10.0 Sp	Sp
3-13	18.0	4	355	82	1	C	2	3.5	5.5 Te	Sp
3-14	28.0	4	355	79	1	C	7.6	0.6	8.2 Te	Sp
3-15	37.1	4	75	32	2	R/B	5.9	7.6	13.5 Tr	Tr
3-16	39.1	4	103	60	3	R	9.1	6.2	12.3 Tr	Tr
3-17	45.7	4	225	72	1	R	3.4	6.6	10.0 C	Sp
3-18	46.6	4	266	70	1	R	1.2	4.1	5.3 Tr	C
3-19	53.6	4	296	90	1	C	5.2	1.7	6.9 C	C
3-20	62.5	4	243	79	3	C/R	4.5	9.7	14.2 Te	Tr
3-21	74.4	4	190	64	10	C/R/B	12.1	2.2	14.3 C	C
3-22	84.3 3T		260	72	1	C	1.5	0.7	2.2 Tr	C
86.4'-91.2' Covered										

Traverse 3, N14W Trend, Grid origin 418, 57' long						***Start 562***	**1615989.62**	**1764522.7**			
						End 598+26.2'	**1615981.93**	**1764551.7**			
	0'-5.8' TrenCh 5.8'-13.0' Covered										
3-23	13.3	3T	261	81	10	C	8	9	17.0	C	C
3-24	18.6	3T	276	90	3	C	1.9	8.7	10.6	Tr	C
3-25	20.8	3T	72	90	1	O	2.4	0.9	3.3	Tr	Tr
3-26	21.7	3T	260	33	1	C	2.5	0.7	3.2	Tr	C
3-27	23.2	3T	279	90	8	C/R	16.2	7.6	23.8	Tr	Tr
3-28	28.6	3T	86	84	4	C/R	1.3	8.1	9.4	C	C
3-29	42.1	3T	41	41	1	C	0.9	2	2.9	C	C
3-30	46.0	3T	274	90	2	C	2	2.9	4.9	C	C
3-31	47.7	3T	48	35	5	C/R	6.3	1.7	8.0	C	Tr
3-32	56.2	3T	200	64	6	C	4	9.5	13.5	Te	C
Traverse 3, N14W Trend, Grid origin 598, 30' long						***Start 598***	**1615981.93**	**1764551.7**			
						End 562	**1615989.62**	**1764522.7**			
3-33	2.6-7.9	3T	264	8	2	C	7.9	5.3	13.2	Tr	Tr
3-34	7.9-10.4	3T	243	12	10	C	2.4	9.1	11.5	Tr	Tr
3-35	10.4-14.2	3T	256	14		O	1.6	8.9	10.5	Tr	Tr
3-36	18.8-21.4	3T	263	13	2	C	4	0.5	4.5	Tr	C
END	**207' total**			**mean**	**3**			**mean**	**9.51**		
				max	**10**			**max**	**23.8**		
				min	**1**			**min**	**2.2**		
fracture density =		**17.4 fractures / 100 ft**									

Traverse 4, N20W Trend, Grid origin 667 + 15.2' N, 75+' long						***Start 667+15.2' N***		**not surveyed**			
						End 595	**1615894.96**	**1764528.3**			
4-1	6	3	82	57	1	C	2.2	5.2	7.4	Tr	C
4-2	9.6	3	99	37	1	C/R	2.5	7.1	9.6	C	C
4-3	16.3	3	130	72	1	C	5	7.3	12.3	Tr	Te
4-4	21	3	75	90	1	R	4.1	1.7	5.8	Tr	Sp
4-5	21.7	3	70	63	1	C	3.2	0.5	3.7	Tr	Tr
4-6	24.5	3	234	87	10	C/R	9.4	11.5	20.9	Tr	C
4-7	29	3	168	70	20	C/R	6.2	5.1	11.3	Tr	Tr
4-8	42.1	3T	138	75	10	C/R	31.5	9.3	40.8	C	Tr
4-9	46.8	3T	250	39	4	C	0.3	5.1	5.4	C	C
4-10	51.3	3T	271	88	10	C/B	1.1	13.4	14.5	Tr	Tr
4-11	55.3	3T	72	90	25	C/R	8	21	29	Tr	Tr
4-12	65.8-69.1	3T	255	18	1	C	6.3	10.4	16.7	C	Tr
4-13	68.3	3T	85	63	1	C	1.9	4.8	6.7	Tr	Te
4-14	74.7	3T	62	65	1	C	1.6	0.7	2.3	Sp	C
4-15	75.7	3T	82	90	8	C/R/B	4.9	3.3	8.2	Tr	C
4-16	81.3	3T	42	90	100	C/R/B	4.6	0.4	5	Tr	C
4-17	75.7-81.3	3T	271	9	6	C	2	1.5	3.5	Tr	C
4-18	74.7-75.7	3T	275	10	1	C	2.2	3.9	6.1	Tr	C
Traverse 4, N20W Trend, Grid origin 667 + 15.2' N, 90' long						***Start 595***	**1615894.96**	**1764528.3**			
						End 487	**1615918.37**	**1764441.4**			
4-19	2.2	3T	314	90	2	C	8.2	1.4	9.6	C	Tr
4-20	0.8-2.8	3T	252	4	20	C	2.7	1.1	3.8	Tr	Tr
4-21	2.8	3T	215	80	50	C/R/B	8.4	12.4	20.8	C	C
4-22	2.8-6.6	3T	252	9	10	C/R/B	1.1	3.4	4.5	Tr	Tr
4-23	6.6	3T	50	82	35	C	1.8	1.1	2.9	Tr	Tr
4-24	7.6	3T	124	64	14	C	3.4	4.1	7.5	Tr	Tr
	10.1-20.3 Covered										
4-25	23.9	4	49	74	1	C	3.2	1.3	4.5	Tr	C
4-26	30.1	4	309	46	2	R	2	2.3	4.3	C	C
4-27	49.8	4	310	62	2	C	0.8	1	1.8	C	Sp
4-28	51.9	4	70	90	1	C	0.3	3	3.3	Tr	C
4-29	74.2	4	129	80	4	C	4.1	1.7	5.8	Tr	C
4-30	78.2	4	51	67	2	C	8	5.2	13.2	C	Tr
4-31	88.1	4	57	90	1	C	7.2	4.7	11.9	Sp	Tr
END	**165' total**			**mean**	**11**			**mean**	**9.78**		
				max	**100**			**max**	**40.8**		
				min	**1**			**min**	**1.8**		
fracture density =		**18.8 fractures / 100 ft**									

Traverse 5, N12W Trend, Grid origin 662, 105' long						***Start 662***	**1615734.66**	**1764547.3**		
						End 554	**1615757.97**	**1764460.5**		
5-1	9.7	3	320	90	8	C/R	1.2	1.3	2.5 C	C
5-2	12.9	3	104	56	1	C	0.4	11.7	12.1 Tr	C
5-3	13.5	3	347	35	1	C/OX	0.6	9.2	9.8 C	Tr
5-4	14.7	3	240	43	1	OX/R	0.6	1.2	1.8 Te	Tr
5-5	22.5	3	94	84	2	C	7.8	8.3	16.1 Tr	C
5-6	22.7	3	218	79	14	C/R/F	6	2.7	8.7 C	Tr
5-7	23.7	3	139	55	1	C	3.5	0.2	3.7 Tr	Tr
5-8	25.3	3	119	64	1	C/R	2.3	2.4	4.7 Te	Tr
5-9	27.6	3	296	90	6	C/R/B	12	7.4	19.4 Tr	Tr
5-10	31.2	3	29	67	1	C	3.1	6.6	9.7 Tr	Tr
5-11	33	3	268	59	1	C	3.4	1.6	5 Tr	Tr
5-12	35.8	3	293	16	2	R	0.5	1.7	2.2 Tr	Te
5-13	36.1	3	51	76	1	R	2	3.3	5.3 Tr	Tr
5-14	41.3	3	295	90	16	C/B/OX	2.1	1.4	3.5 Tr	Tr
5-15	42.3	3	245	88	6	C/R/OX	9	16	25 Tr	C
5-16	~45.7	3	22	2	1	C	4.9	7	11.9 Tr	Tr
5-17	~56.7	3	303	90	50	C/R/B	11	18	29 Tr	C
5-18	59.7	3	265	82	10	C/R	10.6	15	25.6 Tr	C
5-19	63.5-65.7	3T	227	11	25	C/R	5.2	7.1	12.3 Tr	C
5-20	66.5-69	3T	220	11		O	2.4	2.6	5 Tr	Tr
5-21	71.5	3T	238	88	30	C	1.5	11	12.5 Tr	Tr
5-22	72.4-75.4	3T	245	11	10	C	0.3	3.7	4 Tr	Tr
5-23	75.6	3T	98	70	12	C/R	2.8	1	3.8 C	C
5-24	76.7	3T	1	79	10	C/R/B	21	7	28.0 C	C
5-25	82.4-83.1	3T	262	8		O	0.9	1.8	2.7 Tr	Te
5-26	85.0	3T	260	83	10	C	2	5.5	7.5 Tr	C
5-27	86-92	3T	254	7	4	C/R	4	5	9.0 Tr	C
5-28	93.8	4	311	80	10	C	6	3.1	9.1 C	C
5-29	99.8	4	45	69	4	C	1	2.1	3.1 C	C
5-30	100.9-102	4	25	1	1	C	0.9	1.6	2.5 C	C
5-31	104.5	4	29	81	3	C	3.6	2.9	6.5 C	C
Traverse 5, N12W Trend, Grid origin 662, 30' long						***Start 554***	**1615757.97**	**1764460.5**		
						End 482	**1615773.46**	**1764402.5**		
	5.0-24.4 Covered									
5-32	25.7	4	52	30	20	R	2.4	2.1	4.5 C	C
	26.0-31.0 Covered									
5-33	31.8	4	39	45	10	R	2.1	8.5	10.6 C	Tr
5-34	34.5	4	55	35	25	C/R	5.7	2.2	7.9 C	Tr
5-35	39.0	4	87	72	2	C/R	3.7	5.3	9.0 Tr	Tr
5-36	40.3	4	96	86	4	C/R	21.9	6.3	28.2 Tr	Tr
5-37	46.3	4	9	90	2	C	2.8	1.2	4.0 Sp	Tr
5-38	47.4	4	72	52	1	C	1.3	3.5	4.8 Tr	Sp
5-39	48.9	4	38	90	1	C/OX	1.5	2.5	4.0 Tr	Tr
5-40	50.0	4	18	90	1	C/OX	9.4	2.3	11.7 Tr	Tr
5-41	54.7	4	138	83	2	C	14.1	15.4	29.5 Sp	C
5-42	55.7	4	40	68	1	C	0.8	11.6	12.4 Tr	Tr
5-43	58.5	4	41	51	10	C	1.4	3.1	4.5 Tr	Tr
5-44	60.4	4	72	90	2	C	2.1	7.7	9.8 Tr	Tr
END	**135' total**			**mean**	**8**			**mean**	**10.07**	
				max	**50**			**max**	**29.5**	
				min	**1**			**min**	**1.8**	

fracture density = 32.6 fractures / 100 ft

Traverse 6, N76E Trend, Grid origin 599, 60+' long					***Start 599***	**not surveyed**				
					End 597	**not surveyed**				
6-1	7.1	3T	159	32	1	R	1.4	0.8	2.2 Tr	C
8.0' to 23.5' Covered										
6-2	26.0	3T	301	73	70	C	2.5	0.9	3.4 C	C
6-3	26.0-26.9	3T	260	5	2	C	3.9	0.6	4.5 Tr	C
6-4	29.4-30.7	3T	291	11	4	C/R	2.5	0.3	2.8 C	Tr
6-5	30.7	3T	21	25	54	C	1.2	0.4	1.6 C	Tr
6-6	31.5	3T	24	62	20	C/R	1.8	0.8	2.6 C	C
6-7	33.7	3T	141	62	1	C	1.4	0.5	1.9 C	Tr
6-8	34.2	3T	52	59	4	C	1	1.3	2.3 C	C
6-9	34.2-35.9	3T	138	5	4	C	0.8	1.2	2.0 C	Tr
6-10	36.5	3T	34	90	6	C	0.4	1	1.4 C	C
6-11	36.5-41.0	3T	350	5	6	C	1.2	1.5	2.7 C	Tr
41.0' to 50.6' Covered										
6-12	50.8	3T	321	90	4	C	4.6	1.8	6.4 C	C
6-13	50.8-52.7	3T	245	12	1	C	1.1	1.3	2.4 Tr	Tr
6-14	52.8	3T	327	81	2	C	4.8	3.1	7.9 C	C
6-15	54.7	3T	339	90	4	C	1	1.4	2.4 Tr	C
6-16	54.7-56.0	3T	254	14	2	C	1.7	0.6	2.3 C	Tr
6-17	57.1-58.6	3T	315	16	4	C/OT	1.5	0.7	2.2 Tr	Tr
6-18	58.7	3T	217	82	20	C/R	10.5	3	13.5 Tr	C
Traverse 6, N76E Trend, Grid origin 599, 60+' long					***Start 597***	**not surveyed**				
					End 595	**1615894.96**	**1764528.3**			
6-19	59.9	3T	150	65	10	C/ot	1.9	1.5	3.4 C	C
6-20	61.4	3T	305	81	30	C/r	1.1	4.1	5.2 Tr	C
6-21	61.4-68.6	3T	100	1	4	C/r	0.8	2.7	3.5 C	Tr
6-22	68.6	3T	326	77	20	C/r	13.3	2.7	16.0 C	Tr
6-23	69.4	3T	39	62	4	C	2.4	0.8	3.2 C	Tr
6-24	69.4-77.7	3T	240	12		O	6.9	3.8	10.7 Tr	Tr
6-25	77.7	3T	345	90	20	r/C	10.4	49	59.4 C	C
6-26	77.8-83.35	3T	245	6		O	8.3	4.7	13.0 C	Tr
6-27	83.4	3T	351	90	2	C	27	27.4	54.4 C	C
6-28	83.4-90.45	3T	257	5	1	C	4	5.7	9.7 Tr	Tr
6-29	90.5	3T	171	87	4	C	30.7	1.6	32.3 Sp	Tr
6-30	90.5-95.25	3T	260	6	1	C	1.4	2	3.4 C	Tr
6-31	95.3	3T	330	62	1	C	1.4	2	3.4 C	C
6-32	97.2	3T	343	90	1	C	1.1	1.3	2.4 C	C
6-33	97.2-101.4	3T	240	10		O	0.8	4	4.8 C	Tr
6-34	101.6	3T	160	39	2	C	1.3	3.5	4.8 C	C
6-35	103.3	3T	359	90	1	C	28	52.7	80.7 C	Tr
6-36	103.4-108.6	3T	260	20	2	C	2.8	3	5.8 Tr	Tr
6-37	108.7	3T	319	90	2	C/r	16.7	1.7	18.4 Tr	Tr
6-38	108.7-110.55	3T	263	20	2	C	6.1	1.8	7.9 Tr	Tr
6-39	110.55	3T	184	87	8	C/r	10.8	2	12.8 C	C
6-40	110.55-112.35	3T	253	9	10	C	1.7	3.4	5.1 Tr	Tr
6-41	112.35	3T	324	90	10	C/r	2.3	1	3.3 Tr	Tr
6-42	112.4-113.6	3T	260	12	6	C	0.8	0.9	1.7 C	Tr
6-43	113.60	3T	217	84	2	C	2.5	1.2	3.7 C	Tr
6-44	115.90	3T	13	90	30	r/C	17	1.7	18.7 C	C
6-45	116.2-119.8	3T	255	5	10	C	2	1.2	3.2 Tr	Tr

Traverse 6, N76E Trend, Grid origin 599, 60+' long					***Start 595***	**1615894.96**	**1764528.3**			
					End 593	**not surveyed**				
6-46	4.7	3T	285	88	1	C	0.4	0.6	1.0	Tr	Tr
6-47	4.8'-6.1'	3T	80	3	4	C	0.3	0.7	1.0	C	Tr
6-48	6.2	3T	225	61	10	C	1.4	0.9	2.3	C	Tr
6-49	7.9'-11.5'	3T	229	9	2	C/r	0.7	2.6	3.3	C	Tr
6-50	15.0'-17.1'	3T	239	15	1	C	0.5	1.8	2.3	C	Tr
6-51	17.2	3T	323	84	2	C	0.2	1.6	1.8	Tr	Tr
6-52	17.2'-18.25'	3T	260	20	2	C	0.6	1.6	2.2	Tr	Tr
6-53	18.3	3T	184	81	34	C/r/b	0.5	1.6	2.1	C	Tr
6-54	18.7	3T	236	78	1	C	1.9	0.3	2.2	Tr	Tr
6-55	19.3'-20.6'	3T	247	6	2	C	0.3	1.1	1.4	Tr	Tr
6-56	20.6	3T	343	76	1	r/C	0.6	1.2	1.8	C	C
6-57	21.0'-21.5'	3T	245	27	6	C	0.6	1.1	1.7	C	Tr
6-58	21.6	3T	216	65	4	r/C	1.1	1.6	2.7	C	Tr
6-59	31.4	3T	22	90	22	C	1.1	0.1	1.2	C	Tr
6-60	32.4	3T	33	64	1	C	0.9	0.3	1.2	Tr	Tr
6-61	35.0	3T	355	90	10	C	0.7	1.5	2.2	C	C
6-62	35.0'-36.6'	3T	255	36	5	r/C	0.7	2	2.7	C	TR
6-63	42.5	3T	119	78	1	C	1.4	1	2.4	C	Tr
6-64	43.3	3T	347	90	10	C	1.2	1.2	2.4	Tr	Tr
6-65	43.35'-47.8'	3T	277	23	6	C/r	1.9	2.4	4.3	C	Tr
6-66	47.9	3T	201	52	1	C	0.7	2	2.7	C	C
6-67	50.8	3T	310	70	2	C	1.6	1.4	3.0	C	C
6-68	50.85'-56.3'	3T	256	22	10	C	2.5	2.1	4.6	Tr	Tr
6-69	56.3	3T	345	90	15	C/r	2.4	0.5	2.9	C	C
6-70	56.35'-60'	3T	265	16	2	r/C	1.7	5.7	7.4	Tr	Tr
Traverse 6, N76E Trend, Grid origin 599, 60+' long					***Start 593***	**not surveyed**				
					End 591	**1615779.08**	**1764497.2**			
6-71	5.7	3T	152	87	20	C/r	14.9	16.5	31.4	C	C
6-72	6.3	3T	169	36	30	r/C	1.8	6	7.8	C	C
6-73	10.6	3T	42	54	15	C	2.5	4	6.5	Tr	Tr
6-74	14.1-16.2	3T	251	23	2	C/R	1.1	1.2	2.3	C	Tr
6-75	16.2	3T	354	90	10	C	0.4	1.1	1.5	C	Tr
	17.5'-36.0' Covered	3T									
6-76	36.4	3T	276	90	2	C	0.3	1.9	2.2	C	C
6-77	43.4	3T	148	78	2	C	0.8	5.7	6.5	C	C
6-78	43.6	3T	46	62	40	C	0.7	2.1	2.8	C	Tr
	46.4'-55.5' Covered	3T									
6-79	56.0-58.5	3T	238	15		O	1.3	1	2.3	Tr	Tr
6-80	58.5	3T	186	75	6	C	1.9	0.3	2.2	C	C
Traverse 6, N76E Trend, Grid origin 599, 60+' long					***Start 591***	**1615779.08**	**1764497.2**			
					End 589	**1615721.07**	**1764481.6**			
6-81	1.9	3T	306	90	40	C/b/r	24.1	18	42.1	C	C
6-82	1.9'-6.7'	3T	245	20	2	r/C	2.8	2.3	5.1	C	Tr
6-83	6.8	3T	36	90	10	C	16.8	4.3	21.1	Tr	Tr
6-84	6.75'-18.25'	3T	240	19	2	C	3.7	5.7	9.4	C	Tr
6-85	18.3	3T	358	85	12	C/r/ot	10.7	16.8	27.5	C	C
6-86	18.35'-22.9'	3T	233	10	10	C/R	4	1.5	5.5	C	Tr
6-87	22.9	3T	17	90	8	r/C/ot	10.7	1	11.7	C	Tr
6-88	22.9'-29.0'	3T	314	15	2	C	3.8	4	7.8	Tr	Tr
6-89	29.0	3	355	73	40	C/r	11.5	14.6	26.1	C	C
6-90	29.05'-33.7'	3	225	9	4	C/R	3	2.6	5.6	Tr	Tr
6-91	33.8	3	350	38	10	b/r/C	1.1	1	2.1	C	C
6-92	34.9	3	356	20	15	C	2.2	3	5.2	C	C
6-93	34.9'-36.55'	3	210	6	2	C	2	1.9	3.9	C	Tr
6-94	36.6	3	208	43	1	r/ot	1.8	9.8	11.6	C	Tr
	39.0'-51.4' Covered										
6-95	58.0	3	323	90	12	o/C	3.1	4	7.1	C	C
6-96	60.0	3	308	90	1	O	0.7	1.5	2.2	C	Tr
6-97	61.5	3	197	77	2	C	0.9	1.3	2.2	C	C

Traverse 6, N76E Trend, Grid origin 599, 60+' long						***Start 589***	**1615721.07**	**1764481.6**		
						End 587	**1615663.17**	**1764466.1**		
6-98	2.1	3	333	90	1	C	1.1	2	3.1 C	C
6-99	5.3	3	60	42	2	O	1.8	3.3	5.1 C	Tr
6-100	9.3	3	330	82	44	O	0.8	2.2	3.0 C	Tr
6-101	10.4	3	301	90	30	O	0.7	1.7	2.4 C	Tr
6-102	10.9	3	302	90	34	O	1	1.3	2.3 C	Tr
6-103	11.9	3	210	50	20	O	2.7	4	6.7 C	C
6-104	18.3	3	20	84	1	C/R	1.7	1.4	3.1 C	C
6-105	22.7	3	31	60	4	O	3.7	2.5	6.2 C	C
6-106	25.3	3	298	90	50	O	2	4	6.0 Tr	C
6-107	28.1-29.9	3	259	10		O	1.5	1.3	2.8 C	Tr
6-108	32.9	3	338	62	2	C/R	0.9	7.3	8.2 C	C
6-109	32.9-38	3	254	14		O	1.9	4	5.9 C	Tr
6-110	44.4	3	308	90	20	C/R	3.1	2.4	5.5 Tr	Tr
6-111	47.1	3	168	78	40	O	2.3	0.9	3.2 C	Tr
6-112	50.4	3	16	85	2	O	1.2	0.5	1.7 C	Tr
END	**360' total**			**mean**	**10**			**mean**	**7.55**	
				max	**70**			**max**	**80.7**	
				min	**1**			**min**	**1.0**	
fracture density =		**31.1 fractures / 100 ft**								

Traverse 7, N78E Trend, Grid origin 670, 60+' long						***Start 670***	**1615966.36**	**1764609.6**		
						End 668	**not surveyed**			
	0-23 covered									
7-1	24.2-27.4	3	282	11		O	1.5	3.8	5.3 C	Tr
7-2	30.4-32.4	3	288	3		O	1	3.1	4.1 Tr	Tr
7-3	32.6	3	219	72	1	C/R	2.7	1.9	4.6 Tr	Tr
7-4	34.1	3	355	90	10	C/R/B	6.4	7	13.4 Sp	Tr
7-5	34.1-35.6	3	213	13		O	0.6	1.2	1.8 Tr	Tr
7-6	35.7	3	355	90	1	C	3.3	3.5	6.8 Te	Tr
7-7	37.8	3	182	83	6	C/R	5.8	4	9.8 Sp	Sp
7-8	39.6	3	155	62	2	C	9.8	9.5	19.3 C	C
7-9	41.0	3	60	90	2	C/R	5.6	1.3	6.9 Tr	Tr
7-10	47.5	3	305	77	10	C/R/B	0.4	3.5	3.9 Sp	C
7-11	51.4	3	350	24	1	C	2.8	3	5.8 Te	C
7-12	53.4	3	141	48	12	C/R	4	9.1	13.1 C	C
7-13	57.4	3	155	31	1	C	2.8	0.7	3.5 C	Tr
7-14	57.7	3	170	44	6	C	3.4	5	8.4 C	Sp
7-15	59-60.3	3	222	35		O	0.7	0.8	1.5 Tr	Tr
Traverse 7, N78E Trend, Grid origin 670, 77+' long						***Start 668***	**not surveyed**			
						End 666+17'	**not surveyed**			
7-16	1.2	3	161	51	20	C/R	5.8	8.6	14.4 C	Tr
7-17	3.0	3	260	72	15	C/R	1.8	2.9	4.7 Tr	Tr
7-18	5.9	3	174	41	2	C	2.9	3.8	6.7 Te	Tr
7-19	7.1	3	315	86	15	C/R	3.2	17.1	20.3 C	Tr
7-20	11.4	3	326	90	6	C/R/B	1.7	11	12.7 Sp	C
7-21	12.1	3	250	21	10	C	1.9	5	6.9 Tr	Tr
7-22	17.0	3	330	73	20	C/R/B	4.7	4.4	9.1 Tr	Tr
7-23	20.3	3	239	56	2	C/R	0.8	1.1	1.9 Tr	Tr
7-24	21.0	3	240	25	4	C/R	1.9	1.6	3.5 Tr	Tr
7-25	22.9	3	318	90	6	C/R/B	16.2	1.2	17.4 C	Tr
7-26	24.6	3	16	90	4	C/R	12.8	9.3	22.1 Tr	Sp
7-27	27.9	3	330	90	1	C	0.5	5.9	6.4 Sp	Tr
7-28	35.3	3	330	90	28	C/R	0.9	13.1	14.0 Sp	C
7-29	36.4	3	148	67	1	C	6.2	6.7	12.9 Tr	C
7-30	52.4	3	300	73	30	C/R/B	1.5	9.1	10.6 C	C
7-31	53.3	3	355	90	60	C/R/B	2.1	1.3	3.4 C	Tr
7-32	55.4	3	353	90	10	C/R	1.1	1.6	2.7 C	Te
7-33	56.0	3	261	9	2	C/R	1.4	1.3	2.7 C	Tr
7-34	60.6	3	178	21	1	C/R	5.8	0.7	6.5 Tr	Tr
7-35	61.0	3	155	69	1	C/R	1.9	5.2	7.1 Te	C
7-36	62.5	3	141	58	2	C/R	0.9	0.7	1.6 Te	Tr
7-37	66.0	3	297	71	20	C/R/B	2.4	11.2	13.6 Tr	C
7-38	67.2	3	305	90	2	C	2.4	0.3	2.7 Tr	Tr
7-39	68.5	3	65	85	2	C	5.2	0.9	6.1 Tr	Sp
7-40	74.5	3	323	90	4	C	12.3	3.5	15.8 C	C
7-41	75.7	3	301	90	4	C	3.9	2.3	6.2 Tr	C
END	**137' total**			**mean**	**9**			**mean**	**8.30**	
				max	**60**			**max**	**22.1**	
				min	**1**			**min**	**1.5**	
fracture density =		**29.9 fractures / 100 ft**								

Traverse 8, N80E Trend, Grid origin 627, 60+' long						***Start 627***	**not surveyed**				
						End 626 + 26'	**1615742.44**	**1764518.4**			
8-1	3.6	3	2	56	2	C	2.2	3.1	5.3	Tr	Tr
8-2	6.3	3	3	37	4	C/R/OT	1.1	4.9	6.0	Tr	Tr
8-3	8.0	3	300	90	2	C/R	9.4	9.5	18.9	Tr	Sp
8-4	10.8	3	161	55	2	C	8.3	3.1	11.4	Tr	Tr
8-5	13.7	3	345	36	12	C/R	3.4	3.5	6.9	Tr	Tr
8-6	14.1	3	357	53	1	C	3.8	1.9	5.7	Tr	Te
8-7	15.7	3	324	76	10	C	3.2	3.4	6.6	Tr	Tr
8-8	16.7	3	349	71	1	C	1.2	6.2	7.4	Tr	Tr
8-9	17.8	3	353	90	20	C/R/B	8	39.7	47.7	Sp	C
8-10	18.5	3	141	76	1	C	3	13	16.0	Tr	Sp
8-11	21.9	3	358	90	1	C	1.1	5.1	6.2	Tr	Tr
8-12	23.6	3	348	90	2	C	0.5	8.7	9.2	Tr	Sp
8-13	24.4	3	299	90	4	C	3.2	16.5	19.7	Sp	Tr
8-14	27.4	3	9	63	1	C	3.2	1.9	5.1	Tr	Tr
8-15	28.5	3	352	71	1	C	4.5	2.9	7.4	Tr	Tr
8-16	31.7	3	275	72	1	C	1.5	1.6	3.1	Te	Tr
8-17	33.7	3	30	62	4	C	4.6	6.2	10.8	Tr	Tr
8-18	38.2	3	335	62	1	C	2.6	10.9	13.5	Tr	C
8-19	41.4	3	293	90	12	C/R/B	14.5	9.3	23.8	Tr	C
8-20	44.4	3	15	59	4	C	8.1	1.1	9.2	C	Tr
8-21	47.0	3	326	51	2	C/R	6.4	5.7	12.1	C	C
8-22	53.5	3	350	44	8	C/OT	2.2	2.4	4.6	Tr	C
8-23	56.9	3	338	90	22	C/B/F	8	6.1	14.1	C	C
END	**57' total**			**mean**	**5**			**mean**	**11.77**		
				max	**22**			**max**	**47.7**		
				min	**1**			**min**	**3.1**		
fracture density =		**40.4 fractures / 100 ft**									

END	**1891' total**	**mean**	**7**	**mean**	**9.4**
		max	**100**	**max**	**80.7**
		min	**1**	**min**	**1**
fracture density =	**24.1 fractures / 100 ft**				

Notes:
Location coordinates are Northing and Easting in New Mexico State Plane Coordinate System, NM Central Zone, North American Datum 1983
The fracture number is the traverse number followed by the fracture number counting from the beginning of the traverse
Fracture strike orientations are presented according to the right-hand rule
Fracture filling abbreviations: C clay; Ca cataclasite; R roots; O open; OX oxidized; B breccia; F foliated; OT other.
Trace lengths are measured to the south (S) and north (N) of the traverse line.
Termination types: Tr truncated; Te terminates by dying out; SP slays; C covered.

B-2.0 SUBSURFACE FRACTURE DATA GENERATED FROM BOREHOLE OPTICAL TELEVIEWER

Table B-2.0-1
MDA P, Borehole 257

Depth (ft)	Dip Direction (degrees)	Quadrant	Dip Angle (degrees)	Strike Direction RHR (degrees)	True North Adjusted to 11 Degrees East	Lithologic Unit
9.7	344	NW	20	254	243	
33.2	7	NE	40	277	266	
33.4	282	NW	34	192	181	
37.2	187	SW	19	97	86	
37.7	116	SE	63	26	15	
39.8	39	NE	51	309	298	Unit 4I
42.2	315	NW	78	225	214	
46.1	156	SE	44	66	55	
48.4	57	NE	65	327	316	
50.4	43	NE	34	313	302	
54.3	112	SE	26	22	11	
60.6	200	SW	32	110	99	
61.9	6	NE	51	276	265	Unit 3T
63.6	179	SE	29	89	78	
65.9	33	NE	59	303	292	
72.8	77	NE	40	347	336	
73.8	208	SW	21	118	107	
76.2	34	NE	43	304	293	
78.5	230	SW	19	140	129	
80.3	295	NW	23	205	194	
88.2	192	SW	72	102	91	
90.3	353	NW	23	263	282	
99.8	283	NW	45	193	182	
104.7	8	NE	33	278	267	Unit 3
109.6	202	SW	4	112	101	
110.8	259	SW	55	169	158	
113.6	77	NE	78	347	336	
117.3	127	SE	20	37	26	
119.5	286	NW	9	196	185	
131.8	258	SW	30	168	157	
136.5	170	SE	6	80	69	
143.8	33	NE	59	303	292	
152.3	151	SE	45	61	50	

Table B-2.0-2
MDA P, Borehole 273

Depth (ft)	Dip Direction (degrees)	Quadrant	Dip Angle (degrees)	Strike Direction RHR (degrees)	True North Adjusted to 11 Degrees East	Lithologic Unit
12.5	173	SE	32	83	72	
25.2	211	SW	63	121	110	Unit 4I
27.6	85	NE	65	335	324	
56.2	181	SW	40	91	80	
60.2	233	SW	24	143	132	
66.7	62	NE	17	332	321	Unit 3T
75.2	115	SE	23	25	14	
77.4	46	NE	29	299	288	
98.4	214	SW	8	124	113	
110.2	11	NE	13	281	270	
113.5	125	SE	85	35	24	
124.3	272	NW	28	182	171	
126.3	312	NW	19	222	211	
128.4	175	SE	35	85	74	
130.3	143	SE	45	53	42	
136.2	141	SE	45	51	40	
137.8	73	NE	27	343	332	Unit 3
140.7	311	NW	24	221	210	
141.0	356	NW	18	266	255	
142.5	358	NW	18	268	257	
144.5	25	NE	25	295	284	
144.9	172	SE	47	82	71	

Table B-2.0-3
MDA P, Borehole 554

Depth (ft)	Dip Direction (degrees)	Quadrant	Dip Angle (degrees)	Strike Direction RHR (degrees)	True North Adjusted to 11 Degrees East	Lithologic Unit
9.0	255	SW	22	165	154	Unit 3T
9.2	174	SE	18	84	73	
16.4	202	SW	44	112	101	
26.1	56	NE	15	326	315	
27.1	213	SW	39	123	112	
28.4	220	SW	19	130	119	
30.0	52	NE	5	322	311	
39.9	349	NW	20	259	248	
48.3	145	SE	13	55	44	Unit 3
49.8	260	SW	14	170	159	
57.2	193	SW	60	103	92	
77.3	194	SW	86	104	93	
89.5	44	NE	3	314	303	
91.3	0	N	21	270	259	

Table B-2.0-3 (continued)
MDA P, Borehole 554

Depth (ft)	Dip Direction (degrees)	Quadrant	Dip Angle (degrees)	Strike Direction RHR (degrees)	True North Adjusted to 11 Degrees East	Lithologic Unit
92.0	191	SW	20	101	90	
92.5	21	NE	14	291	280	

Table B-2.0-4
MDA P, Borehole 526

Depth (ft)	Dip Direction (degrees)	Quadrant	Dip Angle (degrees)	Strike Direction RHR (degrees)	True North Adjusted to 11 Degrees East	Lithologic Unit
9.3	329	NW	58	239	228	
9.7	141	SE	44	51	40	Unit 3T
10.9	155	SE	54	65	54	
11.8	109	SE	33	19	8	
16.5	208	SW	33	118	107	
25.3	326	NW	63	236	225	
27.0	330	NW	33	240	229	
36.7	85	NE	51	355	344	
39.9	108	SE	21	18	7	
46.4	256	SW	76	166	155	Unit 3
49.3	113	SE	37	23	13	
50.1	65	NE	71	335	324	
50.8	1	NE	38	271	260	
53.6	258	SW	7	168	157	
53.8	32	NE	10	302	291	
54.3	343	NW	23	253	242	
54.5	117	SE	11	27	16	

Table B-2.0-5
MDA P Borehole 557

Depth (ft)	Dip Direction (degrees)	Quadrant	Dip Angle (degrees)	Strike Direction RHR (degrees)	True North Adjusted to 11 Degrees East	Lithologic Unit
36.9	51	NE	7	321	310	
46.9	56	NE	57	326	315	Unit 3
50.7	49	NE	12	319	308	
54.0	348	NW	68	258	247	

Appendix C

Descriptions of Selected Fractures in Cores

Descriptions of Fractures in Core - MDA-P

Borehole 273

Depth (ft)	
2.4 – 2.7	Low angle fracture (30°) Clays: continuous, massive, waxy clay (5YR 5/4 dry) <1 mm thick Mn oxides: absent to very few Fe oxides/hydroxides: absent
28.4	Moderate angle fracture (50°) Clays: absent, stain only on rock matrix Mn oxides: absent Fe oxides/hydroxides: common lithic fragments with white halos
48.3	Low angle fracture (10°) Clays: few, thin, waxy films, <1 mm thick Mn oxides: absent Fe oxides/hydroxides: mafic minerals pervasively altered, no halos
49.8 – 51.4	High angle fracture (70°) and rubble zone Clays: common, massive to foliated, waxy (5YR 5/4 dry) on rubble faces grades to staining across rubble zone Mn oxides: very few Fe oxides/hydroxides: common lithic fragments with white halos
62.4 - 62.6	Vertical fracture Clays: many, foliated to massive, waxy (5YR 4/2 dry) 4-6 mm thick, foliation parallel to fracture wall Mn oxides: few with very few clay intergrowths Fe oxides/hydroxides: mafic minerals pervasively altered, no halos
116.7 – 117.1	High angle fracture (80°) Clays: continuous, massive to foliated, waxy (5YR 4/5 dry) 10-12 mm thick, few phenocryst aggregates locally supported by clay matrix Mn oxides: common, with few clay intergrowths Fe oxides/hydroxides: mafic minerals pervasively altered, no halos

Note: terminology after Birkeland (1984) 0-5% very few, 5-25% few, 25-50% common, 50-90% many, 90-100% continuous.

Field_notes 6_14.doc Created on 12/4/2002 3:36 PM

Descriptions of Fractures in Core - MDA-P

Borehole 554

Depth (ft)	
8.6	High angle fracture (75°) Clays: Common, massive, waxy to dull (5YR 4/3 dry) 2-4 mm thick, few phenocryst aggregates supported by clay matrix Mn oxides: few with few clay intergrowths. Fe oxides/hydroxides: mafic minerals pervasively altered, no halos
37.5	High angle fracture (75°) Clays: common, massive, waxy (5YR 3/4 dry) 1-3 mm thick, grades to stains and thin clay films on fracture wall, few phenocryst aggregates supported by clay matrix Mn oxide: few with very few clay intergrowths Fe oxides/hydroxides: mafic minerals pervasively altered, no halos
47.2	High angle fracture (75°) Clays: staining only, grades to stains on adjacent rubble Mn oxide: very few Fe oxides/hydroxides: mafic minerals pervasively altered, no halos Other: pumice fragment 0.5 – 1 cm altered by hydration of glass
65.4	Low angle fracture (15°) Clays: common, massive, waxy (5YR 3/4 dry) 1-3 mm thick, grades to stains and thin clay films on fracture wall, few phenocryst aggregates supported by silty-clay matrix Mn oxide: very few Fe oxides/hydroxides: mafic minerals pervasively altered, no halos
75.9 - 77.8	High angle fracture (80°) Clays: continuous, foliated to massive, waxy (5YR 4/5 dry) 10-16 mm thick, foliation is locally curvilinear Mn oxides, many to continuous, ≤1 mm thick with common clay intergrowths Fe oxides/hydroxides: Mafic phenocrysts altered with white halos. Alteration of associated rock matrix includes vuggy iron oxides/hydroxides with white halos ~1 cm diameter, vugs 4-6 mm.

Note: terminology after Birkeland (1984) 0-5% very few, 5-25% few, 25-50% common, 50-90% many, 90-100% continuous.

Field_notes 6_14.doc Created on 12/4/2002 3:36 PM

Descriptions of Fractures in Core - MDA-P

Borehole 526

Depth (ft)	
1.0	Low angle fracture (10°) Clays: few, massive (5YR 5/3 dry) 1-2 mm thick Mn Oxide: absent Fe oxides/hydroxides: mafic minerals pervasively altered, no halos Organic mat and fine roots 1-3 mm thick
9.0	Moderate angle fracture (30°) Clays: common, massive, waxy (5YR 6/4 dry) ≤1 mm thick Mn oxide: few, very few clay intergrowths Fe oxides/hydroxides: mafic minerals pervasively altered, no halos
28.8	Moderate angle fracture (50°) Clays: Common, massive to foliated, waxy (5YR 5/4 dry) <1-5 mm thick, few phenocryst aggregates locally supported by clay matrix Mn Oxides: very few with very few clay intergrowths Fe oxides/hydroxides: mafic minerals pervasively altered, no halos
36.5	Moderate angle fracture (50°) Clays: very few, massive (5YR 5/8 dry) ≤1mm thick Mn Oxides: absent Fe oxides/hydroxides: mafic minerals pervasively altered, no halos
43.2	High angle fracture (75°) Clays: few, massive, waxy (5YR 5/8 dry) ≤1 mm thick, grades to common stains and clay films on adjacent rubble zone Mn Oxides: absent Fe oxides/hydroxides: mafic minerals pervasively altered, no halos Other: remnant of small degassing pipe, 1 cm dia. sorted crystals, grain-supported, oxidized and stained
44.4	High angle fracture (75°) Clays: few, massive, waxy (5YR 5/8 dry) ≤1 mm thick Mn Oxides: very few Fe oxides/hydroxides: mafic minerals pervasively altered, no halos Other: pumice fragment 3 cm dia. slightly flattened, altered by hydration (?)

Note: terminology after Birkeland (1984) 0-5% very few, 5-25% few, 25-50% common, 50-90% many, 90-100% continuous.

Field_notes 6_14.doc Created on 12/4/2002 3:36 PM

Descriptions of Fractures in Core - MDA-P

Borehole 516

Depth (ft)

28.5 - 33.7	Vertical fracture Clays: continuous, massive to foliated (5YR 3/3 dry) ≤1 to 6 mm thick, few phenocryst aggregates locally clay supported Mn oxides: very few Fe oxides/hydroxides: mafic minerals pervasively altered, no halos

Note: terminology after Birkeland (1984) 0-5% very few, 5-25% few, 25-50% common, 50-90% many, 90-100% continuous.

Field_notes 6_14.doc Created on 12/4/2002 3:36 PM

Descriptions of Fractures in Core - MDA-P

Borehole 557

Depth (ft)

0.4 Moderate angle fracture (50°)
Clays: common, massive (5YR 5/4 dry) ≤1 mm thick
Mn Oxide: absent
Fe oxides/hydroxides: mafic minerals pervasively altered, with white halos, some unaltered mafic minerals present
Black to dark brown organic mat ≤1 mm thick

20.4 Moderate angle fracture (45°)
Clays: common, massive (5YR 5/4 dry) ≤1 mm thick, grades to thin clay films
Mn oxides: few with very few clay intergrowths
Fe oxides/hydroxides: mafic minerals pervasively altered, incipient halos

55.6 High angle fracture (80°)
Clays: many, foliated to massive (5YR 3/3 dry) 1-3 mm thick, few phenocryst aggregates locally supported by silty-clay, thick clay films on phenocryst aggregates
Mn oxides: few with very few clay intergrowths
Fe oxides/hydroxides: mafic minerals pervasively altered, no halos

65.5 Moderate angle fracture (50°)
Clays: continuous, massive to foliated (5YR 5/4 dry) 10-15 mm thick, few phenocryst aggregates locally supported.by silty-clay, thick clay films on on phenocryst aggregates
Mn oxide: very few
Fe oxides/hydroxides: oxidation of mafic minerals common, no halos

Note: terminology after Birkeland (1984) 0-5% very few, 5-25% few, 25-50% common, 50-90% many, 90-100% continuous.

Field_notes 6_14.doc Created on 12/4/2002 3:36 PM

Descriptions of Fractures in Core - MDA-P

Borehole 257

Depth (ft)

21.9	Moderate angle fracture (50°) Clays: few, foliated to massive, waxy to dull (5 YR 4/4 dry) ≤1 mm thick Black, Mn oxide: common, thin with very few clay intergrowth Fe oxides/hydroxides: Altered andesitic lithic fragment 6-8 mm common with vuggy Fe oxides grading to white halos 2 cm diameter
85.5	High angle fracture (80°) Clays: few, thin, massive, waxy (5YR 5/8 dry) <1 mm thick Mn oxides: absent to very few Fe oxides/hydroxides: oxidation of mafic minerals common
104.9	Low angle fracture (20°) Clays: few, massive, waxy (5YR 5/6 dry) <1 mm thick Mn oxides: common, intergrowths absent Fe oxides/hydroxides: oxidation of mafic minerals common, no halos, lithic fragments 3-4 mm pervasively altered with incipient halos
114.8	High angle fracture (70°) Clays: many, massive to foliated, waxy (5YR 3/2 dry) 6-8 mm thick with common quartz phenocrysts supported by clay matrix Mn oxides: few with very few clay intergrowth Fe oxides/hydroxides: oxidation of mafic minerals common, incipient halos, lithic fragment 10 mm not altered

Note: terminology after Birkeland (1984) 0-5% very few, 5-25% few, 25-50% common, 50-90% many, 90-100% continuous.

Field_notes 6_14.doc Created on 12/4/2002 3:36 PM

Appendix D

Summary Plots of Borehole Geophysics

Geophysical Summary Plot

COLOG Main Office
17301 W.Colfax Ave, Ste 265, Golden, CO 80401
Phone: (303) 279-0171, Fax: (303) 278-0135
E-mail: colog@colog.com

COMPANY:	Roy F. Weston	PROJECT:	MDA-P, Los Alamos Natl Labs
DATE LOGGED:	Sept. 12/Oct. 1, '01	WELL:	257

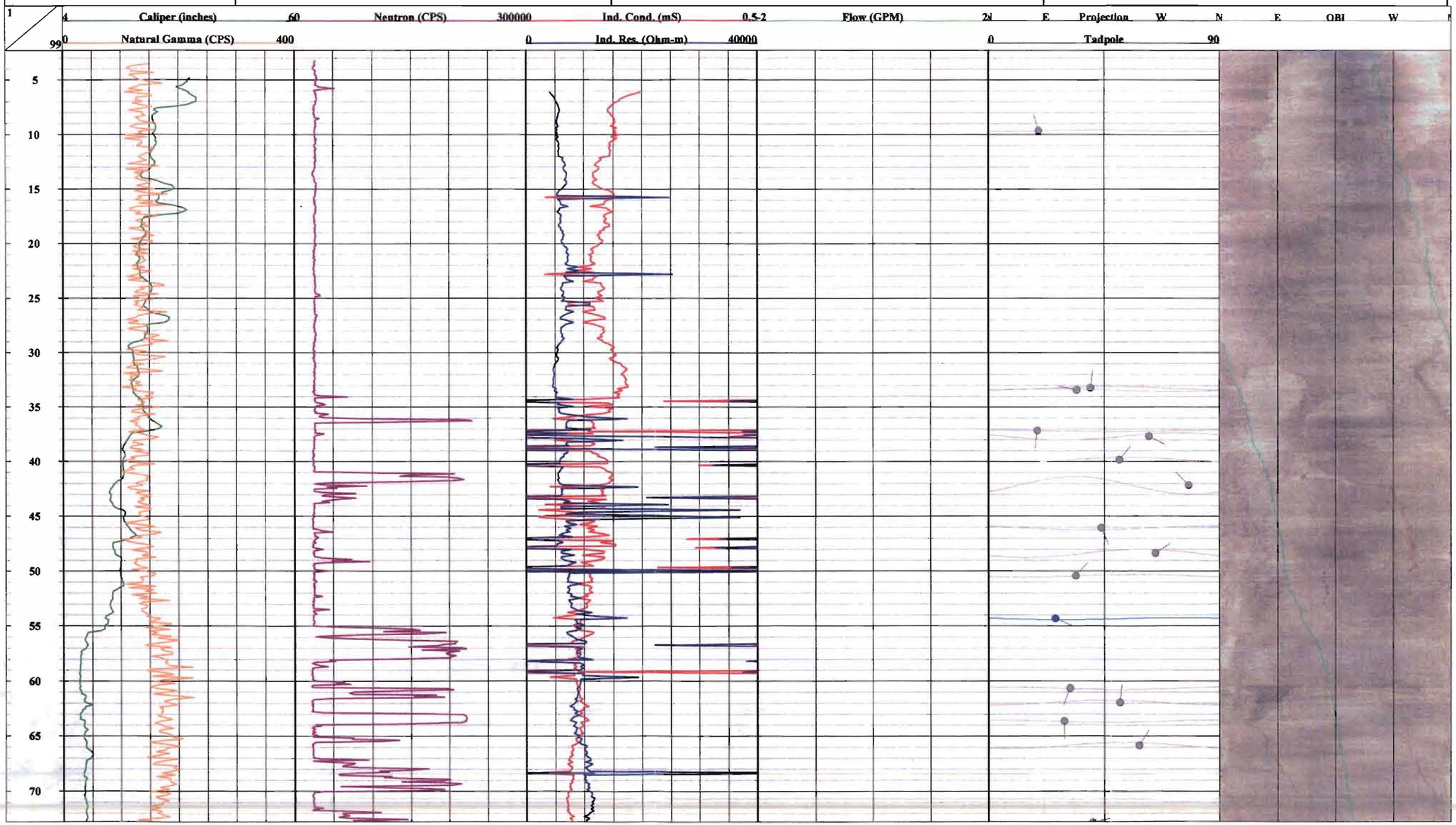

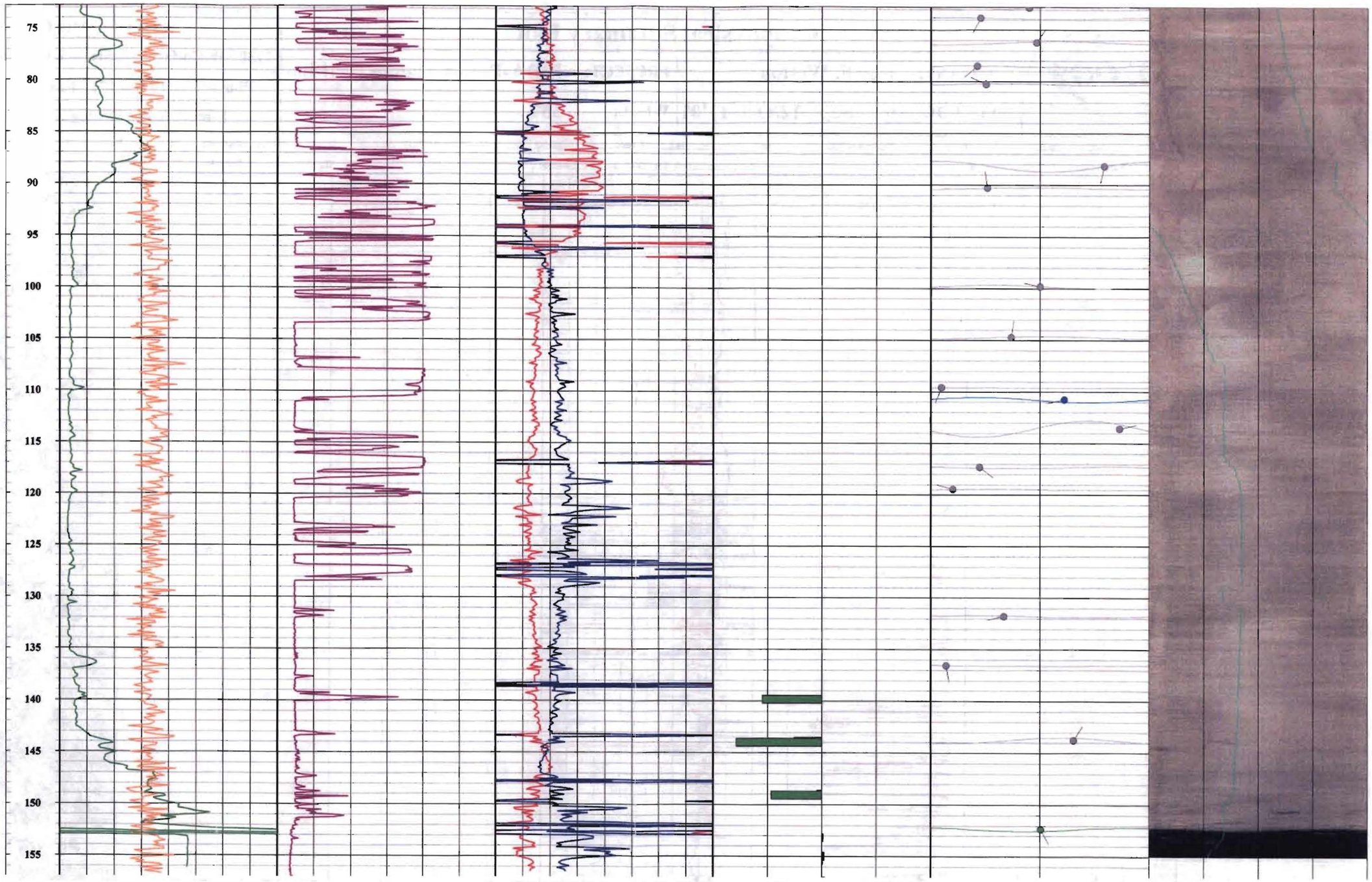
75
80
85
90
95
100
105
110
115
120
125
130
135
140
145
150
155

Geophysical Summary Plot

COLOG Main Office
17301 W.Colfax Ave, Ste 265, Golden, CO 80401
Phone: (303) 279-0171, Fax: (303) 278-0135
E-mail: colog@colog.com

COMPANY:	Roy F. Weston	PROJECT:	MDA-P, Los Alamos Natl Labs
DATE LOGGED:	Sept. 12/Oct. 1, '01	WELL:	257 REPEAT

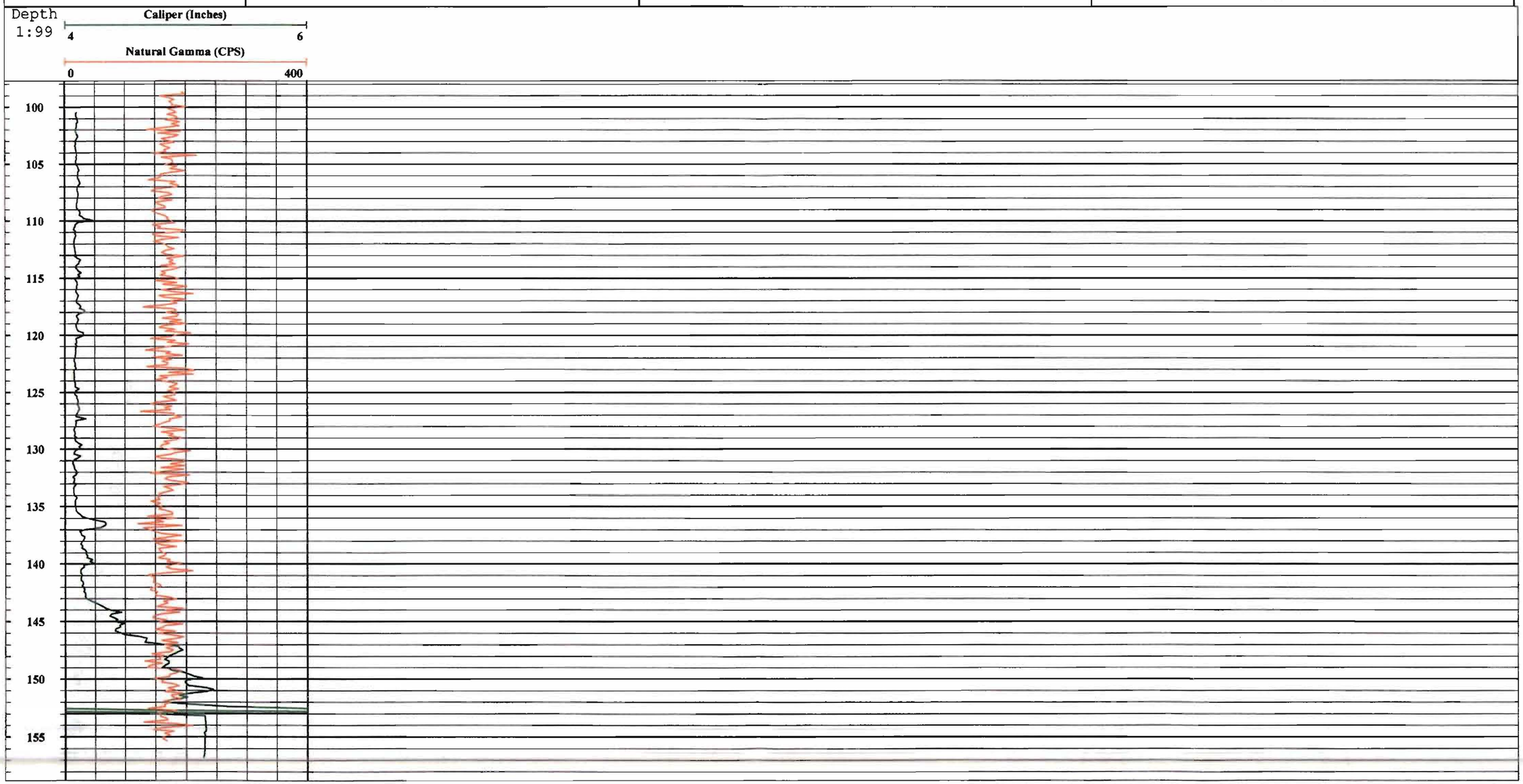

Geophysical Summary Plot

COMPANY: Roy F. Weston, Inc.	PROJECT: MDA-P Los Alamos Natl Labs
DATE LOGGED: Sept. 12/Oct. 1, '01	WELL: 273

COLOG Main Office
17301 W.Colfax Ave, Ste 265, Golden, CO 80401
Phone: (303) 279-0171, Fax: (303) 278-0135
E-mail: colog@colog.com

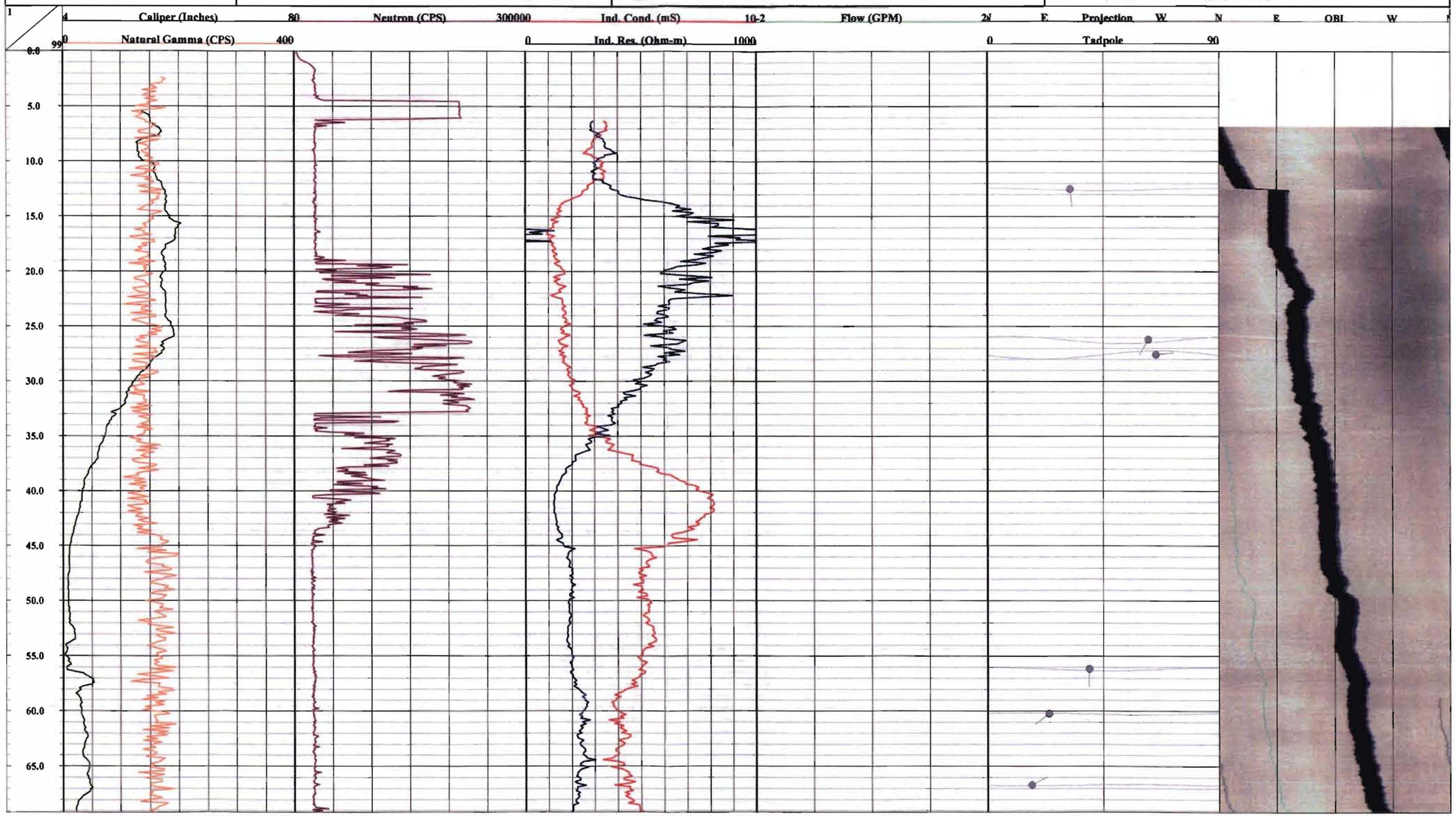

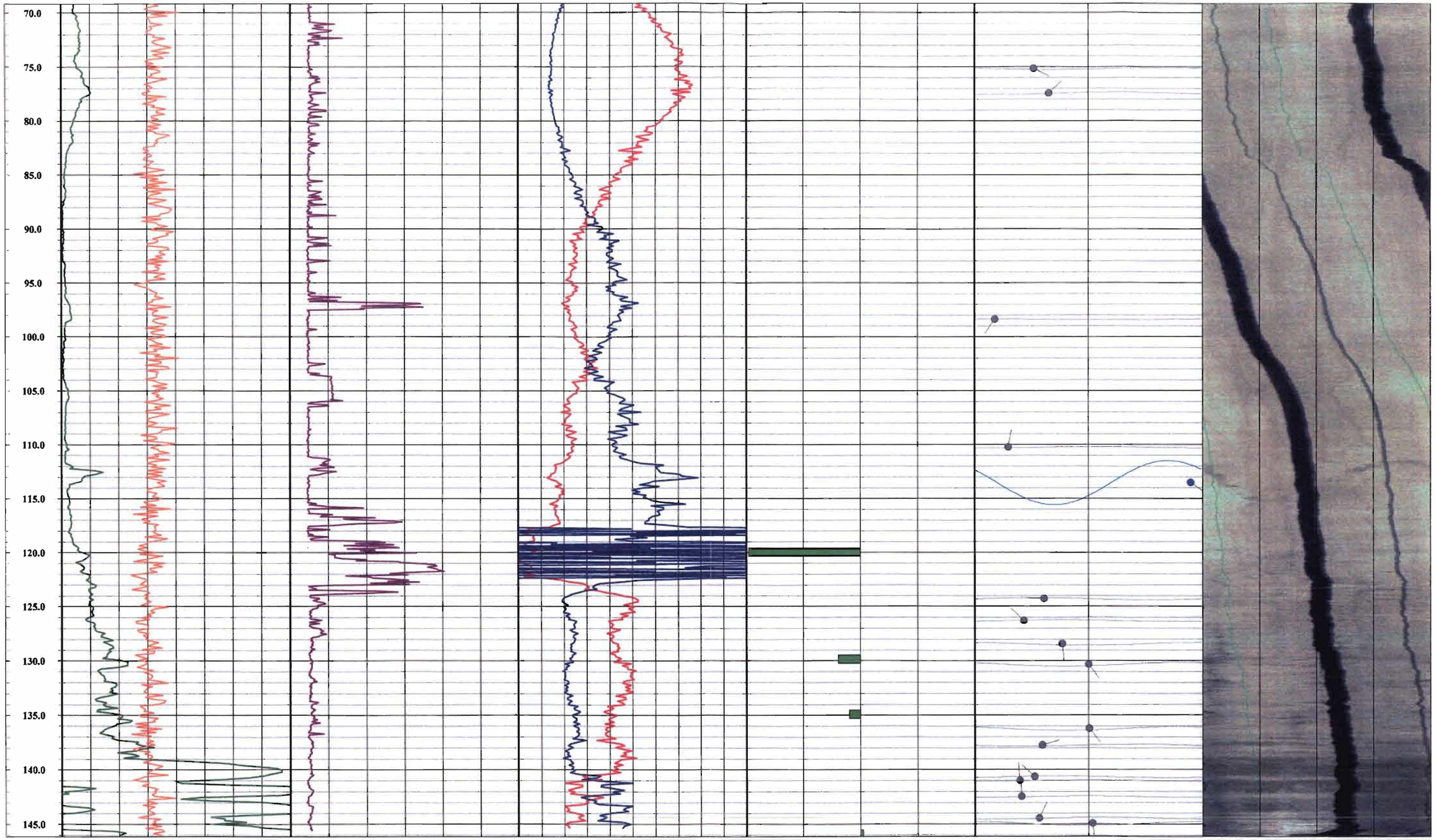
70.0
75.0
80.0
85.0
90.0
95.0
100.0
105.0
110.0
115.0
120.0
125.0
130.0
135.0
140.0
145.0

Geophysical Summary Plot

COMPANY:	Roy F. Weston, Inc.	PROJECT:	MDA-P Los Alamos Natl Labs
DATE LOGGED:	Sept. 12/Oct. 1, '01	WELL:	273 REPEAT

COLOG Main Office
17301 W.Colfax Ave, Ste 265, Golden, CO 80401
Phone: (303) 279-0171, Fax: (303) 278-0135
E-mail: colog@colog.com

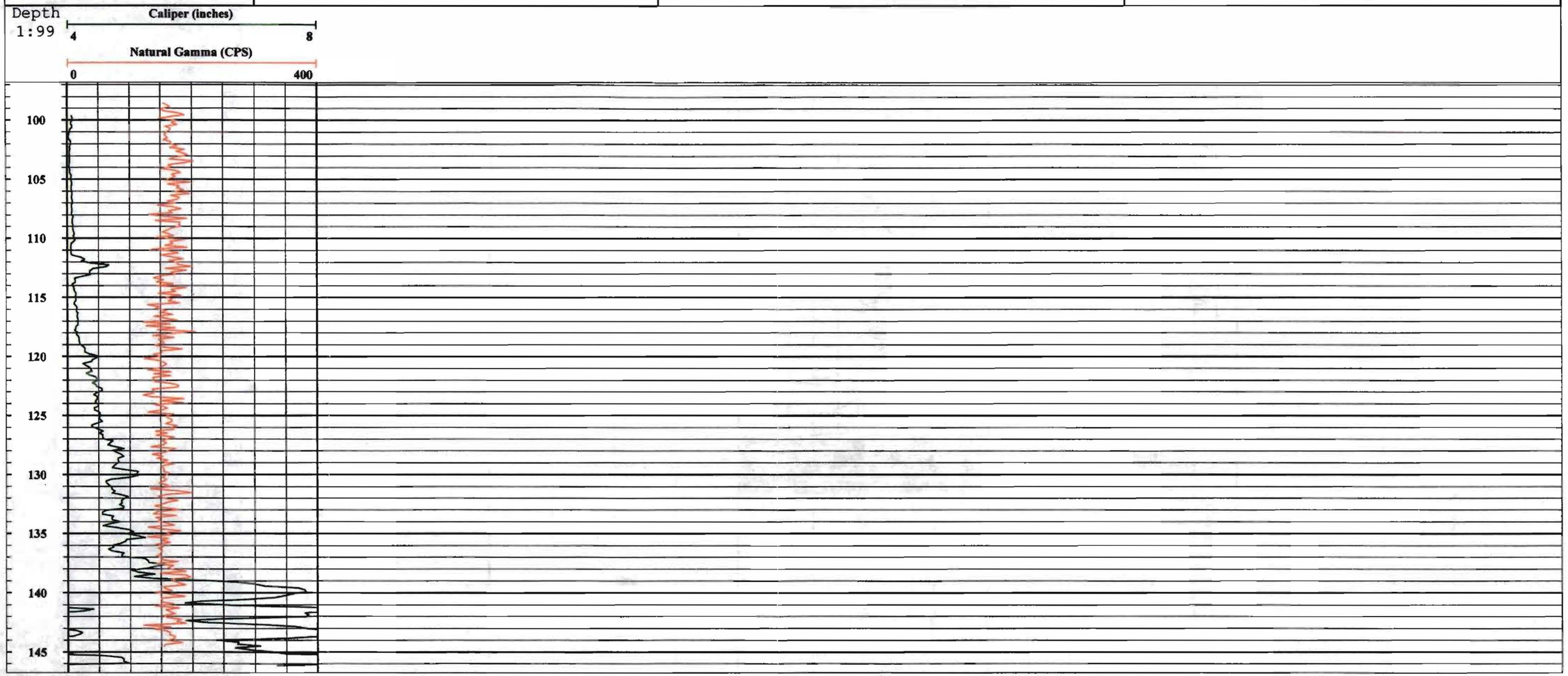

Geophysical Summary Plot

COLOG Main Office
17301 W.Colfax Ave, Ste 265, Golden, CO 80401
Phone: (303) 279-0171, Fax: (303) 278-0135
E-mail: colog@colog.com

COMPANY:	Roy F. Weston	PROJECT:	MDA-P, Los Alamos Natl. Labs
DATE LOGGED:	Sept. 12/Oct. 1, '01	WELL:	526

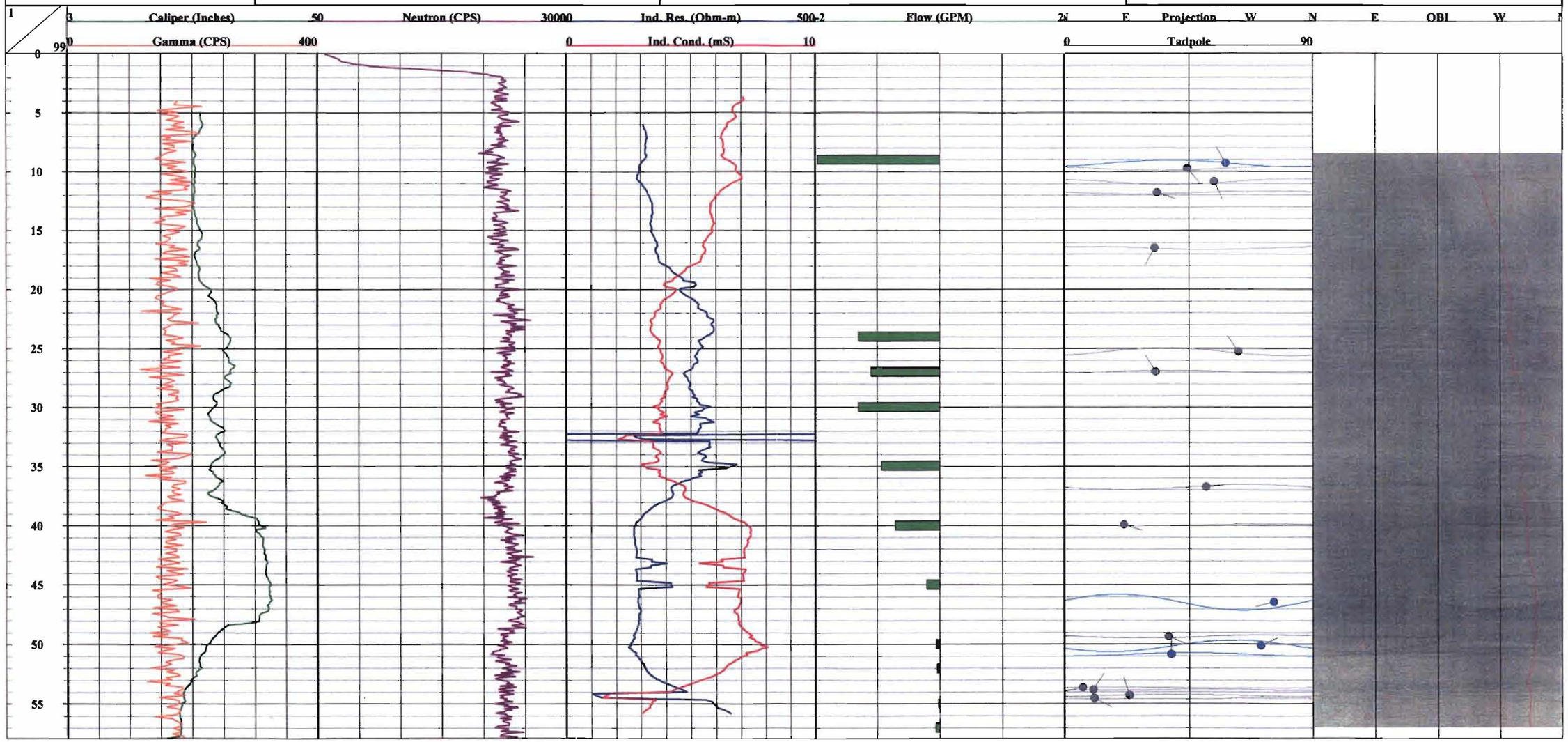

Geophysical Summary Plot

COLOG Main Office
17301 W.Colfax Ave, Ste 265, Golden, CO 80401
Phone: (303) 279-0171, Fax: (303) 278-0135
E-mail: colog@colog.com

COMPANY:	Roy F. Weston	PROJECT:	MDA-P, Los Alamos Natl. Labs
DATE LOGGED:	Sept. 12/Oct. 1, '01	WELL:	526 REPEAT

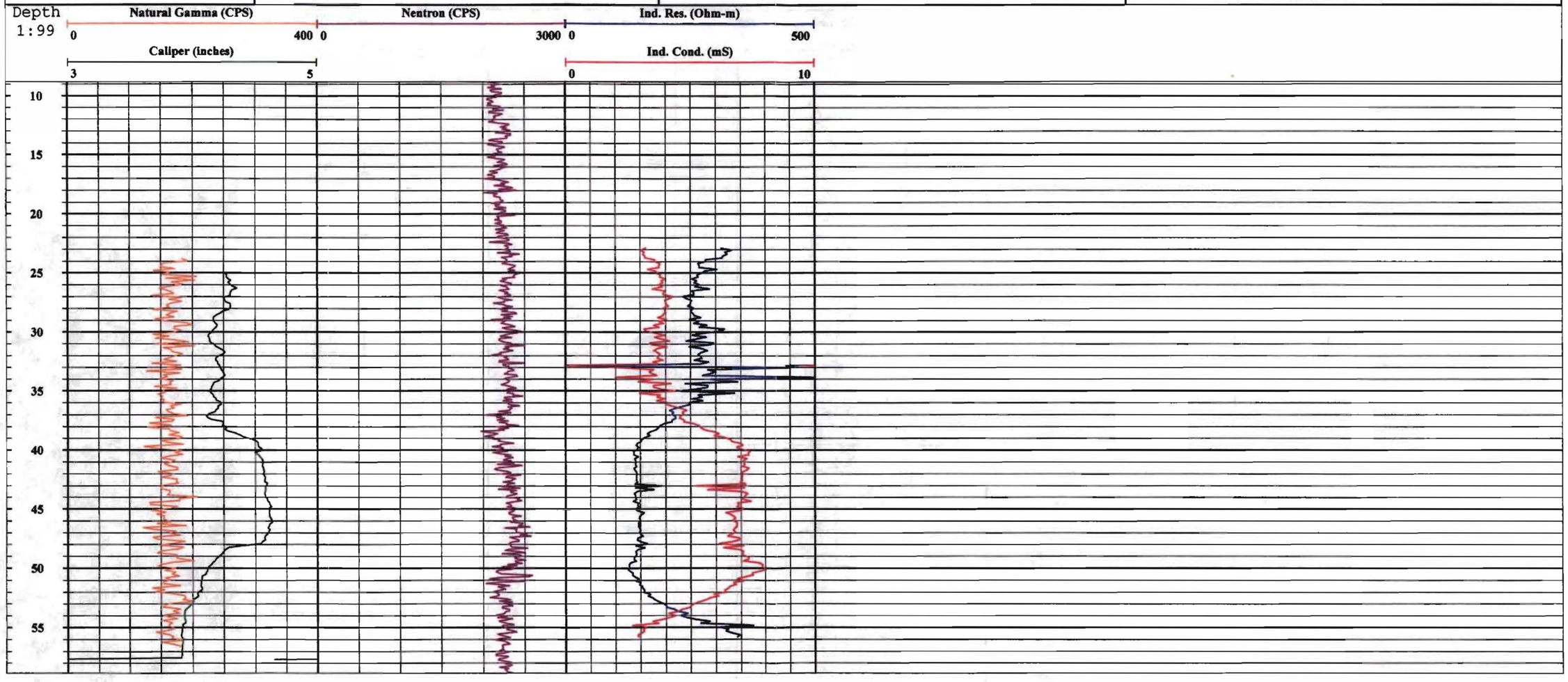

Geophysical Summary Plot

COLOG Main Office
17301 W.Colfax Ave, Ste 265, Golden, CO 80401
Phone: (303) 279-0171, Fax: (303) 278-0135
E-mail: colog@colog.com

COMPANY:	Roy F. Weston, Inc.	PROJECT:	MDA-P, Los Alamos Natl Labs
DATE LOGGED:	Sept. 12/Oct. 1, '01	WELL:	554

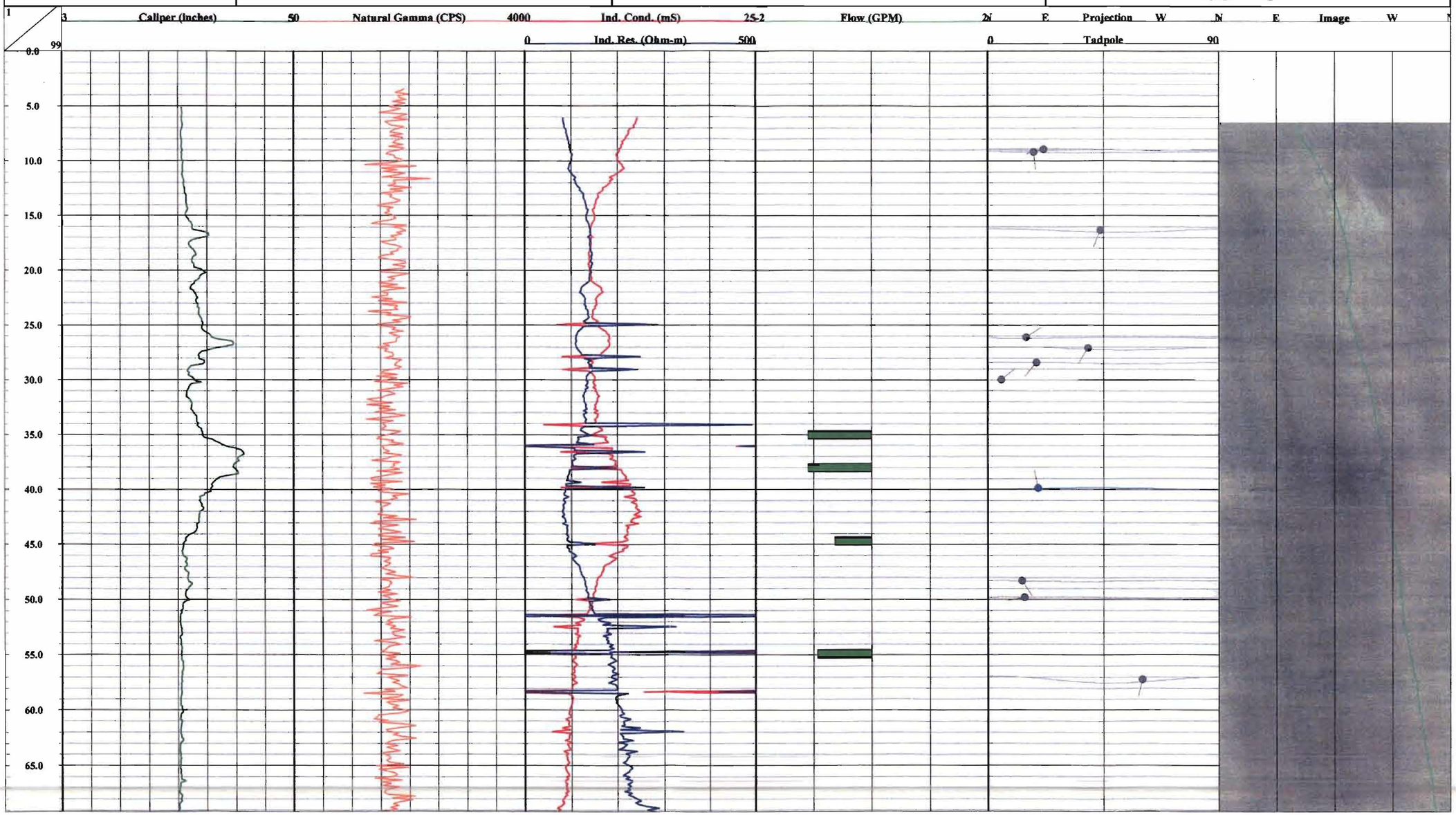

Geophysical Summary Plot

COMPANY:	Roy F. Weston, Inc.	PROJECT:	MDA-P, Los Alamos Natl Labs
DATE LOGGED:	Sept. 12/Oct. 1, '01	WELL:	554 REPEAT

COLOG Main Office
17301 W.Colfax Ave, Ste 265, Golden, CO 80401
Phone: (303) 279-0171, Fax: (303) 278-0135
E-mail: colog@colog.com

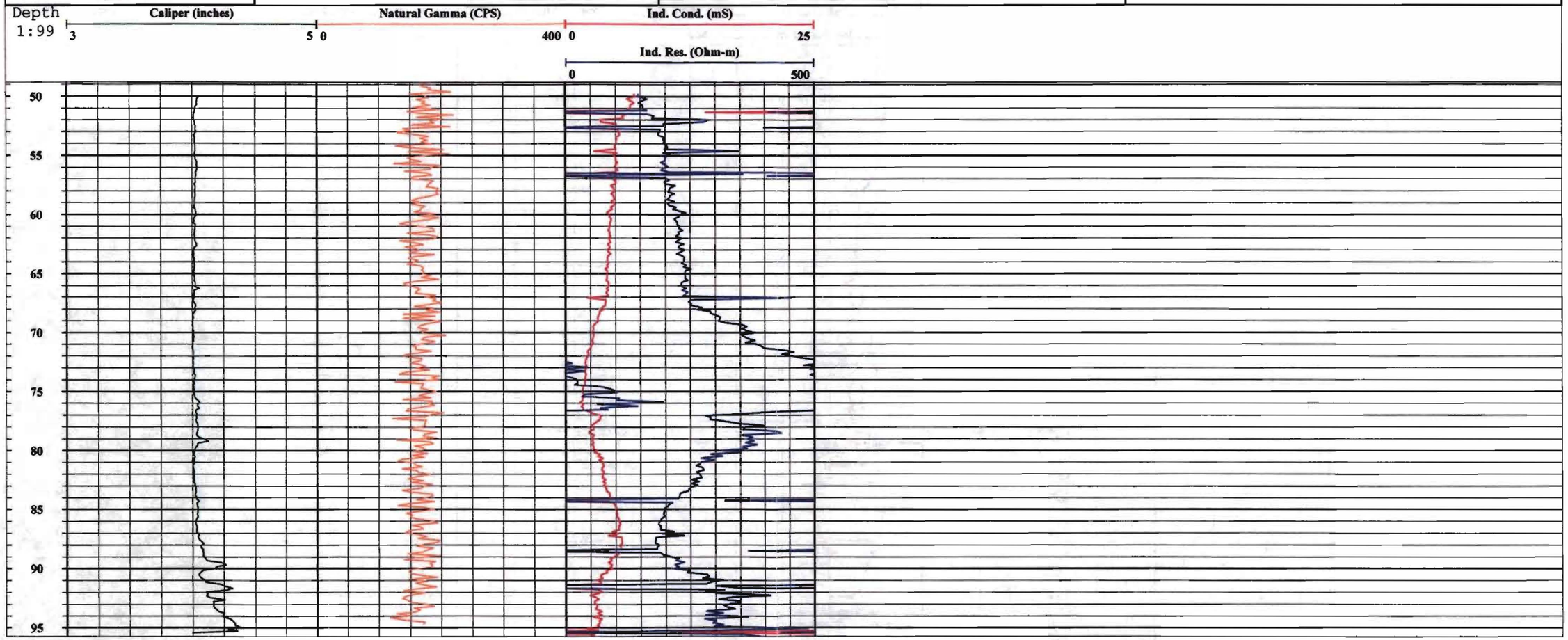

Geophysical Summary Plot

COLOG Main Office
17301 W.Colfax Ave, Ste 265, Golden, CO 80401
Phone: (303) 279-0171, Fax: (303) 278-0135
E-mail: 1051@laynechristensen.com

COMPANY:	Roy F. Weston, Inc.	PROJECT:	MDA-P, Los Alamos Natl Labs
DATE LOGGED:	Sept. 12/Oct. 1, '01	WELL:	557

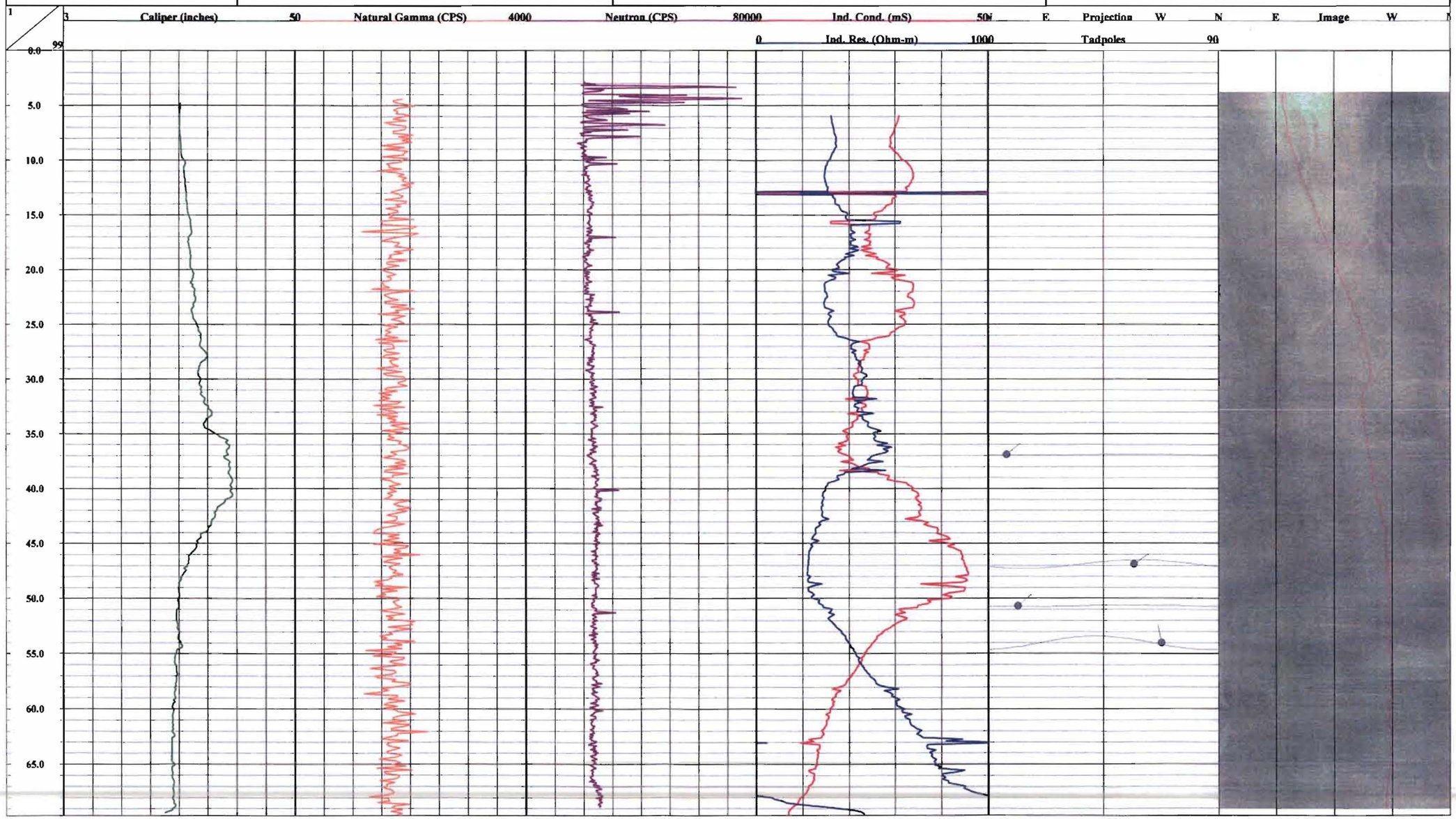

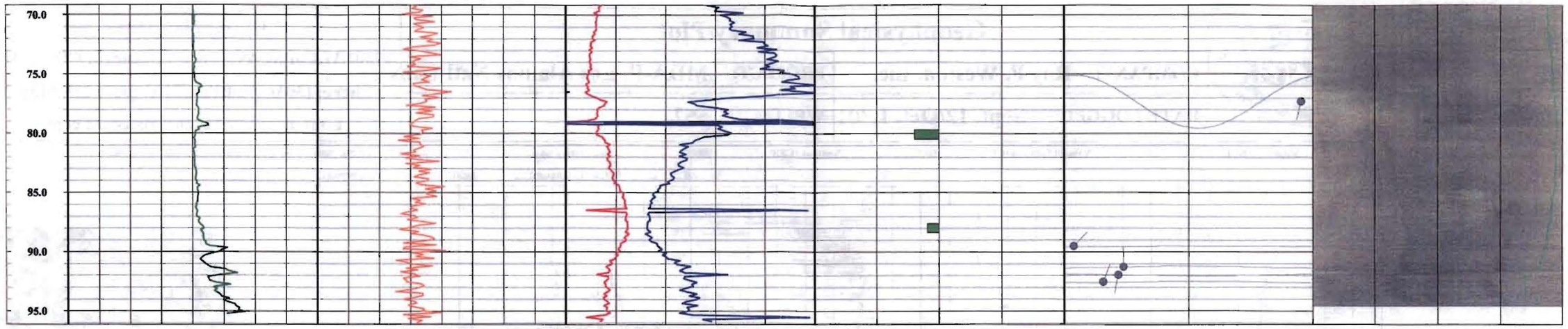
70.0
75.0
80.0
85.0
90.0
95.0

Geophysical Summary Plot

COLOG Main Office
17301 W.Colfax Ave, Ste 265, Golden, CO 80401
Phone: (303) 279-0171, Fax: (303) 278-0135
E-mail: 1051@laynechristensen.com

COMPANY: Roy F. Weston, Inc.	PROJECT: MDA-P, Los Alamos Natl Labs
DATE LOGGED: Sept. 12/Oct. 1, '01	WELL: 557 REPEAT

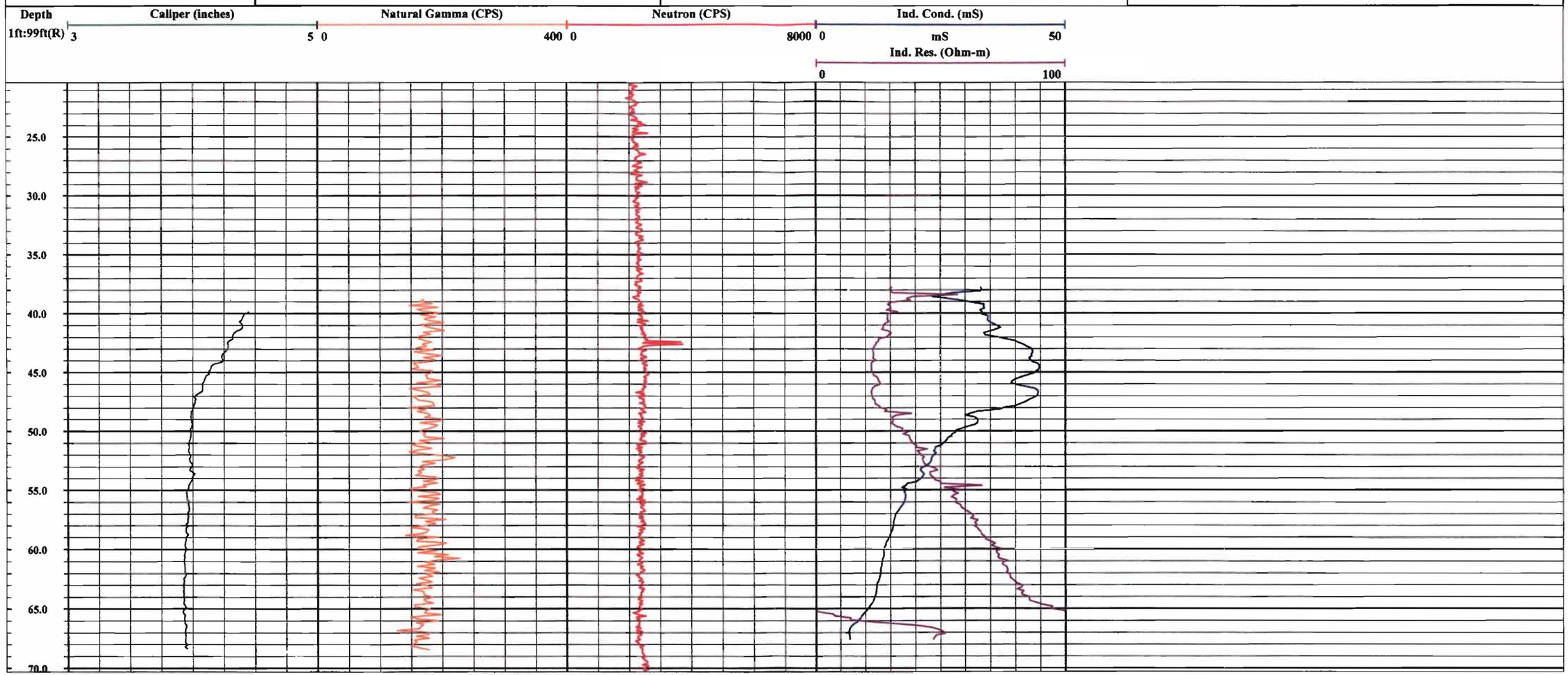

Appendix E

Heat Pulse Flowmeter Data Tables

HEAT PULSE FLOWMETER
BOREHOLE 257

"Depth" "Feet"	"Flow" "Gal./min."	Comments
139.817	-1.1	
144.002	-0.942	
144.002	-1.306	
144.002	-1.581	
144.002	-1.581	
144	**-1.3525**	limit of tool
148.985	-0.124	
149.085	-0.253	
149.085	-0.389	
149.085	-0.465	
149.085	-0.513	
149.085	-0.717	
149	**-0.410167**	
154.964	-0.037	
154.964	-0.053	
154.964	-0.043	
154.964	-0.053	
154.964	-0.088	
155	**-0.0548**	
157.356	-0.058	
157.356	-0.052	
157	**-0.055**	

Note: negative flow
is downward

154.964	0.039
155.363	0.02
155.363	0.016
149.085	-0.717
149.085	-0.942
153.171	0.021
155.064	0.028
155.064	0.027

HEAT PULSE FLOWMETER
BOREHOLE 273

"Depth" "Feet"	"Flow" "Gal./min."	Comments
119.985	-1.962	
129.851	-0.389	
129.851	-0.389	
129.851	-0.389	
129.851	-0.389	
130	**-0.389**	
134.934	-0.181	
134.934	-0.212	
134.934	-0.191	
134.934	-0.201	
134.934	-0.201	
135	**-0.1972**	

Note: negative flow
is downward

HEAT PULSE FLOWMETER

BOREHOLE 526

"Depth" "Feet"	"Flow" "Gal./min."	Comments
8.982	-1.581	
8.983	-1.962	rejected
52.037	-0.046	
57.012	-0.02	
57.012	-0.068	
24.012	-1.306	
24.012	-1.306	
24.012	-1.306	
24.012	**-1.306**	rejected
26.982	-1.1	
26.982	-1.1	
26.982	-1.1	
26.982	**-1.1**	
34.963	-0.942	
34.963	-0.942	
34.963	-0.942	
34.963	**-0.942**	
40.012	-0.717	
40.012	-0.717	
40.012	-0.717	
40.012	**-0.717**	
44.99	-0.212	
44.99	-0.212	
44.99	**-0.212**	
49.974	-0.073	
49.974	-0.061	
49.973	-0.064	
49.974	**-0.066**	
54.975	-0.027	
54.975	-0.051	
54.975	-0.037	
54.975	-0.029	
54.975	**-0.036**	

Note: negative flow is downward

flow	depth	flow/interval	interval
0	1.20	0	
24	1.20	24	0.1	24
27	1.10	27	0.16	3
35	0.94	35	0.22	8
40	0.72	40	0.51	5
45	0.21	45	0.11	5
50	0.10	50	0.06	5
55	0.04	55	0.04	5
59	0.00	59		

rate/foot	Elevation	7421 nearest
	7421	7420
0.004	7397	7400
0.053	7394	7395
0.028	7386	7385
0.102	7381	7380
0.022	7376	7375
0.012	7371	7370
0.008	7366	7365
	7362	7360

HEAT PULSE FLOWMETER
BOREHOLE 554

"Depth" "Feet"	"Flow" "Gal./min."	Comments
35.03	-1.306	
35.03	-1.306	
35.03	-1.306	
35.039	-1.1	
35	**-1.2545**	too low?
38.041	-1.1	
38.041	-1.1	
38.041	-1.1	
38.041	-1.1	
38	**-1.1**	
44.705	-0.636	
44.705	-0.717	
44.705	-0.636	
45	**-0.663**	
54.931	-0.942	
54.931	-0.942	
54.931	-0.942	
54.931	-0.942	
54.931	-0.817	
54.931	-0.942	
55	**-0.921167**	
58.071	-0.717	
58.071	-0.817	
58.071	-0.817	
58.071	-0.817	
58	**-0.792**	
74.961	-0.513	
74.961	-0.513	
74.961	-0.465	
74.961	-0.513	
74.961	-0.465	
75	**-0.61725**	
80.108	-0.389	
80.108	-0.424	
80.108	-0.389	
80.108	-0.389	
80.108	-0.389	
80.108	-0.389	
80	**-0.394833**	
87.982	-0.201	
87.982	-0.201	
87.982	-0.201	
87.982	-0.212	
87.982	-0.191	
88	**-0.2012**	

Nore: negative flow
is downward

Cum Flow	Depth	flow/interval	interval	rate/foot	elevation	7422	rounded
1.60	0	0.30	35	0.009		7422	7420
1.30	35	0.20	3	0.067		7387	7390
1.10	38	0.10	7	0.014		7384	7385
1.00	45	0.08	10	0.008		7377	7375
0.92	55	0.13	3	0.043		7367	7370
0.79	58	0.17	17	0.010		7364	**7365**
0.62	75	0.23	5	0.046		7347	7345
0.39	80	0.19	8	0.024		7342	7340
0.20	88	0.20	8	0.025		7334	7335
0.00	96					7326	7325
	554						

Appendix F

Summary Tables of Geochemical Anion/Cation Analyses

Core 526 East Lobe Leach Results (mg/kg)

Mid-depth (ft)	Unit	Br (mg/kg)	C_2O_4 (mg/kg)	Cl (mg/kg)	F (mg/kg)	NO_2 (mg/kg)	NO_3 (mg/kg)	PO_4 (mg/kg)	SO_4 (mg/kg)	Note
0.3	3t	0	2.38	4.18	11.34	0.83	26.8	0	4.21	—
2.4	3t	0	0.09	2.75	10.89	0	7.9	0.22	3.25	fx[a]
10.25	3t	0	0.53	3.80	5.11	0	7.3	0	2.33	fx
15.25	3	0	0.00	2.65	13.15	0	9.9	0	2.30	—
17.25	3	0	0.55	4.86	2.80	0	13.2	0.07	2.29	fx
25.75	3	0	0.26	4.07	1.69	0	6.2	0	2.32	—
28.55	3	0	0	3.72	1.48	0	3.9	0.17	3.52	fx
35.75	3	0	0.97	3.41	0.58	0	6.7	0	4.86	—
38.4	3	0	0.68	8.68	1.36	0	25.8	0	3.54	fx
44.95	3	0	0	6.06	0.91	0	22.9	0	1.70	—
55.25	3	0	0	2.44	0.35	0	7.3	0.39	0.60	—
59.15	3	0	0	3.63	0.47	0	11.5	0.35	0.63	—
Max.	—	**0**	**2.4**	**8.7**	**13.2**	**0.8**	**26.8**	**0.4**	**4.9**	—
Min.	—	**0**	**0**	**2.4**	**0.3**	**0**	**3.9**	**0.0**	**0.6**	—

[a] fx = fractured.

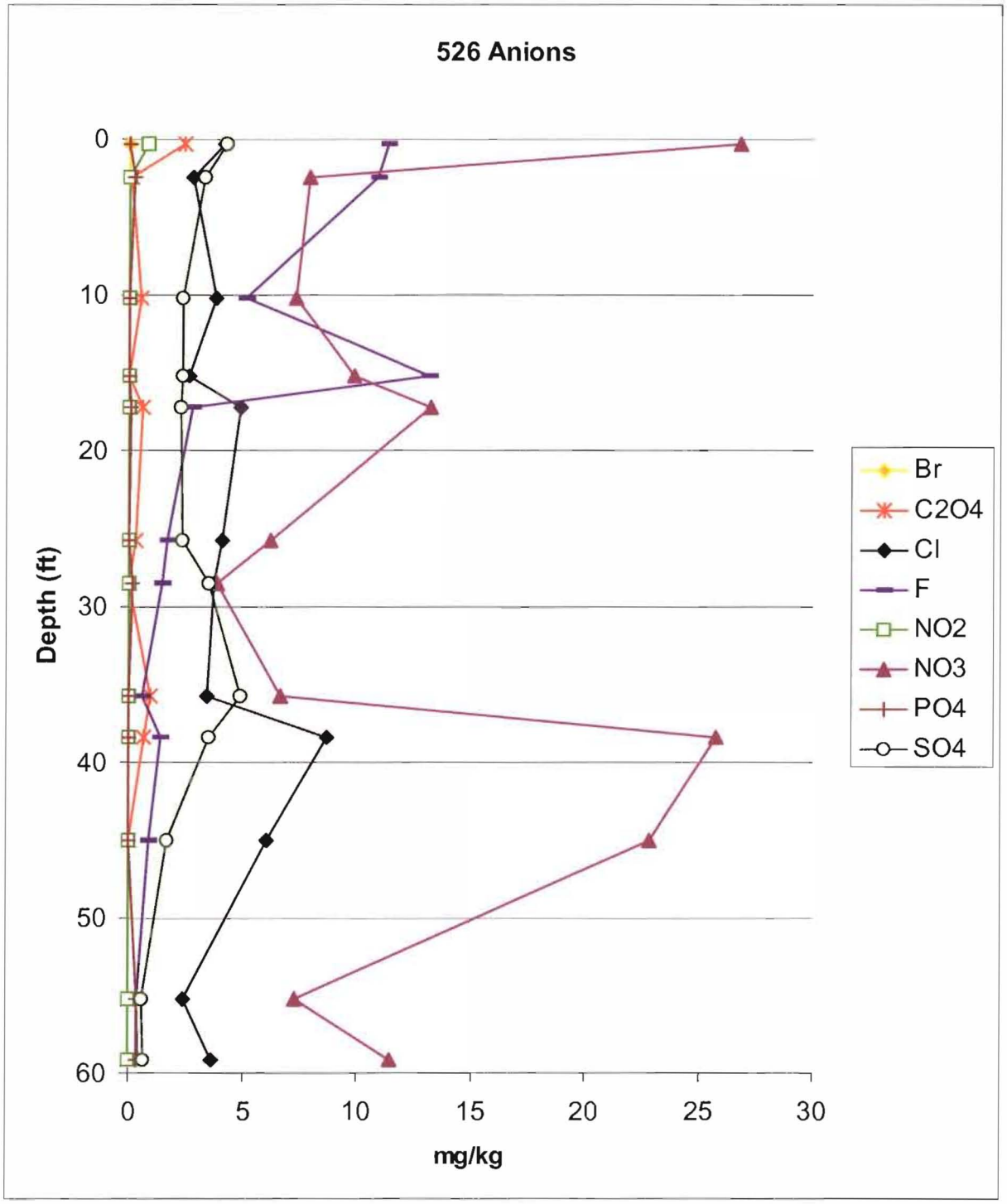
526 Anions
Depth (ft)
0
10
20
30
40
50
60
0
5
10
15
20
25
30
mg/kg
Br
C2O4
Cl
F
NO2
NO3
PO4
SO4

Core 554 West Lobe Leach Results (mg/kg)

Mid-depth (ft)	Unit	Br (mg/kg)	C_2O_4 (mg/kg)	Cl (mg/kg)	F (mg/kg)	NO_2 (mg/kg)	NO_3 (mg/kg)	PO_4 (mg/kg)	SO_4 (mg/kg)	Note
0.25	3t	0	0.8723	4.69	0.33	0.77	0.9	0	17.15	—
1.75	3t	0	0	3.80	0.26	0	15.1	0	66.27	fx[a]
10.95	3t	0	0.06	2.76	0.70	0	10.4	0	15.16	—
20	3	0	0	1.85	0.65	0	4.7	0	10.67	—
30.7	3	0	0.23	2.84	0.63	0	2.2	0.24	7.21	—
38.75	3	0	0	7.13	1.25	0	13.3	0.30	20.47	fx
44.45	3	0	0	7.56	1.00	0.66	7.2	0.26	10.04	fx
50.25	3	0	0	3.35	0.23	0	7.8	0	8.27	—
56.6	3	0	0	3.22	0.42	0	2.0	0.42	3.07	fx
60.05	3	0.02	0	2.26	0.27	0	1.9	0.15	3.01	—
70.25	3	0	0	2.78	0.14	0	1.8	0	3.90	—
77.05	3	0	0.24	7.37	0.16	0	5.6	0	10.00	fx
80.05	3	0.05	0	3.35	0.15	0	2.3	0	2.76	—
89.1	3	0.06	0.09	4.85	0.05	0	2.7	0	1.61	—
Max	**—**	**0.06**	**0.9**	**7.6**	**1.2**	**0.8**	**15.1**	**0.4**	**66.3**	**—**
Min	**—**	**0**	**0**	**1.8**	**0**	**0**	**0.9**	**0**	**1.6**	**—**

[a] fx = fractured.

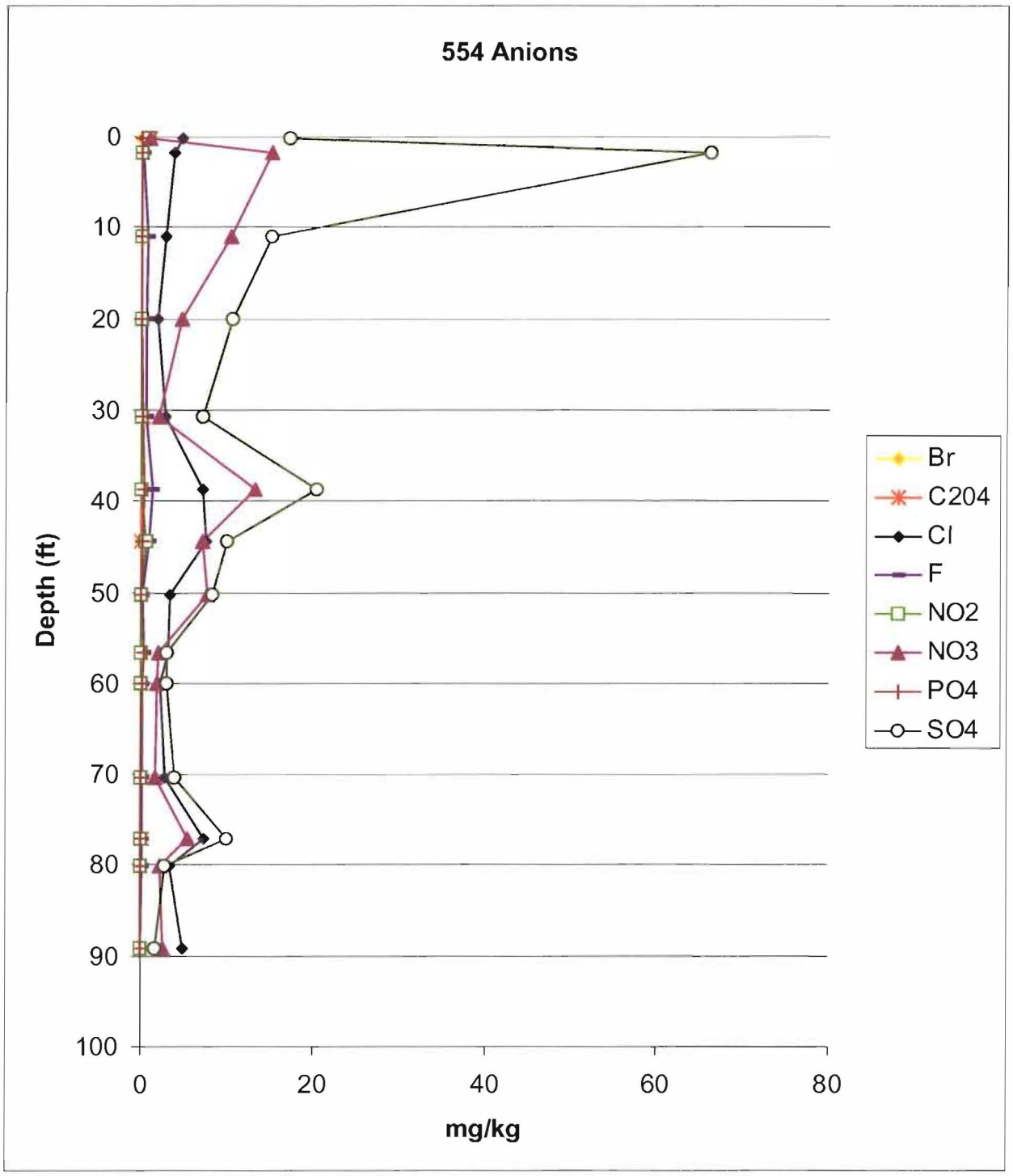
554 Anions
Depth (ft)
0
10
20
30
40
50
60
70
80
90
100
0
20
40
60
80
mg/kg
Br
C204
Cl
F
NO2
NO3
PO4
SO4

Core 273 Old Burn Pad Leach Results (mg/kg)

Mid-depth (ft)	Unit	Br (mg/kg)	C_2O_4 (mg/kg)	Cl (mg/kg)	F (mg/kg)	NO_2 (mg/kg)	NO_3 (mg/kg)	PO_4 (mg/kg)	SO_4 (mg/kg)	Note
0.25	3t	0	0	4.5	0.79	0	0.3	0	1.26	fx[a]
4.95	3t	0	0	5.2	0.67	0	0.3	0	1.84	nrt[b]
16.95	3t	0	0	4.5	0.58	0	0	0	1.24	nrb[c]
22.1	3t	0	0	9.6	0.87	0	0	0	1.30	nrb
33.25	3t	0.07	0	18.6	1.04	0	0.1	0	1.62	nrb
39.55	3t	0	0	23.1	1.09	0	6.2	0	3.49	—
50.5	3t	0	0	42.9	3.53	0	0.2	1.8	1.25	fx
61.3	3t	0	0	21.6	1.86	0	0	0.6	2.24	fx
62.75	3t	0	0	61.9	5.47	0	0	1.1	1.71	fx
74	3t	0	0.20	35.0	2.43	0	0	0.87	1.45	nrb
80.4	3t	0	0.35	58.0	3.18	0	0	0.59	0.80	nrt
90.3	3	0.37	0	5.4	0.73	0	0	0.00	0.36	nrt
94.6	3	0	0	16.7	1.40	0	0	0.44	0.29	fx
100.35	3	0	0	5.0	0.61	0	0.1	0.22	0.52	nrt
105	3	0	0.21	5.1	0.97	0	0.2	0.21	0.49	fx
110.7	3	0	0	5.0	0.22	0	0.6	0	7.43	nrb
113.75	3	0	0	7.8	0.16	0	0.5	0	13.40	fx
117.25	3	0	0	4.8	0.12	0	0.3	0	5.26	fx
119.75	3	0	0	8.0	0.11	0	0.4	0	14.35	rubble
Max	—	**0**	**0.3**	**61.9**	**5.5**	**0.0**	**0.6**	**1.1**	**14.3**	—
Min	—	**0**	**0**	**4.8**	**0.1**	**0**	**0.0**	**0.0**	**0.3**	—

[a] fx = fractured.

[b] nrt = top of no-recovery zone.

[c] nrb = bottom of no-recovery zone.

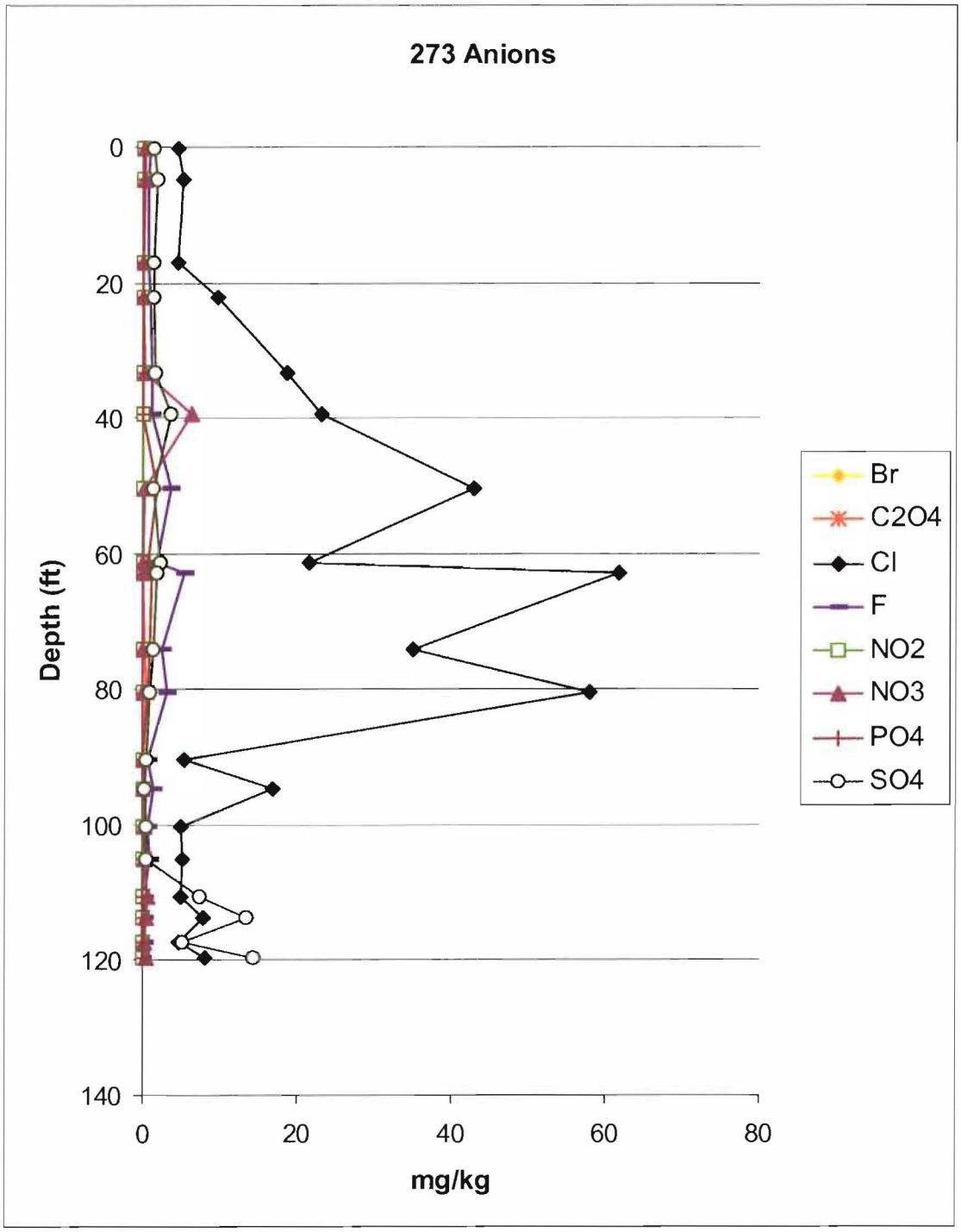
273 Anions
Depth (ft)
0
20
40
60
80
100
120
140
0
20
40
60
80
mg/kg
Br
C2O4
Cl
F
NO2
NO3
PO4
SO4

526 Cations

Mid-depth (ft)	Tuff wt (g)	Ba (mg/kg)	Ca (mg/kg)	K (mg/kg)	Mq (mg/kg)	Na (mg/kg)
0.3	50.05	116.26	8.22	4.55	1.76	25.54
2.4	51.28	1.59	10.23	1.39	2.24	11.49
10.25	50.11	0.95	4.31	0.98	1.11	14.69
15.25	50.01	0.78	11.09	1.41	2.46	15.31
17.25	50.21	0.79	5.12	1.09	1.11	12.67
25.75	50.57	0.54	2.30	1.36	0.57	16.57
28.55	50.01	0.66	1.73	1.57	0.47	24.70
35.75	50.19	0.70	2.38	1.77	0.60	23.51
38.4	50.08	0.22	2.97	2.79	0.37	51.14
44.95	51.24	0.41	3.45	1.93	0.47	22.83
55.25	50.32	0.67	1.29	2.18	0.21	26.90
59.15	50.81	0.38	0.69	1.35	0.10	16.26

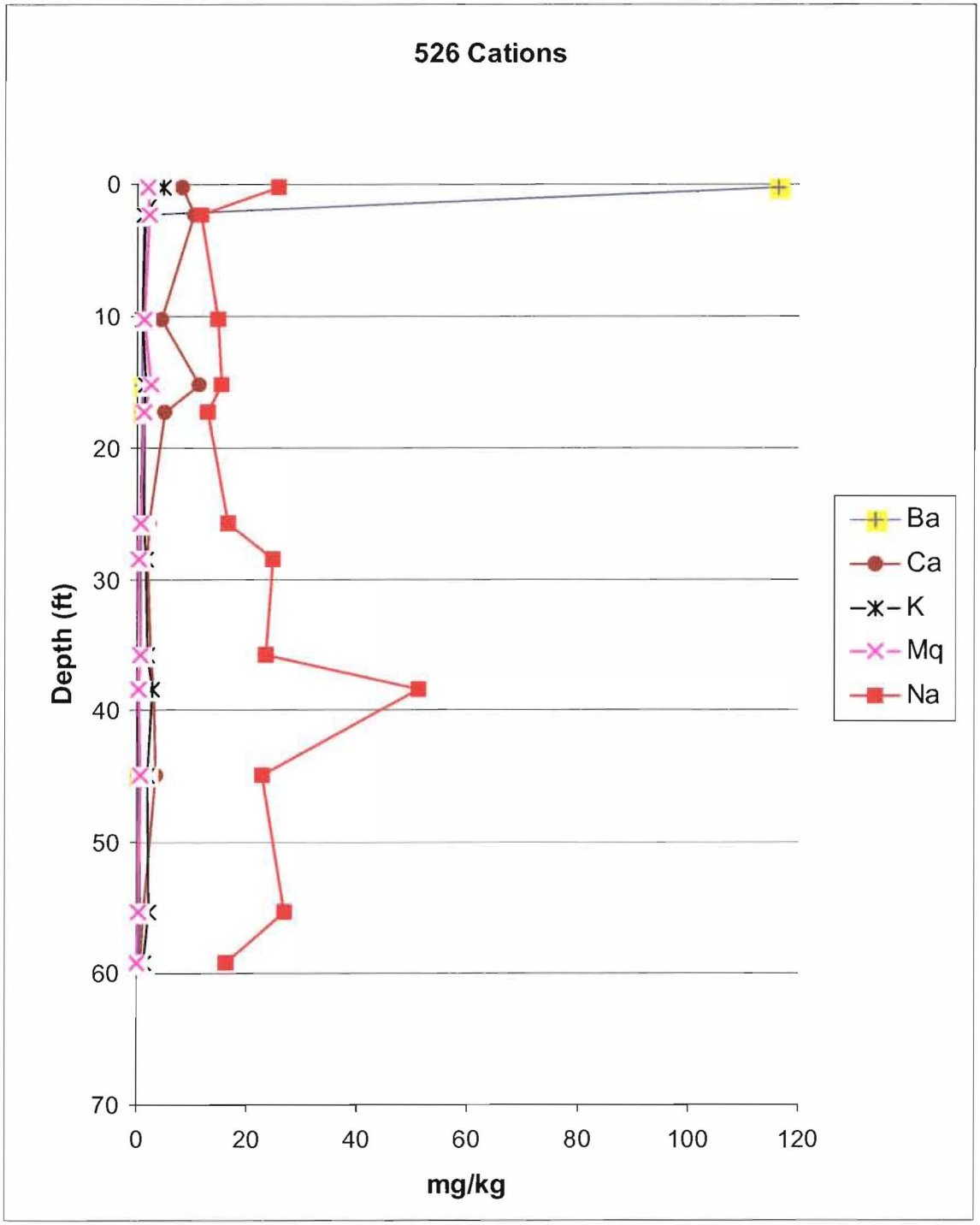
526 Cations
Depth (ft)
0
10
20
30
40
50
60
70
0
20
40
60
80
100
120
mg/kg
Ba
Ca
K
Mq
Na

554 Cations

Mid-depth (ft)	Ba (mg/kg)	Ca (mg/kg)	K (mg/kg)	Mq (mg/kg)	Na (mg/kg)
0.25	0.91	4.68	2.86	0.84	20.8
1.75	0.93	4.78	4.60	1.50	24.4
10.95	0.68	1.73	1.13	0.63	15.6
20	0.09	0.14	0.63	0.10	14.9
30.7	0.21	0.28	1.47	0.44	22.7
38.75	0.22	0.21	1.29	0.34	28.8
44.5	0.26	0.31	1.41	0.47	26.3
50.25	0.10	0.04	0.84	0.07	15.4
56.6	0.17	0.11	0.95	0.23	16.7
60.05	0.12	0.03	0.89	0.06	16.4
70.25	0.22	0.24	0.93	0.15	13.8
76.9	0.47	1.84	1.50	0.65	16.2
80.05	0.48	2.29	1.16	0.69	15.3
89.1	0.35	1.02	0.44	0.42	12.0

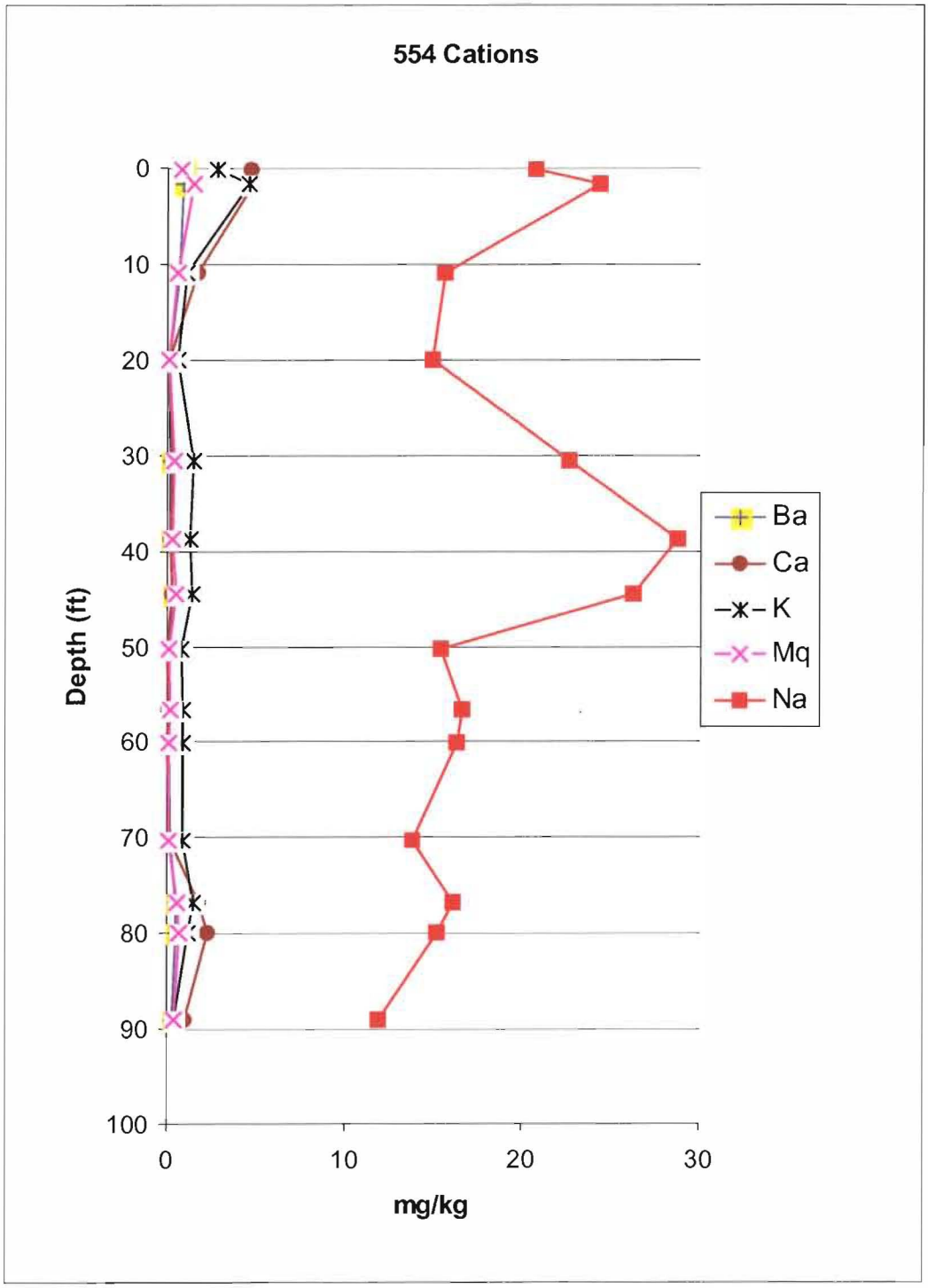
554 Cations
Depth (ft)
0
10
20
30
40
50
60
70
80
90
100
0
10
20
30
mg/kg
Ba
Ca
K
Mq
Na

273 Cations

Mid-depth (ft)	Ba (mg/kg)	Ca (mg/kg)	K (mg/kg)	Mq (mg/kg)	Na (mg/kg)
0.25	0.0105	1.4393	0.9745	0.2399	11.3497
4.95	0.0090	2.9440	1.2553	0.5529	15.9903
16.95	0.0090	3.0951	1.4055	0.6280	12.3804
22.1	0.0809	3.7290	1.8570	0.6889	14.1673
33.25	1.3231	1.5758	1.2934	0.3419	23.4888
39.55	0.7445	0.9269	1.5650	0.1671	32.3646
50.5	0.2251	0.8855	1.8911	0.1201	54.6327
61.3	0.7352	0.6902	1.5605	0.1200	39.4631
62.75	0.2248	2.9520	3.2667	0.6444	75.0750
74	0.2262	2.7144	2.3525	0.7088	48.4068
80.4	0.6306	6.5916	4.9549	2.5676	66.8167
90.3	0.3092	1.0978	1.4998	0.3247	16.6993
94.6	0.4526	1.6747	2.1122	0.7393	26.8548
100.35	0.3133	0.4476	0.8653	0.1044	15.2172
105	0.3863	0.9212	1.3670	0.5349	15.7499
110.7	0.2973	0.4906	2.7653	0.1635	28.0994
113.75	0.6721	3.4949	3.8085	0.9409	42.2670
117.25	0.3155	1.4572	1.9229	0.4056	21.0322
119.75	0.7069	8.6630	4.9331	2.2109	55.6476

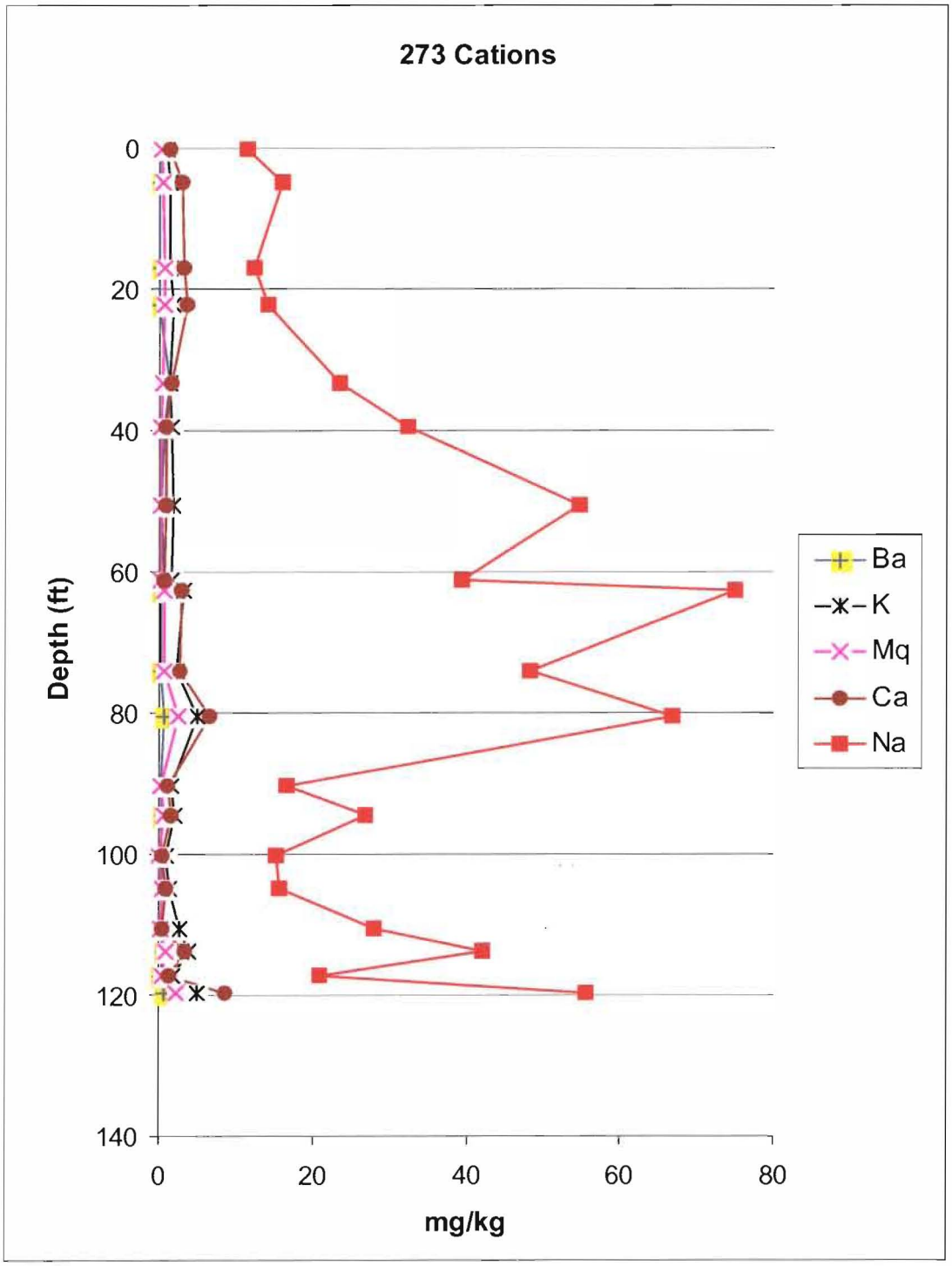
273 Cations
Depth (ft)
0
20
40
60
80
100
120
140
0
20
40
60
80
mg/kg
Ba
K
Mq
Ca
Na

Geologic Map of MDA P: Completion of Phase I Closure Implementation - PLATE 1

- Boreholes - Drilled July 2001, Abandoned October 2001
- Observation Wells, Active (P-1)
- Contour, 2-ft
- Contour, 10-ft
- Contour, 100-ft
- Boundary of Mapped Area
- Culvert
- Fence, Current
- Fence, Removed
- Stream Channel Boundary
- Trench Buried by Fill (Exposed by Excavation)
- Trench, Remnant Exposed
- Road, Dirt
- Road, Paved
- Straw Bales or Wattles for Erosion Control

Faults and Fractures

- Fault
- Fracture
- Traverse Line

6425

Building/Storage Areas

- Active Facility or Structure
- Revetment at Building 389

Results of Erosion Stabilization

- Qrr Rip Rap, Placed for Sediment Control
- Qrc Reclaimed Area, Seeded, Straw Crimp

Unconsolidated Deposits

- Qal Stream Channel Sediment
- Qu Unconsolidated Undifferentiated
- Qt Terrace Undifferentiated
- Qs Forest Floor Soils/Undisturbed

Bedrock - Bandelier Tuff Exposed by Excavation

- Qbt4I Bandelier Tuff Unit 4I
- Qbt3T Bandelier Tuff Unit 3T
- Qbt3 Bandelier Tuff Unit 3

DATA SOURCES FOR PLOT: 200573

Title; Owner; Pub Date; Intended Scale; (ER ID); (GISLab ID)

Geologic Features, Faults, and Fractures; Lewis, C., Lavine, A., Reneau, S., Gardner, J. N., Channell, R. A., and Caldwell, C. W., 2002; Geology of the Western Part of Los Alamos National Laboratory (TA-3 to TA-16), Rio Grande Rift, New Mexico; Los Alamos National Laboratory Report; In preparation; Unknown; (NA); (Unknown)

MDA P Dirt Roads, client supplied; Los Alamos National Laboratory, ER; Unknown; Unknown; (NA); (Unknown)

MDA P Erosion Control (straw bales and wattles), client supplied; Los Alamos National Laboratory, ER; Unknown; Unknown; (NA); (Unknown)

MDA P Line Features (trenches, culverts, stream channel, fences, boundary of mapped area), client supplied; Los Alamos National Laboratory, ER; Unknown; Unknown; (NA); (Unknown)

MDA P Point Features (boreholes, wells), client supplied; Los Alamos National Laboratory, ER; Unknown; Unknown; (NA); (Unknown)

MDA P Reclaimed Areas, client supplied; Los Alamos National Laboratory, ER; Unknown; Unknown; (NA); (Unknown)

MDA P Rip Rap, client supplied; Los Alamos National Laboratory, ER; Unknown; Unknown; (NA); (Unknown)

MDA P Structures, client supplied; Los Alamos National Laboratory, ER; Unknown; Unknown; (NA); (Unknown)

MDA P Topography, client supplied; Los Alamos National Laboratory, ER; Unknown; Unknown; (NA); (Unknown)

MDA P Unconsolidated Undifferentiated Deposit Areas, client supplied; Los Alamos National Laboratory, ER; Unknown; Unknown; (NA); (Unknown)

MDA P Undistrubed Areas, client supplied; Los Alamos National Laboratory, ER; Unknown; Unknown; (NA); (Unknown)

Roads, surfaced; Los Alamos National Laboratory, FWO; Unknown; Unknown; (Unknown); (00007-0002)

Roads, unsurfaced; Los Alamos National Laboratory, FWO; Unknown; Unknown; (Unknown); (00008-0002)

GISLab Los Alamos National Laboratory

RRES

Cartography by: Doug Walther

Date: January 24, 2003 M#: 200573

N

State Plane Coordinate System, New Mexico Central Zone, 1983 North American Datum. Units Feet.

Grid displays New Mexico State Plane coordinates in feet.

1:600

0 50 100 150 200 Feet

0 15 30 45 Meters

DISCLAIMER OF LIABILITY:
Neither the United States Government nor the University of California nor any of their employees, makes any warranty, express or implied, including the warranties of merchantability and fitness for a particular purpose, or assumes any legal liability or responsibility for the accuracy, completeness, or usefulness of any information, apparatus, product, or process disclosed, or represents that its use would not infringe privately owned rights.

Work performed on behalf of RRES-R, Los Alamos National Laboratory, Los Alamos, NM, 87545.